UNIVERSITY OF COPENHAGEN
FACULTY OF SCIENCE

MSc Thesis

Unconventional superconductivity and the Hebel-Slichter peak of the kagome lattice

Yi Dai

Supervisor: Brian Møller Andersen

May 20, 2024

Abstract

To determine the symmetry of the superconducting ground state is a crucial task for understanding unconventional superconductivity. The spin-lattice relaxation rate measured by nuclear magnetic resonance on superconductors is usually thought to be able to probe the symmetry of superconducting order parameter. Materials with kagome lattice structure, such as the AV_3Sb_5 family are possible candidates for unconventional superconductivity. They are already very interesting in the normal state because of the rich band structure and the unique sublattice interference effect. The kagome superconductor was reported to exhibit a Hebel-Slichter peak in the spin-lattice relaxation rate in the superconducting state and this result was interpreted as an evidence for s-wave conventional superconductivity. In this thesis, a theoretical investigation of the spin-lattice relaxation rate of unconventional kagome superconductors is performed. The result shows that despite the existence of a sign-changing gap structure, which sums to zero over the Fermi surface, the d-wave unconventional pairing of the kagome lattice will exhibit a Hebel-Slichter peak in the spin-lattice relaxation rate. This result is further explained in the thesis as an effect of the sublattice interference effect. This thesis, together with the previous study of the robustness of superconducting critical temperature to disorder on the kagome lattice with d-wave order parameter, shows that the unconventional superconductivity of kagome lattice might appear similar to conventional non-sign-changing superconductivity, and further investigation is needed to determine the nature of the superconductivity on the kagome lattice.

Acknowledgements

The last sentence in the acknowledgement of my Bachelor's thesis was from Pascal, 'My heart inclines wholly to know where is the true good, in order to follow it; nothing would be too dear to me for eternity.'[1] Too many things happened in the past three years after my graduation. I said goodbye to something and someone, and said hej hej to something and someone. I miss all of them, my lovely friends, in the past or now, or in the future, I will always miss the moments. Memories are always the source of eternity and infinity to me. I will never hesitate to do the same thing if it happens again. Thanks to all of my friends who made up my memory, which will never happen again in the world, but happens every moment inside me.

First of all, big thanks to Brian and Andreas, for leading me towards this interesting research field. I will never forget the discussions we had in the office, which always give me a lot new ideas and inspirations. I will never forget the cakes Andreas brought at many office nights. Thanks to Magnus, Yongtao and Hans, my office mates, who made the office air hyggligt during the long winter. Thanks to Sofie, for the delightful discussions as well as sharing the kagome notes with me, which helped me a lot in this thesis. Thanks to Mercè, who offered me tremendous help in the CMT1 class and giving me suggestions on finding the supervisor. Too many things to thank for, as well as guiding me to use the cluster. Thanks to Roger, who gives me many useful suggestions in the danish class on my study and thesis. Thanks to Henrik, who had a really helpful discussion about the kagome superconductivity with me. Thanks to all the CMT group members, who made every lunch in the meeting room interesting.

I also want to say thanks to my badminton club members, who always give me passion and motivation to move forward. I won a lot, and also lost a lot, I will try to remember every match.

Thank you, Yifan, for accompanying me from the first day to the last day (it will come soon) during my master's years. I will miss the restaurants we went to, I will miss the voice of the Paris metro, I will also miss the concerts and museums you took me to. All the best with your painting and music. I'm looking forward to seeing you somewhere in a gallery or livehouse of you.

Thank you, the little cats in my little yard, as well as the big cat in 2021. This was a non-ending story, but now we are finally able to move forward. I will always remember, the things you may have already forgotten in the long long summer dream. Also thank you, Sunny Fish, who is always a good friend of mine, thank you for watching and reading my menmories.

Finally, I would like to thank my family, who always supports me with my some-

[1] 'Pensees', Blaise Pascal, translated by W.F. Trotter.

times daydream-like decisions. I love all of you.

”Kamome, Kamome, Kamome,
I want you to listen to my wish.”
— ”Kamome”, Carmen Maki

Table of Contents

Chapter 1

Introduction

1.1 Superconductivity

The disappearance of the electric resistivity of a material under sufficiently low temperatures, known as the famous term 'superconductivity', was initially discovered in 1908 by the Dutch physicist Heike Kamerlingh Onnes in Leiden. About fifty years later, the first satisfying microscopic theory of superconductivity was proposed by John Bardeen, Leon Cooper and John Schrieffer in Illinois. This theory is known as the BCS theory [3, 37], which is very successful in explaining the properties of superconducting materials, for example energy gap, acoustic attenuation rate, electromagnetic absorption, electron tunneling and spin-lattice relaxation rate [37]. As explained in the theory, electrons of opposite spins and momenta will form Cooper pairs near the Fermi surface at low temperatures due to a weak attractive interaction via phonon mediation. Thus the Cooper pairs with effectively zero spin and zero momentum will act as bosons which obey bosonic statistics. Superconducting order parameter, which is from mean-field decoupling of the attraction interaction, can be described using Ginzburg-Landau theory, which explains that the superconducting system shows zero electric resistivity and Meissner effect in low temperature because of spontaneous symmetry breaking.

Even though the BCS theory has achieved a huge success in explaining the superconductivity, the discovery of the high T_c cuprate superconductor in 1986, however, exhibits a case that doesn't follow the conventional BCS regime [4]. The superconducting critical temperature of the cuprate material is much higher than the estimation based on phonon-mediated BCS theory [42]. Moreover, unconventional superconductors show some properties that are quite different from the conventional BCS ones, for example, the resonance peak in the neutron scattering experiment and the absence of Hebel-Slichter peak in the nuclear magnetic resonance experiment. Great theoretical efforts are made to understand unconventional superconductivity [40]. Some micro-

scopic explanations of the unconventional superconductivity other than the phonon-mediated pairing, for example spin fluctuation, are considered as possible candidates.

Phenomenologically, unconventional superconductivity may be understood from the perspective of symmetry of Cooper pairing. Here we briefly introduce the origin of the superconducting order parameter. The pairing Hamiltonian that describes the superconductor pairing can be written as

$$\mathcal{H}(\mathbf{k}) = \mathcal{H}_0(\mathbf{k}) + \sum_{\mathbf{k}\mathbf{k}'} V_{\mathbf{k}\mathbf{k}'} c^\dagger_{\mathbf{k}\uparrow} c^\dagger_{-\mathbf{k}\downarrow} c_{-\mathbf{k}'\downarrow} c_{\mathbf{k}'\uparrow}, \tag{1.1}$$

where $\mathcal{H}_0$ is the kinetic part of the electrons; $V_{\mathbf{k}\mathbf{k}'}$ is the effective pairing interaction induced by phonons (in unconventional superconductors, the interaction can have other origins). $c^\dagger_{\mathbf{k}\sigma}$ and $c_{\mathbf{k}\sigma}$ are the fermionic creation and annihilation operators. The interaction, which is the second term, can be decoupled using the Hartree-Fock mean-field theory [6],

$$\mathcal{H}(\mathbf{k}) = \mathcal{H}_0(\mathbf{k}) - \sum_{\mathbf{k}} \Delta_{\mathbf{k}} c^\dagger_{\mathbf{k}\uparrow} c^\dagger_{-\mathbf{k}\downarrow} - \sum_{\mathbf{k}} \Delta^*_{\mathbf{k}} c_{-\mathbf{k}\downarrow} c_{\mathbf{k}\uparrow}, \tag{1.2}$$

where

$$\Delta_{\mathbf{k}} = -\frac{1}{\mathcal{N}} \sum_{\mathbf{k}'} V_{\mathbf{k}\mathbf{k}'} \langle c_{-\mathbf{k}'\downarrow} c_{\mathbf{k}'\uparrow} \rangle, \tag{1.3}$$

is the superconducting order parameter, where $\mathcal{N}$ is the number of summed points in the momentum space. If we write the kinetic part as $\mathcal{H}_0(\mathbf{k}) = \sum_{\mathbf{k}\sigma} \xi_{\mathbf{k}} c^\dagger_{\mathbf{k}\sigma} c_{\mathbf{k}\sigma}$, then the Hamiltonian can be written in a matrix form

$$\mathcal{H}(\mathbf{k}) = \begin{pmatrix} c^\dagger_{\mathbf{k}\uparrow} & c_{-\mathbf{k}\downarrow} \end{pmatrix} \begin{pmatrix} \xi_{\mathbf{k}} & \Delta_{\mathbf{k}} \\ \Delta^*_{\mathbf{k}} & -\xi_{-\mathbf{k}} \end{pmatrix} \begin{pmatrix} c_{\mathbf{k}\uparrow} \\ c^\dagger_{-\mathbf{k}\downarrow} \end{pmatrix}. \tag{1.4}$$

By defining the so-called Bogoliubov transformation, the Hamiltonian matrix can be diagonalized, and the spinor becomes

$$\begin{pmatrix} \gamma_{\mathbf{k}\uparrow} \\ \gamma^\dagger_{-\mathbf{k}\downarrow} \end{pmatrix} = \begin{pmatrix} u^*_{\mathbf{k}} & v_{\mathbf{k}} \\ -v^*_{\mathbf{k}} & u_{\mathbf{k}} \end{pmatrix} \begin{pmatrix} c_{\mathbf{k}\uparrow} \\ c^\dagger_{-\mathbf{k}\downarrow} \end{pmatrix}. \tag{1.5}$$

Thus Eq. (1.3) can be written as

$$\begin{aligned}\Delta_{\mathbf{k}} &= -\frac{1}{\mathcal{N}}\sum_{\mathbf{k}'} V_{\mathbf{k}\mathbf{k}'}\langle c_{-\mathbf{k}'\downarrow}c_{\mathbf{k}'\uparrow}\rangle \\ &= -\frac{1}{\mathcal{N}}\sum_{\mathbf{k}'} V_{\mathbf{k}\mathbf{k}'}\left[u^*_{\mathbf{k}'}v_{\mathbf{k}'}\left(\langle\gamma_{-\mathbf{k}'\downarrow}\gamma^\dagger_{-\mathbf{k}'\downarrow}\rangle - \langle\gamma_{\mathbf{k}'\uparrow}\gamma^\dagger_{\mathbf{k}'\uparrow}\rangle\right)\right] \\ &= -\frac{1}{\mathcal{N}}\sum_{\mathbf{k}'} V_{\mathbf{k}\mathbf{k}'}u^*_{\mathbf{k}'}v_{\mathbf{k}'}\left[1-2n_F(E_{\mathbf{k}'})\right] \\ &= -\frac{1}{\mathcal{N}}\sum_{\mathbf{k}'} V_{\mathbf{k}\mathbf{k}'}\frac{\Delta_{\mathbf{k}'}}{2E_{\mathbf{k}'}}\left[1-2n_F(E_{\mathbf{k}'})\right],\end{aligned} \tag{1.6}$$

where $E_{\mathbf{k}}$ is the eigenenergies of the Bogoliubov quasi-particles $\gamma^\dagger_{\mathbf{k}\sigma}$ and $\gamma_{\mathbf{k}\sigma}$, i.e. the eigenvalues of the matrix in Eq. (1.4). The final form of Eq. (1.6) is called the BCS gap equation.

Let's consider the the conventional BCS assumption, that the phonon-mediated electron-elecinteraction is independent of the momentum, which means $V_{\mathbf{k}\mathbf{k}'} = V_0$ is a constant. There is a solution for $V_0 < 0$, which is the original solution obtained by BCS,

$$V_{\mathbf{k}\mathbf{k}'} = \begin{cases} V_0 < 0 & \text{if } |\xi_{\mathbf{k}}| \text{ and } |\xi_{\mathbf{k}'}| < \omega_c \\ 0 & \text{otherwise} \end{cases}, \tag{1.7}$$

where ω_c is expected to be of the order of Debye frequency ω_D, which characterizes the cutoff of the phonon spectrum [43].

For the BCS gap equation, there is no non-trivial solution if $V_0 > 0$, which stands for the constant repulsive interaction between electrons. However, if $V_{\mathbf{k}\mathbf{k}'}$ is momentum-dependent, which also results in a momentum-dependent order parameter $\Delta_{\mathbf{k}}$, there can still exist solutions to the gap equation.

The momentum dependence of the superconducting order parameters $\Delta_{\mathbf{k}}$ is classified based on their symmetries. Following the naming convention of the atomic orbitals, the conventional BCS momentum-independent order parameter is called *s*-wave; the different symmetries of $\mathbf{k}$ dependence are called *p*-, *d*-, *f*-wave and so on.

The type of unconventional superconductivity can be identified according to some features. First, the conventional BCS-type *s*-wave order parameter is usually isotropic and does not have node on its Fermi surface; the unconventional superconducting order parameters, however, usually exhibit nodes on the Fermi surface. There are nevertheless exceptions, such as the unconventional $d+id$ order parameter which breaks the time-reversal symmetry can also be nodeless [1]. Another classification of the unconventional superconductivity is the parity of the order parameter. In the triplet superconductors, the order parameter has odd parity and the total spin is $s = 1$; while in the singlet superconductors the parity is even and the total spin is $s = 0$. Furthermore, the unconventional superconducting order parameter will usually have

sign-changing in the **k**-space due to the requirement of the crystal symmetry.

To probe the symmetry of the superconducting order parameter, many experiments are carried out on the superconductors. To name but a few, the heat capacity and penetration depth measurements are supposed to identify the nodal structure of the order parameter; the Knigh shift measurements are expected to identify the singlet/triplet parity; the T_c suppression by impurities and the spin-lattice relaxation rate is believed to be able to tell the sign-changing structure.

1.2 Kagome superconductors

Some superconductors have been identified as unconventional, such as the d-wave cuprates superconductors and the $s_{\pm}$-wave iron pnictide superconductors and the likely spin-triplet superconductor Sr_2RuO_4. For the newly discovered superconductors, it is always an important task to identify the symmetry of the superconducting pairing state, especially for those which shows interesting features that indicate unconventional superconductivity, such as the time-reversal symmetry breaking.

Kagome superconductor AV_3Sb_5 is such a candidate for unconventional superconductivity, which is already very interesting in the normal state because it shows many unconventional electronic states [45]. AV_3Sb_5 mentals exhibit CDW order below T_{CDW} = 78, 104 and 94 K for A = K, Rb, Cs, respectively. In experiments, muon spin relaxation (μSR) studies report possible time-reversal symmetry breaking (TRSB) within the CDW state [20, 23]. And TRSB is also reported in superconducting state [12]. Theoretical studies of the leading superconducting instabilities on the kagome lattice suggests that the $d + id$ symmetry which breaks time-reversal symmetry is the most possible candidate for the unconventional superconductivity [34, 47]. These results motivate us to study the possible unconventional superconducting states in the kagome lattice.

1.3 Structure of thesis

In this thesis, we focus on the superconductivity in the kagome lattice, which is held by AV_3Sb_5 metals. Current research has suggested an singlet and anisotropic picture of the order parameter [45]. But it is still not clear if the order parameter has a sign-changing structure. The nuclear magnetic resonance (NMR) measurement of the spin-lattice relaxation rate has reported a Hebel-Slichter peak in the kagome superconductor, which is usually considered as a evidence for non-sign-changing s-wave superconductivity. However, this conclusion may be not true for the kagome lattice.

In Chapter 2, we review the spin-lattice relaxation rate the Hebel-Slichter peak,

where we explain the reason for the existence of a Hebel-Slichter peak in the conventional BCS superconductors and the absence in unconventional superconductors. In Chapter 3, we take the square lattice as a example, showing that there is a Hebel-Slichter peak in the s-wave case and the peak is absent in the d-wave case because of the sign-changing effect. With these preliminary knowledge of the Hebel-Slichter peak, in Chapter 4 we introduce the exotic kagome superconductor which exhibit so-called sublattice interference effect that render the unconventional d-wave superconductor robust to disorder on the kagome lattice. Finally, we show in Chapter 5 that the unconventional d-wave kagome superconductors can exhibit the Hebel-Slichter peak despite a fully compensated sign-changing gap structure. To make the structure of the thesis clear and easier to read, I put the long derivations in the appendices, which may also provide necessary steps to the results.

Chapter 2

NMR and spin-lattice relaxation rate

2.1 Introduction to NMR

Nuclear magnetic resonance (NMR) is a fundamental method of studying the superconducting materials [5, 14, 43]. In NMR relaxation measurement, the sample is placed in a static magnetic field at first. By applying a second time-dependent oscillating magnetic field, which is perpendicular to the first one, the nuclear magnetization of the sample will precess around the second time-dependent field when this field is oscillating at a certain frequency. Then by switching off the oscillating magnetic field, the nuclear magnetization will relax back to the original thermal equilibrium state. The relaxation time of the longitudinal component of the nuclear magnetization along the static magnetic field is called T_1, and the relaxation time of the transverse component is called T_2.

The longitudinal relaxation time T_1 is also called spin-lattice relaxation time, because the relaxation process requires the redistribution of nuclear magnetic energy levels, and the exchange of energy happens between spins and the lattice [14]. By contrast, the relaxation along the transverse direction does not require energy exchange, but the dephasing by the spin-spin interaction is needed for the process. Thus T_2 is also called spin-spin relaxation time.

In this thesis, we focus on the spin-lattice relaxation rate, which is defined as the inverse of the spin-lattice relaxation time T_1^{-1}. In many cases it is referred to as $1/T_1T$ both in experiments and theories [8, 27, 32], because it is proportional to the imaginary part of spin susceptibility. Usually $1/T_1T$ behaves very differently in the normal states and the superconducting states, and can show the famous Hebel-Slichter peak in the latter case.

2.2 Spin-lattice relaxation rate and spin susceptibility

In the early work by T. Moriya [25, 26, 28], he derived the relation between spin-lattice relaxation rate and the imaginary part of spin susceptibility

$$\alpha \equiv \frac{1}{T_1 T} = \frac{C}{\omega}\frac{1}{\mathcal{N}}\sum_{\mathbf{q}} \mathrm{Im}\chi_0^{+-}(\mathbf{q},\omega), \tag{2.1}$$

where $\mathcal{N}$ denotes the number of points summed over in the Brillouin zone (BZ). ω is the resonance frequency which is very small. C is a constant given by

$$C = 2\gamma_n^2\gamma_e^2 k_B |A|^2, \tag{2.2}$$

where the γ_n and γ_e are the nuclear and the electronic gyromagnetic ratios, k_B the Boltzmann constant, g the Landé factor, and μ_B the Bohr magneton. A is the magnetic hyperfine coupling and is approximated to be a constant. The derivation from the hyperfine contact Hamiltonian to Eq. (2.1) is shown in Appendix A.

We should be reminded that ω in Eq. (2.1) is very small, but it is still a finite number. This very small but finite number is important to avoid the divergence in the relaxation rate.

This relation reduces the calculation of $1/T_1T$ to the imaginary part of spin susceptibility in momentum $\mathbf{q}$ and frequency ω

$$\begin{aligned}
\chi_0^{+-}(\mathbf{q},\omega) = \frac{1}{\mathcal{N}}\sum_{\mathbf{k},E>0}\Bigg[&\left(1-\frac{\xi_{\mathbf{k}}\xi_{\mathbf{k+q}}+\Delta^*_{\mathbf{k+q}}\Delta_{\mathbf{k}}}{E_{\mathbf{k}}E_{\mathbf{k+q}}}\right)\frac{1-f(E_{\mathbf{k}})-f(E_{\mathbf{k+q}})}{\omega+E_{\mathbf{k+q}}+E_{\mathbf{k}}+i\eta}\\
&+\left(1-\frac{\xi_{\mathbf{k}}\xi_{\mathbf{k+q}}+\Delta^*_{\mathbf{k+q}}\Delta_{\mathbf{k}}}{E_{\mathbf{k}}E_{\mathbf{k+q}}}\right)\frac{f(E_{\mathbf{k}})+f(E_{\mathbf{k+q}})-1}{\omega-E_{\mathbf{k+q}}-E_{\mathbf{k}}+i\eta}\\
&+\left(1+\frac{\xi_{\mathbf{k}}\xi_{\mathbf{k+q}}+\Delta^*_{\mathbf{k+q}}\Delta_{\mathbf{k}}}{E_{\mathbf{k}}E_{\mathbf{k+q}}}\right)\frac{f(E_{\mathbf{k}})-f(E_{\mathbf{k+q}})}{\omega+E_{\mathbf{k+q}}-E_{\mathbf{k}}+i\eta}\\
&+\left(1+\frac{\xi_{\mathbf{k}}\xi_{\mathbf{k+q}}+\Delta^*_{\mathbf{k+q}}\Delta_{\mathbf{k}}}{E_{\mathbf{k}}E_{\mathbf{k+q}}}\right)\frac{f(E_{\mathbf{k+q}})-f(E_k)}{\omega+E_{\mathbf{k}}-E_{\mathbf{k+q}}+i\eta}\Bigg],
\end{aligned} \tag{2.3}$$

where η is an infinitesimal positive factor arising from the analytical continuation. ξ_k is the electron dispersion, Δ_k the superconducting order parameter, $E_k = \sqrt{\xi_k^2+\Delta_k^2}$ denotes the energy of superconducting quasiparticles, and $f(E_k)$ is the Fermi-Dirac distribution function

$$f(E_k) = \frac{1}{e^{E_k/k_BT}+1}. \tag{2.4}$$

Because of the Nambu particle-hole symmetry, we can sum only over momentum points with positive E_k. For further details on the derivation for spin susceptibility formula and summing over positive energy, I have shown in Appendix B.

For the superconducting states, the imaginary part of the first term and the second term vanish. To illustrate this, we take the first term in Eq. (2.3) as the example. The last half of this term

$$\frac{1 - f(E_{\mathbf{k}}) - f(E_{\mathbf{k+q}})}{\omega + E_{\mathbf{k+q}} + E_{\mathbf{k}} + i\eta} \tag{2.5}$$

gives a Dirac delta function for the imaginary part according to the Cauchy's principal value $(\omega + i\eta)^{-1} = \mathcal{P}\frac{1}{\omega} - i\pi\delta(\omega)$,

$$-\pi\left[1 - f(E_{\mathbf{k}}) - f(E_{\mathbf{k+q}})\right]\delta(\omega + E_{\mathbf{k+q}} + E_{\mathbf{k}}). \tag{2.6}$$

In the superconducting state, the energy of superconducting quasiparticle $E_k = \sqrt{\xi_k^2 + \Delta_k^2}$ is always larger than a very small $\omega \to 0$. Thus the first two terms give zero. In contrast, they will give contribution to $\chi_0^{+-}(\mathbf{q}, \omega)$ in the normal state when $\xi_k = 0$. Since we mainly focus on the superconducting states which cause the Hebel-Slichter peak, we can neglect these two terms in the discussion.

In the prevalent discussion about the Hebel-Slichter peak [42, 43], one usually only consider the conventional superconducting pairing state. Here we follow their discussion and use the real, momentum independent superconducting order parameter Δ in this chapter. However, we will consider the momentum dependent unconventional superconducting order parameters in the following chapters.

When Δ is real, the third and the fourth term can be combined, and the imaginary part is given by

$$-\frac{2\pi}{\mathcal{N}}\sum_{\mathbf{k},E>0} 2\left(1 + \frac{\xi_{\mathbf{k}}\xi_{\mathbf{k+q}} + |\Delta|^2}{E_{\mathbf{k}}E_{\mathbf{k+q}}}\right)\left(f(E_{\mathbf{k}}) - f(E_{\mathbf{k+q}})\right)\delta(\omega + E_{\mathbf{k+q}} - E_{\mathbf{k}}). \tag{2.7}$$

Now we consider the relaxation rate, where we sum over both $\mathbf{k}$ and $\mathbf{q}$. This term only gives non-zero contribution close to the Fermi surface, in which Δ dominate and $\xi_k \approx 0$. Furthermore, since E_k is homogeneous in $\mathbf{k}$-space, we can convert the $\mathbf{k}$-sum to the E-integral [37]. We rename $E_{\mathbf{k}}$ and $E_{\mathbf{k+q}}$ as E and E' for the moment. The spin-lattice relaxation rate expression with E-integral is

$$\alpha_s \propto -\frac{1}{\omega}\int_0^\infty dE \int_0^\infty dE' \left(1 + \frac{|\Delta|^2}{EE'}\right)\left(f(E) - f(E')\right)\delta(\omega + E' - E)D_s(E)D_s(E'), \tag{2.8}$$

where $D(E)$ denotes the density of states (DOS) of energy E. at superconducting state. The factor 2π is absorbed into the constant C. This expression can be simplified

by combine one of the integral and the δ function together,

$$\frac{2}{\omega}\int_0^\infty dE\left(1+\frac{|\Delta|^2}{E(E+\omega)}\right)(f(E)-f(E+\omega))\,D_s(E)D_s(E+\omega). \tag{2.9}$$

Remember that we want ω to be very small, then $(f(E)-f(E+\omega))/\omega$ just gives the derivative of the Fermi function $\partial f/\partial E$ at energy E,

$$2\int_0^\infty dE\left(1+\frac{|\Delta|^2}{E(E+\omega)}\right)\left(-\frac{\partial f}{\partial E}\right)D_s(E)D_s(E+\omega). \tag{2.10}$$

This is the commonly agreed expression for spin-lattice relaxation rate in textbooks [14, 37, 42, 43]. The factor

$$\left(1+\frac{|\Delta|^2}{EE'}\right), \tag{2.11}$$

where here $E' = E+\omega$, is referred to as F_+ coherence factor, which is relevant for quasiparticle creation and annihilation in NMR experiment. In contrast, another type of coherence factor $\left(1-\frac{|\Delta|^2}{EE'}\right)$ is referred to as F_- for quasiparticle scattering in ultrasound experiments [42].

2.3 Hebel-Slichter peak

In March 1959, less than two years from the publication of the groundbreaking BCS theory in December 1957, Hebel and Slichter calculated the spin-lattice relaxation rate using the BCS theory for the first time [15]. In this paper, they measured the relaxation rate in the superconducting state of Aluminum. The relaxation rate in the superconducting state increases at first as the temperature increases, but drops just below the critical temperature.

Using the BCS theory, they calculated the relaxation rate curve and it agrees with the experiment semiquantitatively. This is seen as an important confirmation of the BCS theory [37].

Now we show the calculation in the books [37, 42, 43], where the approximation is applied for $D_s(E)$,

$$\frac{D_s(E)}{D_n(E)} \approx \frac{E}{\sqrt{E^2-|\Delta|^2}}, \tag{2.12}$$

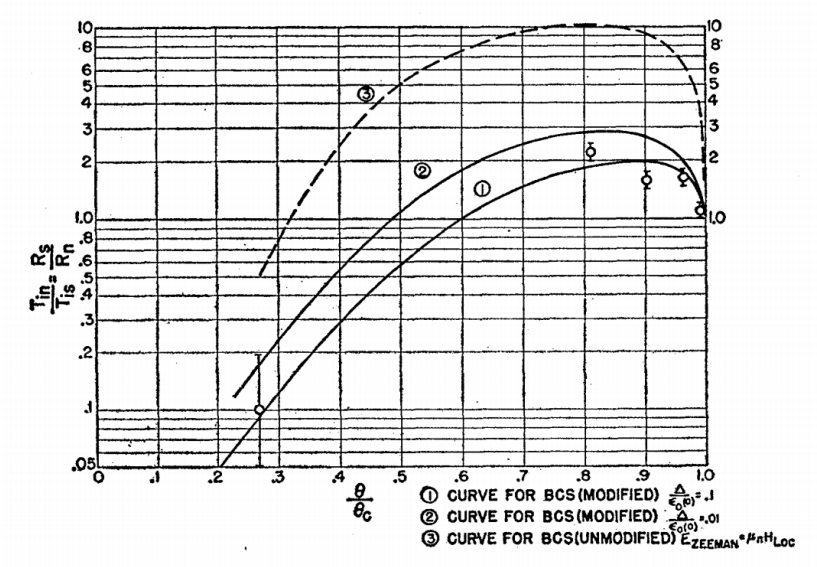

Figure 2.1: The relaxation rate measurement cited from the original paper by Hebel and Slichter [15]. They vertical axis is the relaxation rate α_s/α_n, where α_n is the relaxation rate extrapolated from the normal state. The horizontal axis is the temperature T/T_c, where T_c is the critical temperature in the BCS theory.

and insert this into Eq. (2.10),

$$\begin{aligned}\frac{\alpha_s}{\alpha_n} \approx & 2\int_\Delta^\infty dE\left(1+\frac{|\Delta|^2}{E(E+\omega)}\right)\left(-\frac{\partial f}{\partial E}\right)\frac{E}{\sqrt{E^2-|\Delta|^2}}\frac{E+\omega}{\sqrt{(E+\omega)^2-|\Delta|^2}}, \\ = & 2\int_\Delta^\infty dE\frac{E(E+\omega)+|\Delta|^2}{\sqrt{[(E+\omega)^2-|\Delta|^2]\,[E^2-|\Delta|^2]}}\cdot\left(-\frac{\partial f}{\partial E}\right).\end{aligned} \tag{2.13}$$

The derivative of the Fermi function is

$$\left(-\frac{\partial f}{\partial E}\right) = \frac{1}{2T(1+\cosh(E/T))}, \tag{2.14}$$

and we take the temperature dependence order parameter $\Delta(T)$ solved self-consistently from the BCS gap equation [37],

$$\Delta_{\mathbf{k}'} = -\frac{1}{\mathcal{N}}\sum_{\mathbf{k}} V_{\mathbf{k}\mathbf{k}'}\frac{\Delta_{\mathbf{k}}}{2E_{\mathbf{k}}}\tanh\frac{\beta E_{\mathbf{k}}}{2}, \tag{2.15}$$

where $\beta = 1/k_BT$.

As mentioned above, a finite but small ω is important in Eq. (2.13). If $\omega = 0$, the value will be divergent because of the divergence of the square of superconducting density of states, thus a finite ω is needed to avoid the divergence.

As shown in Fig. 2.3, the relaxation rate in the superconducting states calculated from Eq. (2.14) increases above the normal states just below T_c, which is the famous Hebel-Slichter peak. Now let's move our eyes from the peak. As the temperature

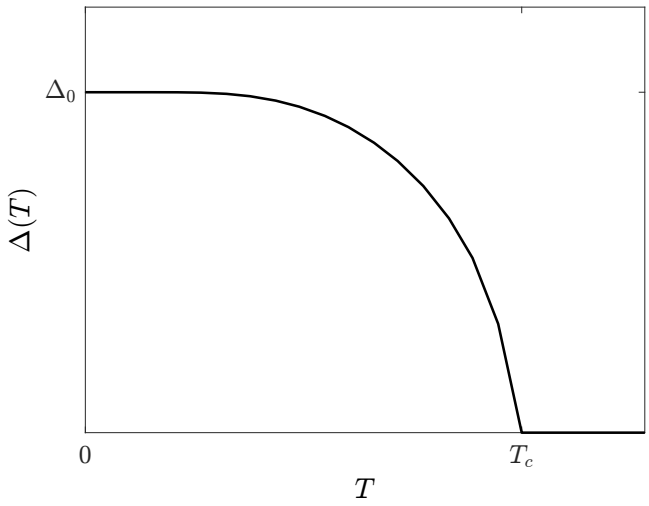

Figure 2.2: T dependence of superconducting order parameter Δ solved from BCS gap equation.

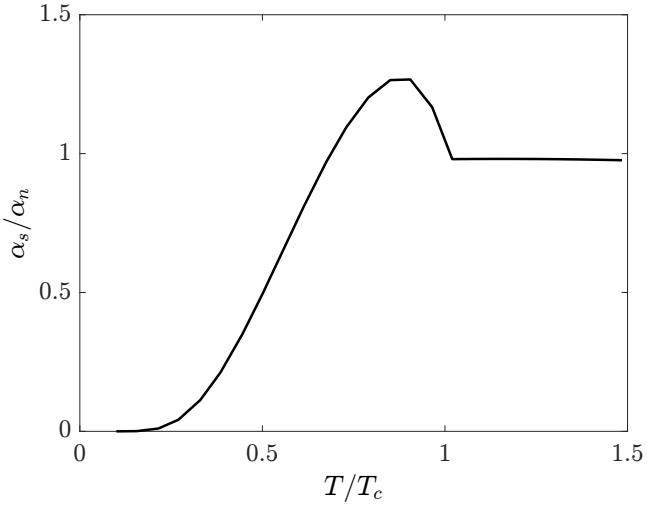

Figure 2.3: T dependence of the spin-lattice relaxation rate ratio α_s/α_n. The pronounced Hebel-Slichter peak is shown right below the critical temperature T_c

increases from the peak, the rate drops to 1 quickly because of the fast decaying behavior of Δ near T_c as shown in Fig. 2.2. As the temperature decreases from the peak and goes to $T \to 0$, the relaxation rate drops to near 0. The reason is explained in the next section.

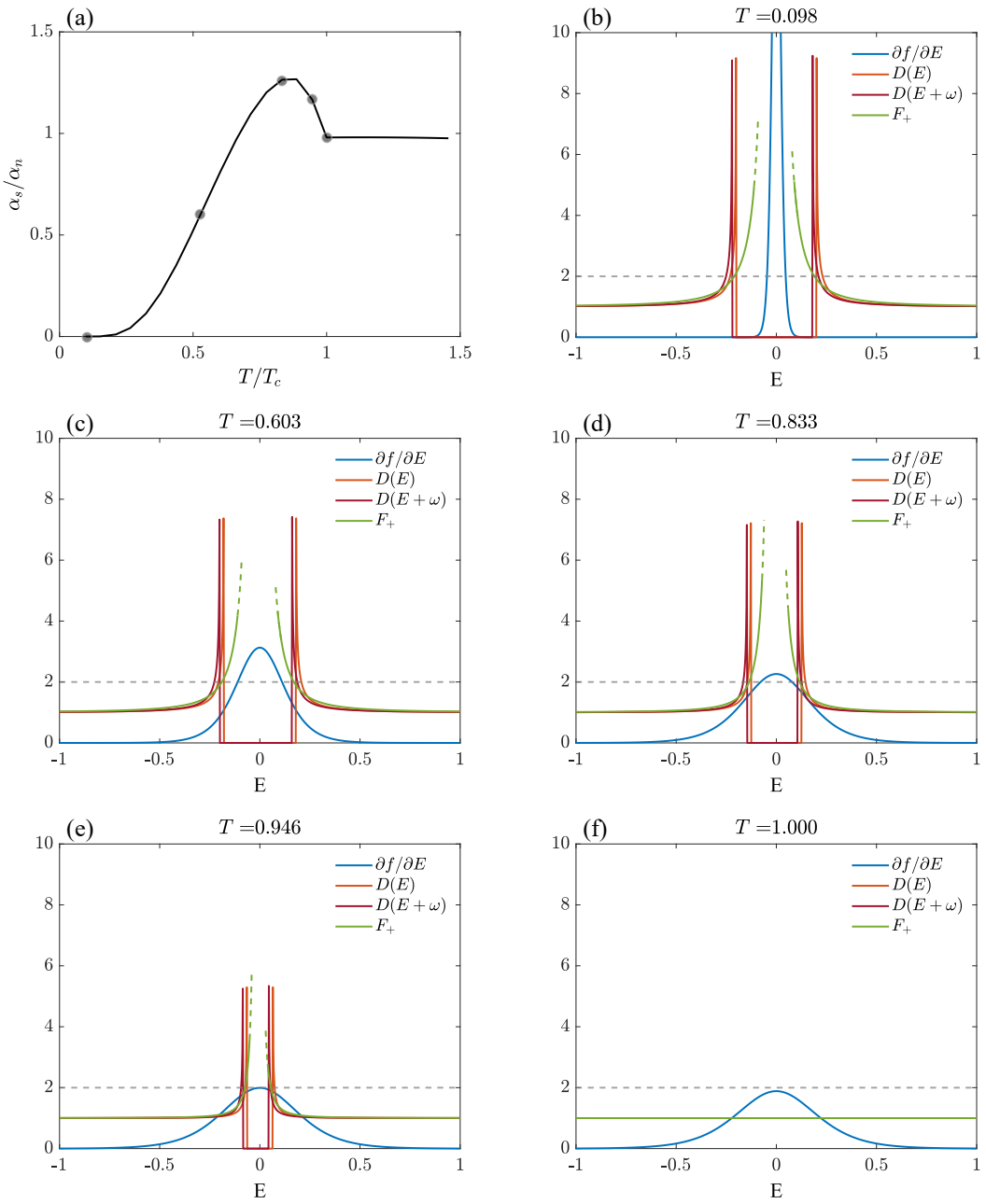

Figure 2.4: (a) T dependence of the relaxation rate. The black dots denote the temperatures which are chosen for panels (b-f). (b)-(f) The distributions of the four terms F_+, $-(\partial f/\partial E)$, $D(E)$ and $D(E+\omega)$ along E axis.

2.4 Why is there a Hebel-Slichter peak?

In Eq (2.13), we inserted the approximation of the density of states in the superconducting states. Combined with other terms, it simplifies the expression of relaxation rate. However, in order to better understand why there is a Hebel-Slichter peak, we can write down the different terms in the expression separately and look how they contribute to the integral,

$$\frac{\alpha_s}{\alpha_n} \approx 2 \int_{\Delta}^{\infty} dE \cdot F_+(E) \cdot \left(-\frac{\partial f}{\partial E}\right) \cdot D(E) \cdot D(E+\omega), \tag{2.16}$$

where

$$F_+(E) = 1 + \frac{|\Delta|^2}{E(E+\omega)}, \tag{2.17}$$

$$\left(-\frac{\partial f}{\partial E}\right) = \frac{1}{2T(1+\cosh(E/T))}, \tag{2.18}$$

$$D(E) = \frac{E}{\sqrt{E^2 - |\Delta|^2}}, \tag{2.19}$$

$$D(E+\omega) = \frac{E+\omega}{\sqrt{(E+\omega)^2 - |\Delta|^2}}. \tag{2.20}$$

As shown in Fig 2.4 (a), we choose some points that correspond to the certain featured stages of the relaxation rate curve. The temperature of the first point is $0.098T_c$, and the corresponding terms Eq. (2.17)-(2.20) are shown in Fig 2.4 (b). The peaks of the density of states $D(E)$ and $D(E+\omega)$ are split by the finite ω, thus the product of the two terms will not be divergent. The derivative of Fermi function $\partial f/\partial E$ shows a very sharp peak at $E \approx 0$ when $T \approx 0$. In contrast, for larger E at $T \approx 0$, for example $E = \Delta$, there is $\partial f/\partial E \approx 0$. Thus the product of three terms in total will give zero, as $\partial f/\partial E$ is inside the gap of the DOS.

When the temperature increases, as shown in Fig 2.4 (c), the $\partial f/\partial E$ distribution becomes broader. As a result, the tails of $\partial f/\partial E$ will pick up the peaks in the DOS, and give a non-zero contribution to the relaxation rate. As the temperature further increase in Fig 2.4 (d-e), $\partial f/\partial E$ spreads more out, and the gap in the DOS becomes smaller since the order parameter decreases as the temperature increases. This means that the peak in the DOS enters into the center of the $\partial f/\partial E$ distribution. Finally in Fig 2.4 (f) at $T = T_c$, the superconducting gap closes and the system enters the normal state.

There are two competing factos in the curve. The first one is that when the temperature increases, the $-\partial f/\partial E$ function becomes broader and will enhance the relaxation rate together with the peak in the DOS. But there is another factor that

might decrease the relaxation rate, i.e., the peaks in the DOS is becoming smaller as the the temperature increase, and finally is wiped out as the system enters the normal state.

I leave the conclusion of the above discussion for a second, and now let's talk about another factor that we haven't considered yet, which is the coherence factor $F_+(E)$. It is easy to see from Eq. (2.17) that there is always $F_+(E) \approx 2$ at $E = \pm|\Delta|$, which means the coherence factor $F_+(E)$ doubles the contribution to the relaxation rate from the energies that lies at the superconducting gap $E = \pm|\Delta|$. However, for the energy E further away from $E = \pm|\Delta|$, how the enhancement to the relaxation rate from F_+ varies with E is not that clearly seen from this equation. To describe the enhancement, we can take the slope of the F_+ function at $E = \pm|\Delta|$ as a quantity that reflects the enhancement,

$$\frac{\partial F_+(T)}{\partial E}\Big|_{E=\pm|\Delta(T)|} = \frac{2\Delta(T)+\omega}{(\Delta(T)+\omega)^2}. \tag{2.21}$$

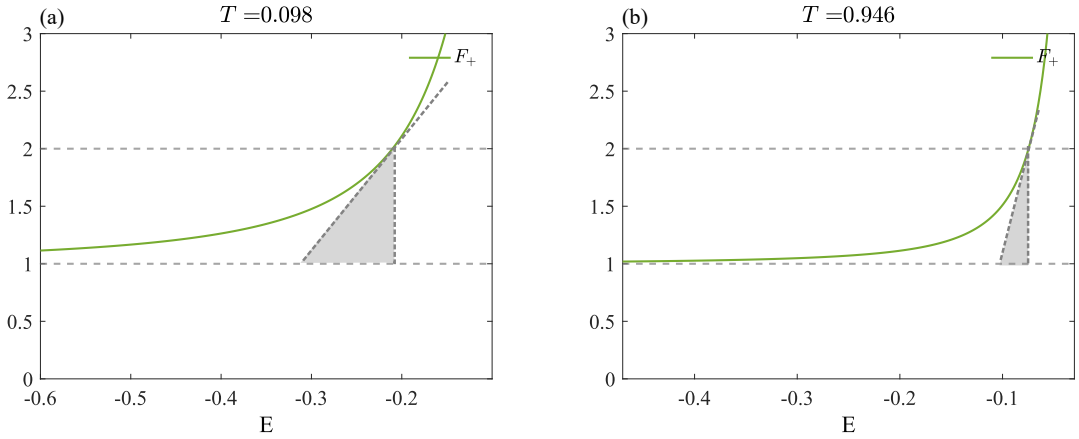

Figure 2.5: (a) Zooming in of F_+ in the negative side of E at $T \to 0$, (b) at $T \to T_c$. The dashed line that is tangent with F_+ at $E = -|\Delta(T)|$ is a linear function with slope $\frac{\partial F_+}{\partial E}$. The gray area indicates the degree of enhancement to relaxation rate from F_+. F_+ shown in the left panel will give more enhancement to the relaxation rate than in the right panel.

As shown in Fig. 2.5, $\frac{\partial F_+}{\partial E}$ is smaller at low temperature $T \to 0$ and large $\Delta(T \to 0)$, which gives the enhancement to a larger area in the E axis. By contrast, at $T \to T_c$ and fast decreasing $\Delta(T \to T_c)$, the slope will be very large, which means only a very small area near $E = \pm|\Delta|$ is enhanced. Finally at $T = T_c$, the slope goes to ∞, which means there is no area got enhanced.

The temperature dependence of $\frac{\partial F_+}{\partial E}$ is shown in Fig 2.6. At temperature below $T/T_c = 0.7$, The slope does not change much and gives a relatively stable enhancement to the relaxation rate. However, as the temperature further increase, the slope starts increasing fast because of the fast decay of Δ. As a result, the enhancement to the

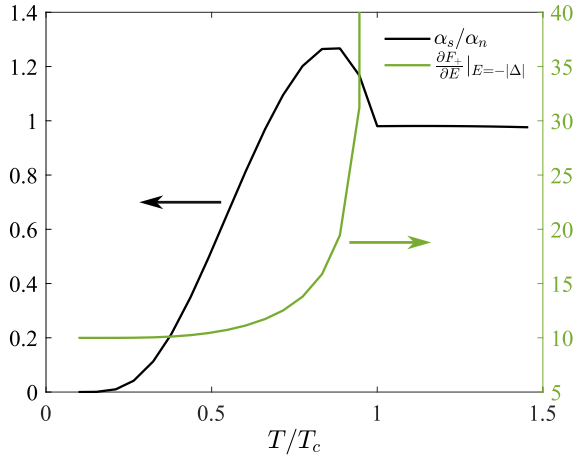

Figure 2.6: The black curve shows the temperature dependence of α_s/α_n. The green curve shows the temperature dependence of the slope of the coherence factor $\frac{\partial F_+}{\partial E}$ at $E = -|\Delta(T)|$.

relaxation rate also decreases fast.

Now we have all the factors that might contribute to the peak ready: 1) the sharp peak of DOS, 2) the broadening of $\partial f/\partial E$, and 3) the coherence factor F_+ that enhances the relaxation rate.

Let's consider the DOS and the Fermi function first. By evaluating the temperature dependence of

$$2\int_{\Delta}^{\infty} dE \cdot \left(-\frac{\partial f}{\partial E}\right) \cdot D(E) \cdot D(E+\omega), \tag{2.22}$$

which is Eq. (2.16), but the coherence factor $F_+(E)$ is set to be 1. Figure. 2.7 shows that there is no peak in such a function. By comparing the result of Fig. 2.7 with Fig. 2.3, we can draw a conclusion that there will not be a Hebel-Slichter peak if we only consider factors 1) and 2). Those two factors, however, only guarantees that the relaxation rate at $T \to T_c$ is larger than it at $T \to 0$, but they will not guarantee that the relaxation rate in the superconducting state exceeds the normal state. In fact, as we will discuss in the next section, in unconventional superconductors, where the coherence factor is usually 1 because of the sign-changing effect, the Hebel-Slichter peak is usually not found, which verifies the above argument.

Taking those factors together, we can now make a brief summary of the origin of the Hebel-Slichter peak. At low temperature $T \to 0$, the Fermi function term is localized inside the gap of the DOS, thus the relaxation rate is greatly suppressed and the value is almost zero. As the temperature increases, the Fermi function term start to overlap with the peak of the DOS. Because of the enhancement from the coherence factor, the rate is further boosted to above the normal state. Thereafter, the DOS and the Fermi function term together continues increasing as shown in Fig. 2.7, but the

enhancement from the coherence factor is decreasing quickly as T goes close to T_c. As the enhancement vanishes, the relaxation rate drops back to the normal state at T_c. Considering these processes together, it results in a peak just below T_c.

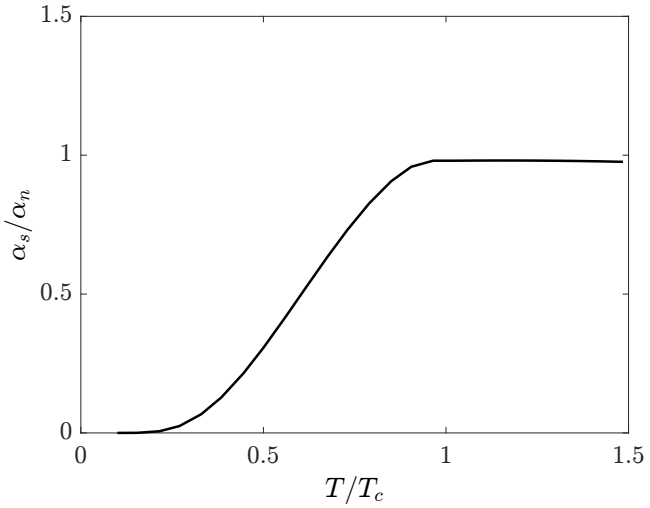

Figure 2.7: T dependence of the value in Eq. (2.22). No Hebel-Slichter peak appears.

2.5 Absence of Hebel-Slichter peak in unconventional superconductors

In experiments, there are many evidences supporting the absence of Hebel-Slichter peak in unconventional (most of them have d-wave symmetries) superconductors [2, 9, 21, 22]. The explanation for the absence of peak can be that the positive and negative $\Delta_{\mathbf{k}}$ cancels with each other and gives zero in total. As a result, the coherence factor F_+ is always 1 thus gives no enhancement to the relaxation rate as shown in Fig. 2.7.

However, the explanation above is not perfect. First of all, the density of states of the unconventional superconductors are usually different from the convention ones. Thus the approximation of density of states in Eq. (2.12) is no longer appropriate. Usually, the DOS of unconventional superconductors are not fully gapped, while the conventional ones does, which may cause different behaviors in the relaxation rate. Furthermore, Eq. (2.3) is derived for the single-band BdG Hamiltonian, but for multi-band systems, the expression may differ. In fact, as we will show in this thesis, kagome lattice is a system that does not follow this argument that the unconventional superconductivity will render the absence of Hebel-Slichter peak. By contrast, the Hebel-Slichter peak is possible to exist even though the superconducting order parameter is sign-changing.

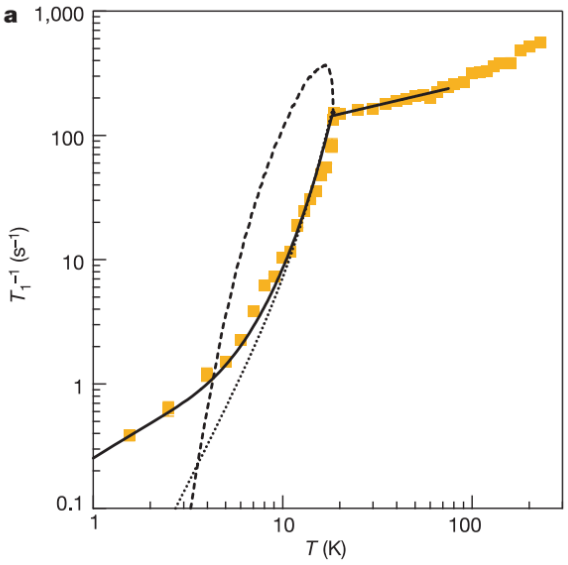

Figure 2.8: The spin-lattice relaxation rate of $PuCoGa_5$ in the normal and superconducting states. The dashed line is the relaxation rate calculated from *s*-wave BCS theory. The Hebel-Slichter peak is absent in the measurement of the superconducting state. Image from [9].

Chapter 3

The Hebel-Slichter peak in the square lattice

As we discussed in the end of last chapter, by directing setting coherence factor $F_+ = 1$, the Hebel-Slichter peak becomes absent from the spin-lattice relaxation rate. However, this argument is not fully satisfying to explain the absence of Hebel-Slichter peak in the d-wave superconductors, since we did not use the realistic d-wave DOS in Eq.(2.22). In this chapter, we consider a simple lattice model, i.e. the square lattice, and calculate the spin-lattice relaxation rate of this model. In this case, the DOS is realistic for the square lattice and there is no approximation upon it.

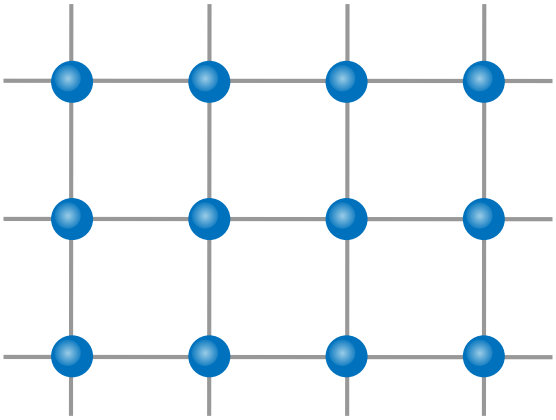

Figure 3.1: Illustration of the square lattice.

3.1 The lattice

The tight-binding model of the square lattice in momentum space is

$$\mathcal{H}_0 = \sum_{\mathbf{k}\sigma} \left[-2t\left(\cos k_x + \cos k_y\right) - \mu\right] c^\dagger_{\mathbf{k}\sigma} c_{\mathbf{k}\sigma}. \tag{3.1}$$

Now we consider the superconductivity. The mean-field Hamiltonian of the superconducting part is

$$\mathcal{H}_{\mathrm{SC}} = -\sum_{\mathbf{k}} \Delta_{\mathbf{k}} c^\dagger_{\mathbf{k}\uparrow} c^\dagger_{-\mathbf{k}\downarrow} - \sum_{\mathbf{k}} \Delta^*_{\mathbf{k}} c_{-\mathbf{k}\downarrow} c_{\mathbf{k}\uparrow}. \tag{3.2}$$

In the conventional (s-wave) BCS theory of superconductivity, the order parameter $\Delta_{\mathbf{k}}$ is independent of the momentum vector $\mathbf{k}$. According to this, we can define the s-wave superconducting order parameter $\Delta^s_{\mathbf{k}} = \Delta_0$ in this lattice. However, the order parameters, which are $\mathbf{k}$ dependent, are also allowed as the solutions of the BCS gap equation Eq. (2.15) [42]. Here we take the order parameter with the $d_{x^2-y^2}$ symmetry $\Delta^d_{\mathbf{k}} = \frac{\Delta_0}{2}\left(\cos k_x - \cos k_y\right)$.

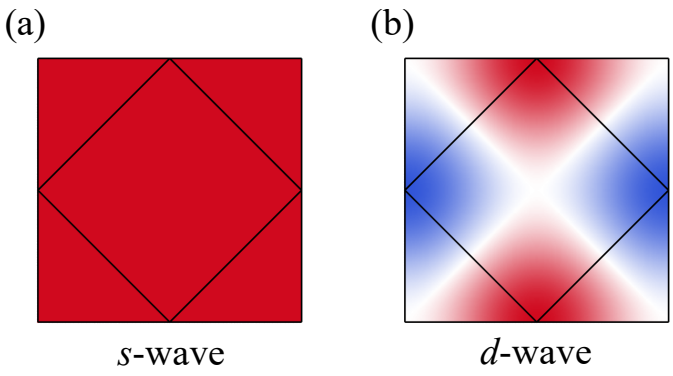

Figure 3.2: The s-wave and d-wave order parameter (a) and (b) in the first Brillouin zone. The black lines indicate the Fermi surface at $\mu = 0$.

3.2 The B factor and relaxation rate

The spin susceptibility is calculated from Eq. (2.3), which is quite general for one-band BCS Hamiltonian. As we have discussed in the last chapter, only the last two terms in Eq. (2.3) are non-zero in the superconducting states. Thus we can write it as

$$\chi_0^{+-}(\mathbf{q},\omega) \approx \frac{1}{\mathcal{N}} \sum_{\mathbf{k},E>0} \left[\left(1 + \frac{\xi_{\mathbf{k}}\xi_{\mathbf{k+q}} + \Delta^*_{\mathbf{k+q}}\Delta_{\mathbf{k}}}{E_{\mathbf{k}}E_{\mathbf{k+q}}} \right) \frac{f(E_{\mathbf{k}}) - f(E_{\mathbf{k+q}})}{\omega + E_{\mathbf{k+q}} - E_{\mathbf{k}} + i\eta} \right. \\ \left. + \left(1 + \frac{\xi_{\mathbf{k}}\xi_{\mathbf{k+q}} + \Delta^*_{\mathbf{k+q}}\Delta_{\mathbf{k}}}{E_{\mathbf{k}}E_{\mathbf{k+q}}} \right) \frac{f(E_{\mathbf{k+q}}) - f(E_k)}{\omega + E_{\mathbf{k}} - E_{\mathbf{k+q}} + i\eta} \right]. \tag{3.3}$$

The coherence factor, which in the expression above is

$$\left(1 + \frac{\xi_{\mathbf{k}}\xi_{\mathbf{k+q}} + \Delta^*_{\mathbf{k+q}}\Delta_{\mathbf{k}}}{E_{\mathbf{k}}E_{\mathbf{k+q}}} \right), \tag{3.4}$$

is the key to the spin-lattice relaxation rate, as we have explained in Chapter 2.4. Since we have set $E_{\mathbf{k}}$ to be always positive, while $\xi_{\mathbf{k}}$ can be both positive and negative, $\xi_{\mathbf{k}}\xi_{\mathbf{k+q}}$ will finally be cancelled. Thus only $\Delta^*_{\mathbf{k+q}}\Delta_{\mathbf{k}}$ remains as the important factor in this term.

We want to see how $\Delta^*_{\mathbf{k+q}}\Delta_{\mathbf{k}}$ looks for the s-wave and the d-wave cases. However, it is defined in both $\mathbf{k}$ and $\mathbf{q}$ space, so it is not convenient to directly plot it. Instead, we can define

$$B(\mathbf{q},\mathbf{k}_n) = \frac{\Delta^*_{\mathbf{k}_n+\mathbf{q}}\Delta_{\mathbf{k}_n}}{E_{\mathbf{k}_n}E_{\mathbf{k}_n+\mathbf{q}}}, \tag{3.5}$$

where $\mathbf{k}_n$ is chosen from the $\mathbf{k}$ points on the Fermi surface, which potentially gives the largest contribution to the spin susceptibility.

As shown in Fig. 3.3, $B(\mathbf{q},\mathbf{k}_n)$ is always positive in the $\mathbf{q}$ space for the s-wave order parameter, since the order parameter is isotropic and non sign-changing in the $\mathbf{k}$ space. In contrast, $B(\mathbf{q},\mathbf{k}_n)$ is half positive and negative in $\mathbf{q}$ space. This is due to the sign-changing structure of the order parameter in the $\mathbf{k}$ space.

As the result, the sum $\sum_{\mathbf{q}} B(\mathbf{q},\mathbf{k}_n)$ is a finite number between 0 and 1 for s-wave case, which will appear in the coherence factor and will give an enhancement to the spin susceptibility and spin-lattice relaxation rate. The d-wave case is different, where the positive and negative parts in the $\mathbf{q}$ space cancel each other and as a consequence give no enhancement to the relaxation rate.

The spin-lattice relaxation rates for the square lattice are calculated according to Eq. (2.1) and are shown in Fig. 3.4. As seen, in the d-wave case, there is no peak as the system enters the superconducting state. This is consistent with the experiments which report the absence of Hebel-Slichter peak in the unconventional d-wave superconductors.

This result in this simple system tells us that the argument in Chapter 2.4 is still valid if we directly evaluate Eq. (2.3) without the approximation of the DOS. However, we should notice that this system is still a one-band model. In the next chapter, we

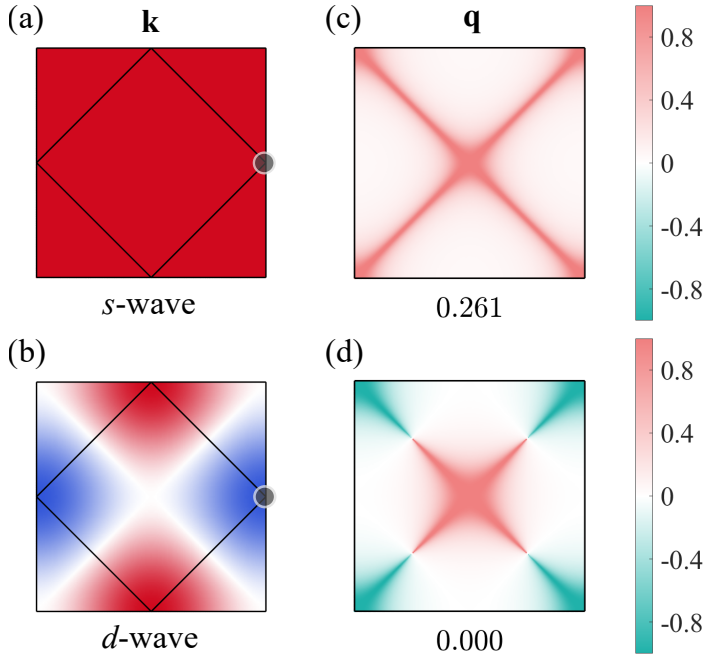

Figure 3.3: (a-b) The s-wave and d-wave order parameter in the first Brillouin zone. The black lines indicate the Fermi surface at $\mu = 0$. (c-d) The corresponding $B(\mathbf{q}, \mathbf{k}_n)$ for s-wave and d-wave order parameters. $\mathbf{k}_n$ is chosen from the black dot in (a) and (b). The number below (c) and (d) indicate the sum $\sum_{\mathbf{q}} B(\mathbf{q}, \mathbf{k}_n)$ in the first Brillouin zone.

will introduce the kagome lattice, which has the multi-band structure in the $\mathbf{k}$ space.

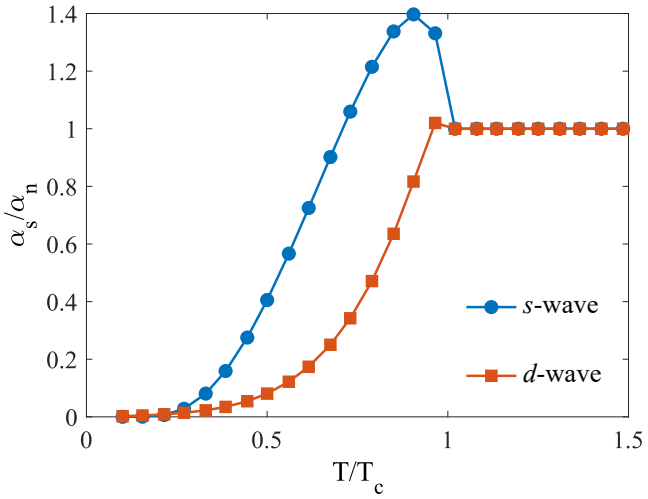

Figure 3.4: The temperature dependence of the spin-lattice relaxation rate for the s-wave and d-wave order parameters. The vertical axis is the spin relaxation rate α_s in the superconducting state divided by α_n in the normal state. All cases are plotted for $\mathcal{N} = 4 \times 10^4$ and $\omega = \eta = 0.015$. As seen, there is no Hebel-Slichter peak in the d-wave case, since the enhancement from the coherence factor is wiped out by the sign-changing structure of the order parameter.

Chapter 4

Introduction to the kagome lattice

4.1 Crystal and band structure

We briefly introduce the structure of the kagome metals AV_3Sb_5, where A stands for an alkali atom, which can be either potassium (K), rubidium (Rb) or Cesium (Cs) [29].

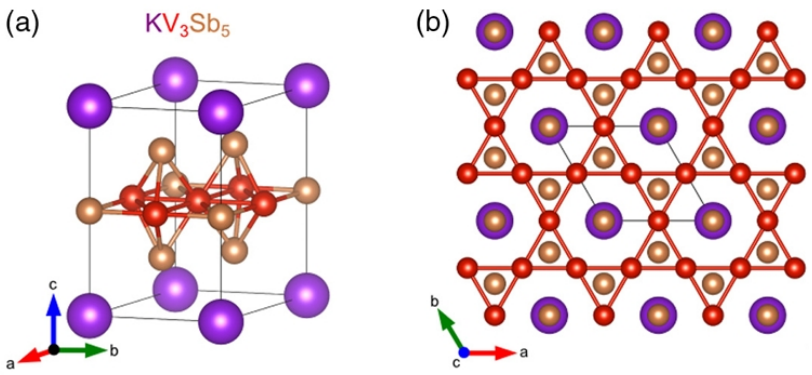

Figure 4.1: The crystal structure of the kagome mentals A(K)V_3Sb_5. The purple, yellow and red spheres denote the alkali (in the figure potassium), vanadium and antimony atoms. The plane where the vanadium atoms are located is named as the *ab* plane, and the axis perpendicular to the plane is called *c*. Panel (a) and (b) show the view from the side and from above. Image from [29].

The layered structure of AV_3Sb_5 is illustrated in Fig. 4.1. The vanadium atoms which lie in the *ab* plane form a kagome lattice. The alkali atoms which lie in another layer of *ab* plane form a hexagonal lattice. The antimony atoms have two sublattices Sb1 and Sb2. Antimony atoms in Sb1 form a hexagonal net and are in the center of the kagome hexagons consisting of vanadium atoms. The atoms in Sb2 form a graphene-like sheet below and above the kagome layer.

The band structure can be calculated via density functional theory (DFT), which has an excellent agreement with the angle resolved photoemission spectroscopy (ARPES)

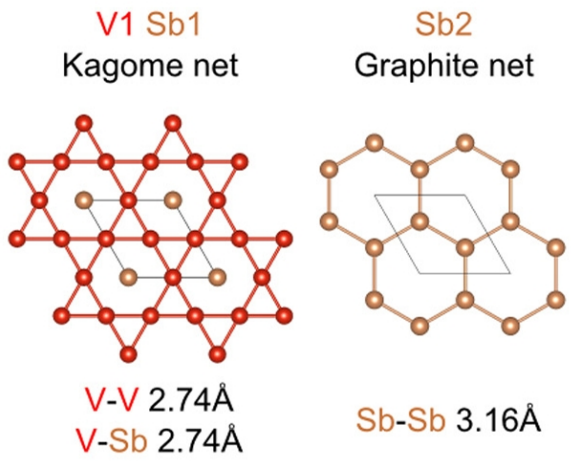

Figure 4.2: The sublattice Sb1 and Sb2 which consist of antimony and vanadium atoms. Image from [29]

measurement[7, 16]. As shown in Fig. 4.3, the Dirac cone at K point and the Van-Hove singularity at M point are dominated by the vanadium atoms. And by comparing the result from path in the vanadium atoms plane Γ-M-K with that from the alkali atoms plane A-L-H, we find that there is not a significant k_z dependence. Thus we can model the AV_3Sb_5 metals with a 2D kagome lattice which consists of vanadium atoms.

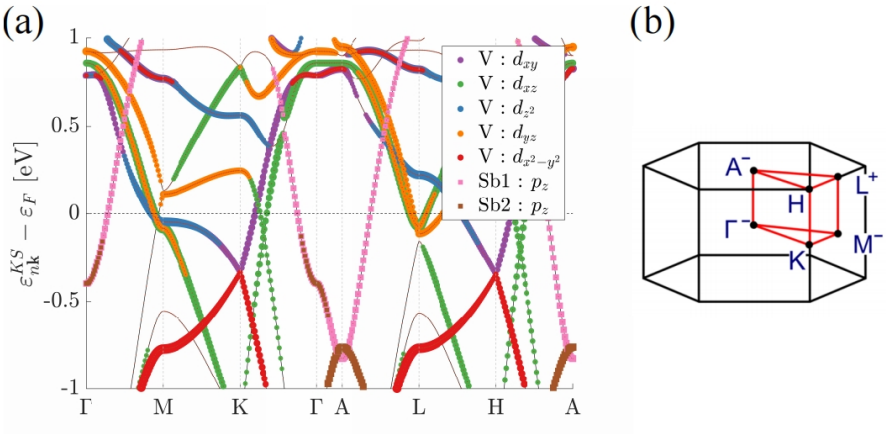

Figure 4.3: Panel (a) shows the energy band calculated using DFT, where the high-symmetry path is shown in panel (b). Image from [18]

4.2 Tight-binding model

To depict the normal state behaviors of the AV_3Sb_5 metals, it is convenient to use a minimal tight-binding (TB) model, which describes the electrons moving on the lattice via nearest neighbor hopping.

The kagome lattice is illustrated in Fig. 4.4, with the definition of the primitive lattice vectors

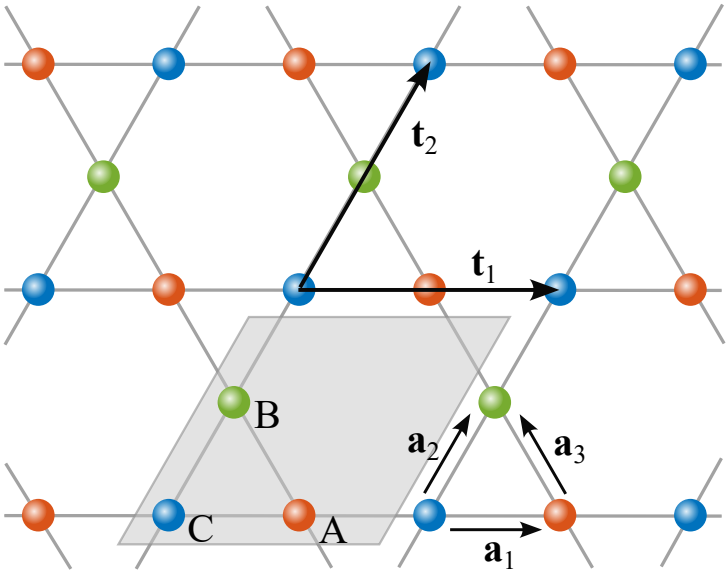

Figure 4.4: Illustration of the kagome lattice. The different sublattice sites are labeled by A, B, C with colors orange, greeen and blue.

$$\mathbf{t}_1 \equiv (1\ 0)\,, \quad \mathbf{t}_2 \equiv \left(\frac{1}{2}\ \frac{\sqrt{3}}{2}\right). \tag{4.1}$$

With the relation $\mathbf{g}_i \cdot \mathbf{t}_j = 2\pi\delta_{ij}$, the primitive reciprocal lattice vectors can be derived

$$\mathbf{g}_1 = 2\pi\left(1\ -\frac{1}{\sqrt{3}}\right), \quad \mathbf{g}_2 = 2\pi\left(0\ \frac{2}{\sqrt{3}}\right). \tag{4.2}$$

With the definitions of the lattice vectors and reciprocal vectors, we can write down the tight-binding Hamiltonian of the kagome lattice

$$\mathcal{H}_0 = -t \sum_{\mathbf{R},s,\bar{s},\sigma} \left[c^\dagger_{\bar{s},\mathbf{R},\sigma} c_{s,\mathbf{R},\sigma} + c^\dagger_{\bar{s},\mathbf{R}+2\mathbf{a}_{s\bar{s}},\sigma} c_{s,\mathbf{R},\sigma}\right] - \mu \sum_{\mathbf{R},s,\sigma} c^\dagger_{s,\mathbf{R},\sigma} c_{s,\mathbf{R},\sigma}, \tag{4.3}$$

where the fermionic operators c and $c^\dagger$ denote the creation and annihilation operator. The subscript s denotes sites $\{A, B, C\}$ in the unit cell and $\bar{s}$ denotes different sites of $\{A, B, C\}$ to s also in the unit cell; σ denotes spin $\{\uparrow, \downarrow\}$. The first term describes the nearest neighbor interactions between sites in the same unit cell. The second also describes the the nearest neighbor interactions but between the adjacent unit cells. The last term describes the filling of the electrons, where μ denotes the chemical

potential. The index **R** denotes the unit cells. The vectors that connect the three sublattice sites are defined as

$$\begin{aligned} \mathbf{a}_{CA} &= \mathbf{a}_1 \equiv \frac{1}{2}(1\ 0)\,, \\ \mathbf{a}_{CB} &= \mathbf{a}_2 \equiv \frac{1}{2}\left(\frac{1}{2}\ \frac{\sqrt{3}}{2}\right), \\ \mathbf{a}_{AB} &= \mathbf{a}_3 \equiv \frac{1}{2}\left(-\frac{1}{2}\ \frac{\sqrt{3}}{2}\right). \end{aligned} \tag{4.4}$$

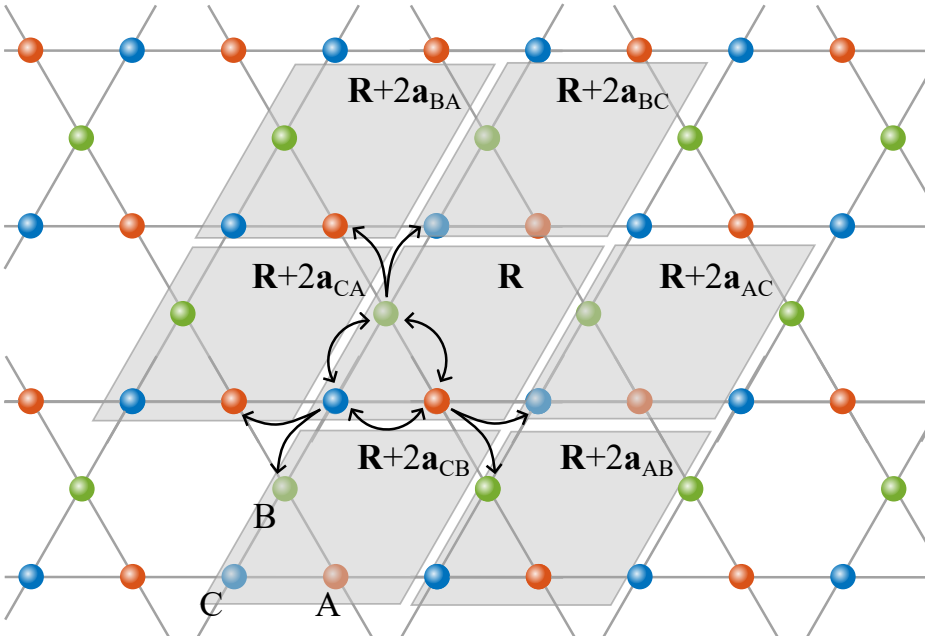

Figure 4.5: Illustration of the nearest neighbor hopping of the kagome lattice. The text labels the unit cell **R** and its adjacent unit cells.

By Fourier transformation

$$c_{s,\mathbf{R},\sigma} = \frac{1}{\mathcal{N}} \sum_{\mathbf{k}\epsilon BZ} e^{i\mathbf{k}\cdot\mathbf{R}} c_{s,\mathbf{k},\sigma}, \tag{4.5}$$

The Hamiltonian can be rewritten as

$$\mathcal{H}_0 = \sum_{\mathbf{k}\epsilon BZ,\sigma} \left(c^\dagger_{A,\mathbf{k},\sigma}\ c^\dagger_{B,\mathbf{k},\sigma}\ c^\dagger_{C,\mathbf{k},\sigma}\right) H_0(\mathbf{k}) \left(c_{A,\mathbf{k},\sigma}\ c_{B,\mathbf{k},\sigma}\ c_{C,\mathbf{k},\sigma}\right)^T, \tag{4.6}$$

where $\mathcal{N}$ denotes the number of points in the first Brillouin Zone (BZ). $H_0(\mathbf{k})$ is a

matrix

$$H_0(\mathbf{k}) = \begin{pmatrix} -\mu & -2t\cos k_3 & -2t\cos k_1 \\ -2t\cos k_3 & -\mu & -2t\cos k_2 \\ -2t\cos k_1 & -2t\cos k_2 & -\mu \end{pmatrix}. \tag{4.7}$$

Here we use the definition $k_i \equiv \mathbf{k}\cdot\mathbf{a}_i$. From the definition of the vectors in the unit cell in Eq. (4.4), we can find this relation

$$\mathbf{a}_1 = \mathbf{a}_2 - \mathbf{a}_3, \quad k_1 = k_2 - k_3. \tag{4.8}$$

We should note that the matrix elements in Eq. (4.7) are not periodical in the first BZ. We could either calculate the physical properties with the size of the k-grid twice that of the first BZ, or apply a unitary transformation $T^{-1}(\mathbf{k})H_0(\mathbf{k})T(\mathbf{k})$, where

$$T(\mathbf{k}) = \begin{pmatrix} e^{-ik_1} & 0 & 0 \\ 0 & e^{-ik_2} & 0 \\ 0 & 0 & 1 \end{pmatrix}, \tag{4.9}$$

and the Hamiltonian matrix in the new basis becomes

$$\tilde{H}_0(\mathbf{k}) = -\begin{pmatrix} \mu & t(1+e^{2ik_3}) & t(1+e^{-2ik_1}) \\ t(1+e^{-2ik_3}) & \mu & t(1+e^{-2ik_2}) \\ t(1+e^{2ik_1}) & t(1+e^{2ik_2}) & \mu \end{pmatrix}. \tag{4.10}$$

We want to know the band structure of the model, thus we need to diagonalize the Hamiltonian. Using relation eq. (4.8), and applying Euler's formula $e^{2ik_i} + e^{-2ik_i} = 2\cos(2k_i)$, the determinant of the Hamiltonian matrix yields

$$\xi^3 - \xi(6+2[\cos(2k_1)+\cos(2k_2)+\cos(2k_3)]) - 4 - 2(\cos(2k_1)+\cos(2k_2)+\cos(2k_3)) - \mu = 0. \tag{4.11}$$

The solutions to the equation are

$$\begin{aligned} \xi_3(\mathbf{k}) &= 2t - \mu, \\ \xi_2(\mathbf{k}) &= t\left(-1 + \sqrt{2[\cos(2k_1)+\cos(2k_2)+\cos(2k_3)]+3}\right) - \mu, \\ \xi_1(\mathbf{k}) &= t\left(-1 - \sqrt{2[\cos(2k_1)+\cos(2k_2)+\cos(2k_3)]+3}\right) - \mu. \end{aligned} \tag{4.12}$$

According to Eq. (4.12), the energy bands is plotted in Fig. 4.6. As seen, the bands feature a Van-Hove singularity [44] at the M point, which leads to a divergence of DOS. Furthermore, at K point the middle and lower bands meet and form a Dirac

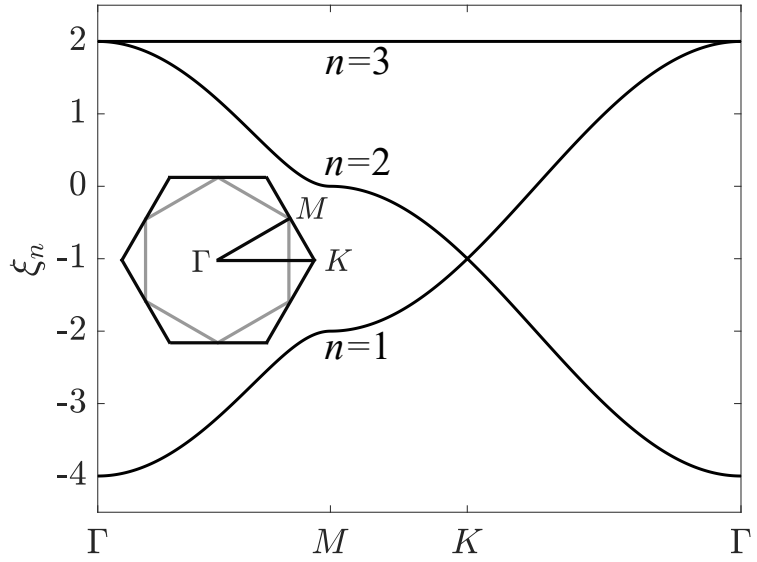

Figure 4.6: Energy bands ξ_n of the kagome lattice at the filling $\mu = 0$. The plot is along the high-symmetry path shown in the inset. The gray lines inside the first BZ denote the Fermi surface at $\mu = 0$. In this plot, the M point is $\left(\pi \ \frac{\pi}{\sqrt{3}}\right)$ and the K point is $\left(\frac{4\pi}{3} \ 0\right)$

cone. Those two features match the result from the DFT calculation as shown in Fig. 4.3.

Besides the band structure, which is mathematically the eigenvalues of the matrix Eq. (4.7), we also want to know the eigenvectors of the this matrix, which will tell us the information about how the matrix transform from the sublattice space to the band space. We can define the unitary transformation that diagonalize H_0 through $U^{-1}(\mathbf{k})H_0(\mathbf{k})U(\mathbf{k})$

$$U(\mathbf{k}) = \begin{pmatrix} u_{A,1,\mathbf{k}} & u_{A,2,\mathbf{k}} & u_{A,3,\mathbf{k}} \\ u_{B,1,\mathbf{k}} & u_{B,2,\mathbf{k}} & u_{B,3,\mathbf{k}} \\ u_{C,1,\mathbf{k}} & u_{C,2,\mathbf{k}} & u_{C,3,\mathbf{k}} \end{pmatrix}, \tag{4.13}$$

which also transform the operators from $c_{\alpha,\mathbf{k},\sigma}$ to $\gamma_{n,\mathbf{k},\sigma}$ via

$$\begin{pmatrix} u_{A,1,\mathbf{k}} & u_{A,2,\mathbf{k}} & u_{A,3,\mathbf{k}} \\ u_{B,1,\mathbf{k}} & u_{B,2,\mathbf{k}} & u_{B,3,\mathbf{k}} \\ u_{C,1,\mathbf{k}} & u_{C,2,\mathbf{k}} & u_{C,3,\mathbf{k}} \end{pmatrix}^{-1} \begin{pmatrix} c_{A,\mathbf{k},\sigma} \\ c_{B,\mathbf{k},\sigma} \\ c_{C,\mathbf{k},\sigma} \end{pmatrix} = \begin{pmatrix} \gamma_{1,\mathbf{k},\sigma} \\ \gamma_{2,\mathbf{k},\sigma} \\ \gamma_{3,\mathbf{k},\sigma} \end{pmatrix}. \tag{4.14}$$

We use the notation α to denote the sublattice indices, and n to denote the band indices. Figure 4.7 shows the square of the eigenvectors of the middle band $|u_{\alpha,2,\mathbf{k}}|^2$ and the lower band $|u_{\alpha,1,\mathbf{k}}|^2$. As seen in the middle band, the weights on the M points in the first BZ are perfectly localized with one of the sublattice indices. For example,

at M1 point there are $|u_{C,2,\mathbf{k}}|^2 = 1$ and $|u_{A,2,\mathbf{k}}|^2 = |u_{B,2,\mathbf{k}}|^2 = 0$. However, such property is not held by the lower band, where two of the sublattice indices blend at the M points.

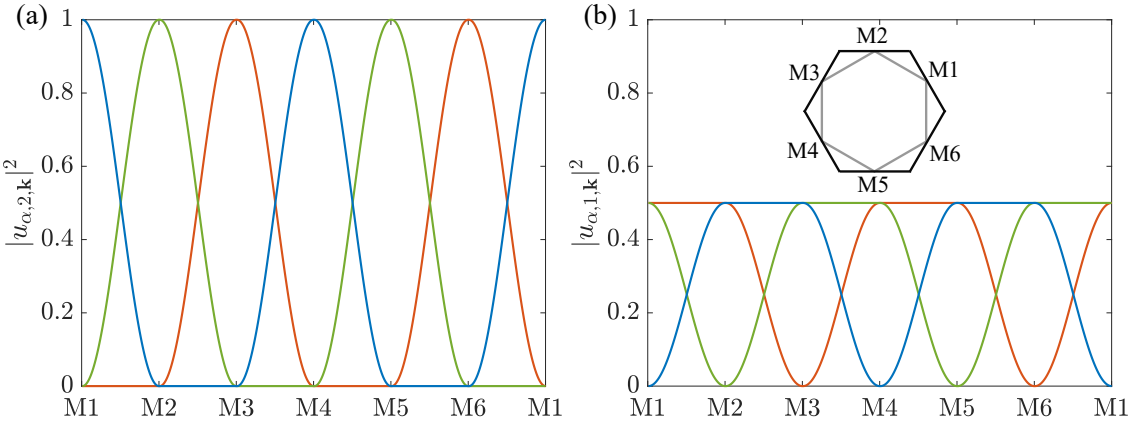

Figure 4.7: The sublattice weights $|u_{\alpha,n,\mathbf{k}}|^2$ of the middle band and the lower band are shown in panels (a) and (b), which is plotted along the certain path illustrated in the inset of (b). The color refers to the sublattice indices, where the color red stands for sublattice A, green for B and blue for C.

Apart from the unique feature with the name sublattice interference, that the sublattice weights are nearly perfectly nest at the M points, there is a more general feature arising together with the sublattice interference effect. As shown in Fig. 4.8, there is area where the sublattice weights are zero in the BZ. This property is not only at the upper Van Hove point, but quite general for the middle band. This feature, together with the well-known sublattice interference, can lead to some unusual behaviors, such as the robustness of sign-changing gap structures to disorder on the kagome lattice to the impurities [17], and the presence of Hebel-Slichter peak in the unconventional kagome superconductors.

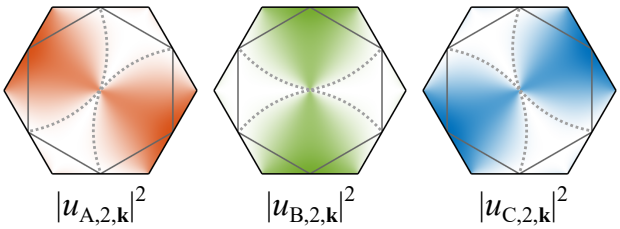

Figure 4.8: The sublattice weights $|u_{\alpha,n,\mathbf{k}}|^2$ of the middle band $n = 2$ in the first BZ. The color refers to the sublattice indices, where the color red stands for sublattice A, green for B and blue for C. The dashed lines sketch the area where the sublattice weights are zero.

4.3 Superconductivity

In 2020, the kagome mental CsV_3Sb_5 was reported to enter the superconducting state at a critical temperature $T_c \approx 2.5$ K [30]. The other members of the AV_3Sb_5 family were also reported superconductivity shortly after with $T_c \approx 0.9$ K[31, 46]. One of the tasks of understanding the nature of the superconductivity in the materials is to determine the pairing symmetry of the superconducting order parameter. [36, 38, 45]. There are some properties of the pairing nature to be identified , e.g. singlet vs. triplet, node vs. nodeless and sign-changing vs. non-sign-changing. In the following we will introduce some experiments that can help determine them.

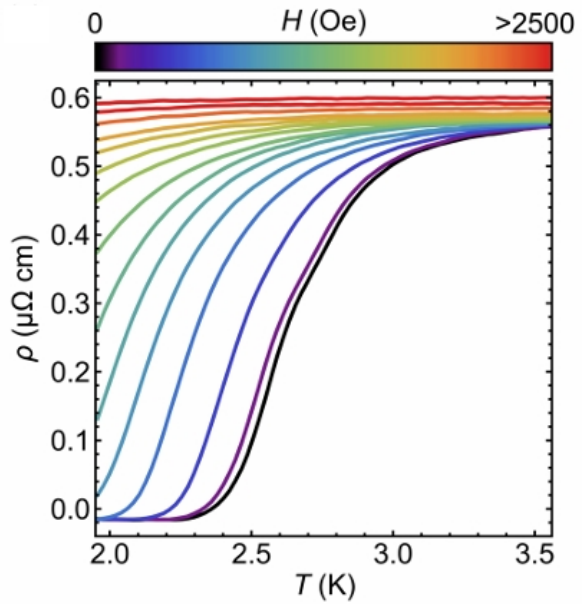

Figure 4.9: The electric resistivity measured for CsV_3Sb_5 mental at low temperature with different amplitudes of magnetic field. The resistivity drops to zero at the critical temperature T_c approximately 2.5 K [30].

Let's first look at the experiment potentially determining nodal/nodeless gap structure. The magnetic penetration depth measurement are expected to identify the nodal/nodeless structure of the superconducting gap. The measurement on CsV_3Sb_5 mental with tunneling diode oscillator technique [11] reports the $T^{2.9}$ dependence of the penetration depth $\Delta\lambda$, which deviates from a T or T^2 behavior expected for line or point nodal structure. This result is closer to an exponential behavior, which points to a nodeless gap structure. Another penetration depth experiment with muon spin rotation/relaxation (μSR) technique that measures the bulk property reports nodeless and anisotropic structure [13].

The ARPES is another tool which can directly measure the superconducting gap structure in the momentum space. The measurement on $Cs(V_{0.93}Nb_{0.07})_3Sb_5$ and $Cs(V_{0.86}Ta_{0.14})_3Sb_5$ [49] reports a fully-gapped and isotropic structure of the order pa-

rameter. In this measurement, the doping of niobium or tantalum atoms substituting some vanadium atoms is aimed at increasing the critical temperature, which helps improve the accuracy of the APRES measurement. However, in a recent research, an anisotropic, even near nodal gap is observed in CsV_3Sb_5 without doping [24]. Furthermore, the doping is proposed to be able to change the superconducting gap from anisotropic to isotropic [35].

Those experimental evidences have slowly pushed the understanding of the gap structure forward to converge to a nodeless, but anisotropic picture [45], although the doping might influence the (an)isotropic symmetry.

Another very basic property of the pairing state is the spatial parity, i.e. the total spin $s = 0$ spin-singlet pairing or the total spin $s = 1$ spin-triplet pairing. The Knight shift measurement is expected to probe this property. For the spin-singlet case, the spin shift is expected to decrease upon entering the superconducting state and can vanish at $T \to 0$. By contrast, for the spin-triplet case, the spin shift can remain finite or a constant along certain directions [14, 19]. Such measurements was applied to the kagome mental CsV_3Sb_5 [27], and the shift for all directions decrease below T_c, which points to the spin-singlet pairing.

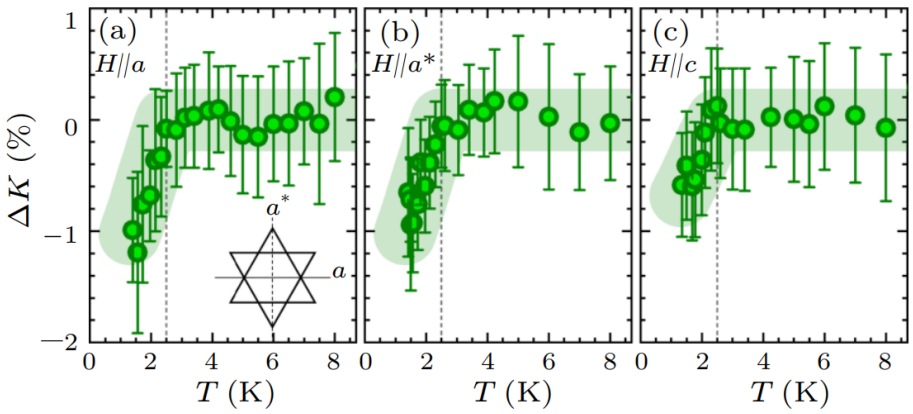

Figure 4.10: The Knight shift measurement along different directions of the kagome lattice. a and a^* are two orthogonal directions on the kagome plane, while c is perpendicular to the plane. Image from [27].

Finally, the (non)sign-changing property is also a very crucial property that distinguishes conventional and unconventional superconductors. In the conventional phonon-mediated superconductors, the order parameter Δ is always non-sign-changing, which represents an effectively always attractive interaction between electrons due to the phonon mediation [37, 42]. However, if the microscopic mechanics of superconductivity is not (only) due to the phonon mediation, a sign-changing gap structure is also allowed as a solution of the BCS gap equation.

Experimentally, it is commonly believed that the atomic-scale disorder will cause

a strong suppression of the critical temperature T_c for the superconductors with a sign-changing gap structure. By contrast, the conventional non-sign-changing s-wave pairing is relatively not sensitive to disorder [17, 45]. Such experiments was carried out for CsV_3Sb_5, and no significant critical temperature suppression was observed [35, 48]. Those results were explained as an evidence for a non-sign-changing gap structure according to the conventional picture that a sign-changing gap is more sensitive to lattice disorder. However, as shown in Fig. 4.11 (b), the recent theoretical study on the suppression of critical temperature due to the lattice disorder suggests that the d-wave gap structures are not sensitive to the disorders as well [17]. This unusual behavior is due to the sublattice effect which wipes out the sign-changing effect.

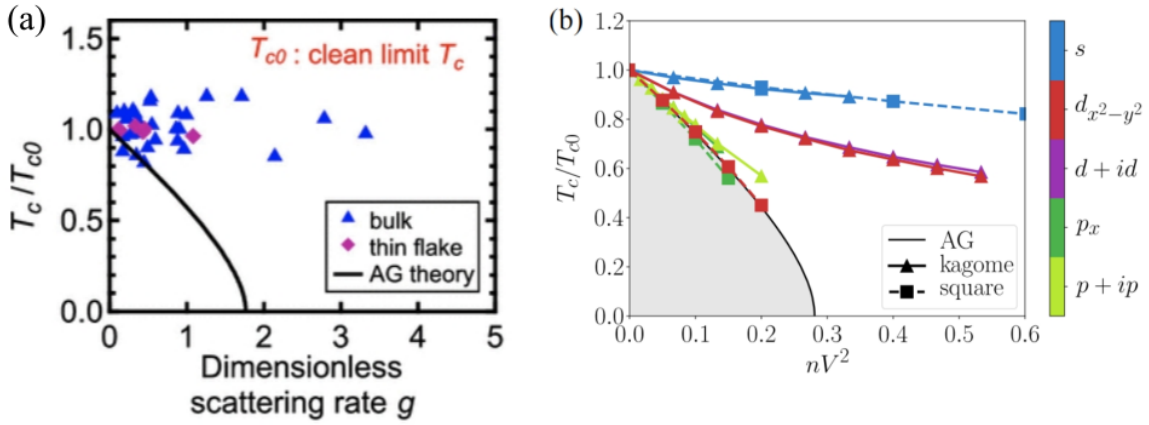

Figure 4.11: The critical temperatures T_c/T_{c0} as a function of amount of impurities. (a) Experiment result on CsV_3Sb_5. Image from [48]. (b) Theoretical calculation for different symmetries. Image from [17].

Moreover, the NMR spin-lattice relaxation rate measurement, as we have detailedly discussed in the previous chapters, is another probe that is believed to be sensitive to the sign-changing gap structure. The spin-lattice relaxation rate was measured for CsV_3Sb_5, and a clear Hebel-Slichter peak was observed. This was considered as a strong sign for a conventional non-sign-changing s-wave gap structure [27].

4.4 Nambu formalism

To theoretically study the superconducting states, it is usual to write down the Hamiltonian using the mean-field Nambu formalism [37, 43],

$$\mathcal{H} = \sum_{\mathbf{k}} \Psi_{\mathbf{k}}^{\dagger} \hat{H}(\mathbf{k}) \Psi_{\mathbf{k}}, \tag{4.15}$$

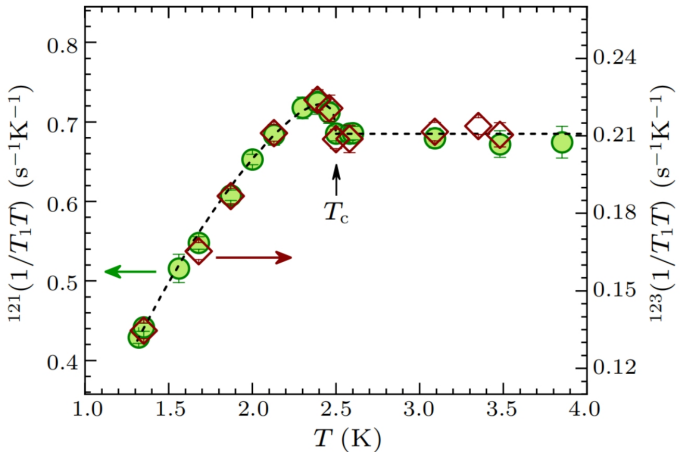

Figure 4.12: Temperature dependence of the spin-lattice relaxation rate of CsV_3Sb_5. Image from [27].

where

$$\hat{H}(\mathbf{k}) = \begin{pmatrix} H_0(\mathbf{k}) & -\Delta(\mathbf{k}) \\ -\Delta(\mathbf{k})^\dagger & -H_0^T(-\mathbf{k}) \end{pmatrix}, \tag{4.16}$$

and $\Psi_\mathbf{k}^\dagger = \begin{pmatrix} c_{\mathbf{k}\uparrow}^\dagger & c_{-\mathbf{k}\downarrow} \end{pmatrix}$ with $c_{\mathbf{k}\sigma}^\dagger = \begin{pmatrix} c_{\mathbf{k}\sigma A}^\dagger & c_{\mathbf{k}\sigma B}^\dagger & c_{\mathbf{k}\sigma C}^\dagger \end{pmatrix}$. H_0 is the tight-binding Hamiltonian matrix defined in Eq. (4.6).

Additional to the tight-binding Hamiltonian, the order parameter $\Delta(\mathbf{k})$ describes the superconducting pairing state. Different from the square lattice in (see Chapter 3), due to the sublattice structure, the tight-binding Hamiltonian of the kagome lattice is in a matrix form. Accordingly, the order parameter $\Delta(\mathbf{k})$ is also a matrix. To derive the matrix for the order parameters with different symmetries, techniques from group theory is used [18]. Since the experimental results points to singlet pairing, the s-wave and d-wave stands out as the leading candidates. In the following we will only briefly introduce the matrices of order parameters we used to describe s-wave and d-wave pairing. Detailed group theory analysis for the kagome lattice structure is presented in the previous works [18, 34].

The kagome lattice is exhibits D_6 point group symmetry. The character table is shown in Table 4.1. For the on-site (OS) pairing, the A_1 (s-wave) and E_2 ($d_{x^2-y^2}$ and d_{xy}-wave) singlet pairing is allowed for the symmetry.

The order parameters can be written accroding to the lattice harmonics function

$$\Delta_\Gamma = \Delta_0 f_{\mathrm{OS},\Gamma}, \tag{4.17}$$

D_6	E	$2C_6$	$2C_3$	C_2	$3C_2'$	$3C_2''$
A_1	1	1	1	1	1	1
A_2	1	1	1	1	-1	-1
B_1	1	-1	1	-1	1	-1
B_2	1	-1	1	-1	-1	1
E_1	2	1	-1	-2	0	0
E_2	2	-1	-1	2	0	0

Table 4.1: The character table of the D_6 point group.

where [17]

$$f_{\mathrm{OS},s} = \frac{1}{\sqrt{3}} \begin{pmatrix} +1 & 0 & 0 \\ 0 & +1 & 0 \\ 0 & 0 & +1 \end{pmatrix}, \tag{4.18}$$

$$f_{\mathrm{OS},d_{x^2-y^2}} = \frac{1}{\sqrt{6}} \begin{pmatrix} +1 & 0 & 0 \\ 0 & -2 & 0 \\ 0 & 0 & +1 \end{pmatrix}, \tag{4.19}$$

$$f_{\mathrm{OS},d_{xy}} = \frac{1}{\sqrt{2}} \begin{pmatrix} +1 & 0 & 0 \\ 0 & 0 & 0 \\ 0 & 0 & -1 \end{pmatrix}. \tag{4.20}$$

Now we consider how to transform the order parameters from the sublattice space to the band space. With the Hamiltonian in the Nambu formalism Eq. (4.16), if $\Delta(\mathbf{k}) = 0$, it is just the tight-binding Hamiltonian in another basis

$$\hat{H}(\mathbf{k}) = \begin{pmatrix} H_0(\mathbf{k}) & 0 \\ 0 & -H_0^T(-\mathbf{k}) \end{pmatrix}. \tag{4.21}$$

The unitary transformation $U(\mathbf{k})$ that diagonalizes the tight-binding Hamiltonian matrix H_0 is defined in Eq. (4.13). Then the unitary transformation in the Nambu formalism is defines as

$$\mathbf{U}(\mathbf{k}) = \begin{pmatrix} U(\mathbf{k}) & \\ & U^*(\mathbf{k}) \end{pmatrix} = \begin{pmatrix} u_{A,1,\mathbf{k}} & u_{A,2,\mathbf{k}} & u_{A,3,\mathbf{k}} & & & \\ u_{B,1,\mathbf{k}} & u_{B,2,\mathbf{k}} & u_{B,3,\mathbf{k}} & & & \\ u_{C,1,\mathbf{k}} & u_{C,2,\mathbf{k}} & u_{C,3,\mathbf{k}} & & & \\ & & & u^*_{A,1,\mathbf{k}} & u^*_{A,2,\mathbf{k}} & u^*_{A,3,\mathbf{k}} \\ & & & u^*_{B,1,\mathbf{k}} & u^*_{B,2,\mathbf{k}} & u^*_{B,3,\mathbf{k}} \\ & & & u^*_{C,1,\mathbf{k}} & u^*_{C,2,\mathbf{k}} & u^*_{C,3,\mathbf{k}} \end{pmatrix}. \tag{4.22}$$

Before the next step, to make it clear, we can write down the Nambu Hamiltonian

Eq. (4.16) without abbreviation

$$\hat{H}(\mathbf{k}) = \begin{pmatrix} -\mu & -2t\cos k_3 & -2t\cos k_1 & -\Delta_{AA}(\mathbf{k}) & -\Delta_{AB}(\mathbf{k}) & -\Delta_{AC}(\mathbf{k}) \\ -2t\cos k_3 & -\mu & -2t\cos k_2 & -\Delta_{BA}(\mathbf{k}) & -\Delta_{BB}(\mathbf{k}) & -\Delta_{BC}(\mathbf{k}) \\ -2t\cos k_1 & -2t\cos k_2 & -\mu & -\Delta_{CA}(\mathbf{k}) & -\Delta_{CB}(\mathbf{k}) & -\Delta_{CC}(\mathbf{k}) \\ -\Delta^*_{AA}(\mathbf{k}) & -\Delta^*_{BA}(\mathbf{k}) & -\Delta^*_{CA}(\mathbf{k}) & \mu & 2t\cos k_3 & 2t\cos k_1 \\ -\Delta^*_{AB}(\mathbf{k}) & -\Delta^*_{BB}(\mathbf{k}) & -\Delta^*_{CB}(\mathbf{k}) & 2t\cos k_3 & \mu & 2t\cos k_2 \\ -\Delta^*_{AC}(\mathbf{k}) & -\Delta^*_{BC}(\mathbf{k}) & -\Delta^*_{CC}(\mathbf{k}) & 2t\cos k_1 & 2t\cos k_2 & \mu \end{pmatrix}. \tag{4.23}$$

The unitary transformation acting on the Nambu Hamiltonian results in

$$\mathbf{U}^\dagger(\mathbf{k})\hat{H}(\mathbf{k})\mathbf{U}(\mathbf{k}) = \begin{pmatrix} U^\dagger(\mathbf{k})H_0(\mathbf{k})U(\mathbf{k}) & -U^\dagger(\mathbf{k})\Delta(\mathbf{k})U^*(\mathbf{k}) \\ -U^T(\mathbf{k})\Delta^*(\mathbf{k})U(\mathbf{k}) & -U^T(\mathbf{k})H_0(\mathbf{k})U^*(\mathbf{k}) \end{pmatrix}, \tag{4.24}$$

where the upper right and the lower left elements are the order parameters in the band space. Let' look at the upper right element

$$\begin{aligned} & -U^\dagger(\mathbf{k})\Delta(\mathbf{k})U^*(\mathbf{k}) \\ &= -\begin{pmatrix} u_{A,1,\mathbf{k}} & u_{B,1,\mathbf{k}} & u_{C,1,\mathbf{k}} \\ u_{A,2,\mathbf{k}} & u_{B,2,\mathbf{k}} & u_{C,2,\mathbf{k}} \\ u_{A,3,\mathbf{k}} & u_{B,3,\mathbf{k}} & u_{C,3,\mathbf{k}} \end{pmatrix} \begin{pmatrix} \Delta_{AA}(\mathbf{k}) & \Delta_{AB}(\mathbf{k}) & \Delta_{AC}(\mathbf{k}) \\ \Delta_{BA}(\mathbf{k}) & \Delta_{BB}(\mathbf{k}) & \Delta_{BC}(\mathbf{k}) \\ \Delta_{CA}(\mathbf{k}) & \Delta_{CB}(\mathbf{k}) & \Delta_{CC}(\mathbf{k}) \end{pmatrix} \begin{pmatrix} u_{A,1,\mathbf{k}} & u_{A,2,\mathbf{k}} & u_{A,3,\mathbf{k}} \\ u_{B,1,\mathbf{k}} & u_{B,2,\mathbf{k}} & u_{B,3,\mathbf{k}} \\ u_{C,1,\mathbf{k}} & u_{C,2,\mathbf{k}} & u_{C,3,\mathbf{k}} \end{pmatrix}, \\ &= \begin{pmatrix} \tilde{\Delta}_{11}(\mathbf{k}) & \tilde{\Delta}_{12}(\mathbf{k}) & \tilde{\Delta}_{13}(\mathbf{k}) \\ \tilde{\Delta}_{21}(\mathbf{k}) & \tilde{\Delta}_{22}(\mathbf{k}) & \tilde{\Delta}_{23}(\mathbf{k}) \\ \tilde{\Delta}_{31}(\mathbf{k}) & \tilde{\Delta}_{32}(\mathbf{k}) & \tilde{\Delta}_{33}(\mathbf{k}) \end{pmatrix}, \end{aligned} \tag{4.25}$$

which is the order parameter in the band space. Since we usually choose the filling of the Fermi surface crossing only the middle band, we can mainly focus on the intra-band pairing $\tilde{\Delta}_{22}(\mathbf{k})$. Figure 4.13 shows the order parameter on the middle band.

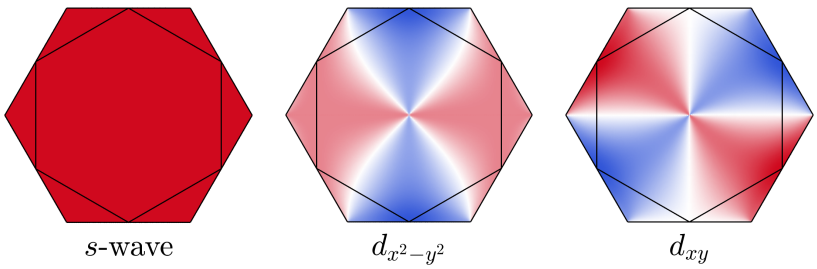

Figure 4.13: The on-site order parameters with different symmetries in the first BZ of the $\mathbf{k}$ space. The black lines denote the Fermi surface at the filling $\mu = 0$.

Nearest-neighbor pairing should also be taken into account. However, since we are

mostly interested in the d-wave pairing which corresponds to the E_2 irreducible representation, and the nearest neighbor pairing will not contribute to the order parameter near the Fermi surface as seen in Fig. 4.14, we can consider only the on-site d-wave pairing terms.

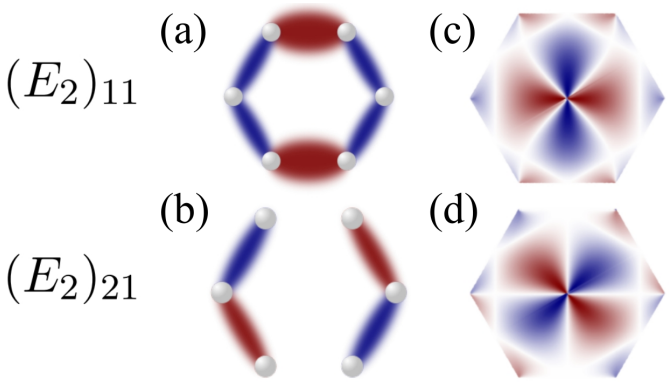

Figure 4.14: The nearest neighbor order pairing with E_2 irreducible representation. (a-b) the real space pairing interaction; (c-d) the momentum space order parameters. Image from [18].

Chapter 5

The Hebel-Slichter peak in the kagome lattice

In the previous chapters, we introduced the origin of the Hebel-Slichter peak, and explained the reason for its absence in the unconventional superconductors. However, those analyses were only carried out on the one-band model, such as the monoatomic square lattice. The kagome lattice, as we introduced in the last chapter, can be described with three sublattice indices, which results in three energy bands and the 3×3 matrix structure of the Hamiltonian and order parameter. The question is very simple: is there a Hebel-Slichter peak in the kagome lattice, even with unconventional superconducting order parameters? To answer this question, in this chapter, we will first start by introducing the expression for the spin susceptibility with multi-bands structure. Then we will derive an effective one-band model to explain the underlying physics.

5.1 Multi-band spin susceptibility

As we have introduced in the last chapter, we can write the Hamiltonian of the kagome lattice with Nambu formalism

$$\mathcal{H} = \sum_{\mathbf{k}\epsilon BZ} \Psi_{\mathbf{k}}^{\dagger} \hat{H}(\mathbf{k}) \Psi_{\mathbf{k}}, \tag{5.1}$$

where the matrix $\hat{H}(\mathbf{k})$ is shown in Eq. (4.23) ,and the corresponding basis is

$$\begin{aligned} \Psi_{\mathbf{k}}^{\dagger} &= \left(c_{A,\mathbf{k},\uparrow}^{\dagger}, c_{B,\mathbf{k},\uparrow}^{\dagger}, c_{C,\mathbf{k},\uparrow}^{\dagger}, c_{A,-\mathbf{k},\downarrow}, c_{B,-\mathbf{k},\downarrow}, c_{C,-\mathbf{k},\downarrow} \right), \\ \Psi_{\mathbf{k}} &= \left(c_{A,\mathbf{k},\uparrow}, c_{B,\mathbf{k},\uparrow}, c_{C,\mathbf{k},\uparrow}, c_{A,-\mathbf{k},\downarrow}^{\dagger}, c_{B,-\mathbf{k},\downarrow}^{\dagger}, c_{C,-\mathbf{k},\downarrow}^{\dagger} \right)^{T}. \end{aligned} \tag{5.2}$$

We have shown in the tight-binding model of the kagome lattice, that the Hamiltonian is not periodical in the first BZ. Thus we can apply a unitary transformation such

that the matrix is periodical in the first BZ. The unitary transformation is defined as

$$T_{\text{Nambu}}(\mathbf{k}) = \begin{pmatrix} T(\mathbf{k}) & 0 \\ 0 & T^T(-\mathbf{k}) \end{pmatrix}, \tag{5.3}$$

where $T(\mathbf{k})$ is defined in Eq.(4.9). Then the Hamiltonian under the new basis $T^{-1}_{\text{Nambu}}(\mathbf{k})\hat{H}(\mathbf{k})T_{\text{Nambu}}(\mathbf{k})$ can be written explicitly

$$\tilde{\hat{H}}(\mathbf{k}) = \begin{pmatrix} -\mu & -t(1+e^{2ik_3}) & -t(1+e^{-2ik_1}) & -\Delta_{AA}(\mathbf{k}) & -\Delta_{AB}(\mathbf{k}) & -\Delta_{AC}(\mathbf{k}) \\ -t(1+e^{-2ik_3}) & -\mu & -t(1+e^{-2ik_2}) & -\Delta_{BA}(\mathbf{k}) & -\Delta_{BB}(\mathbf{k}) & -\Delta_{BC}(\mathbf{k}) \\ -t(1+e^{2ik_1}) & -t(1+e^{2ik_2}) & -\mu & -\Delta_{CA}(\mathbf{k}) & -\Delta_{CB}(\mathbf{k}) & -\Delta_{CC}(\mathbf{k}) \\ -\Delta^*_{AA}(\mathbf{k}) & -\Delta^*_{AB}(\mathbf{k}) & -\Delta^*_{AC}(\mathbf{k}) & \mu & t(1+e^{-2ik_3}) & t(1+e^{2ik_1}) \\ -\Delta^*_{BA}(\mathbf{k}) & -\Delta^*_{BB}(\mathbf{k}) & -\Delta^*_{BC}(\mathbf{k}) & t(1+e^{2ik_3}) & \mu & t(1+e^{2ik_2}) \\ -\Delta^*_{CA}(\mathbf{k}) & -\Delta^*_{CB}(\mathbf{k}) & -\Delta^*_{CC}(\mathbf{k}) & t(1+e^{-2ik_1}) & t(1+e^{-2ik_2}) & \mu \end{pmatrix}. \tag{5.4}$$

To diagonalize the Hamiltonian, we can define the Bogoliubov transformation

$$\mathbf{U}_\mathbf{k} = \begin{pmatrix} u^*_{A,1,\mathbf{k}} & u^*_{A,2,\mathbf{k}} & u^*_{A,3,\mathbf{k}} & -v_{A,1,\mathbf{k}} & -v_{A,2,\mathbf{k}} & -v_{A,3,\mathbf{k}} \\ u^*_{B,1,\mathbf{k}} & u^*_{B,2,\mathbf{k}} & u^*_{B,3,\mathbf{k}} & -v_{B,1,\mathbf{k}} & -v_{B,2,\mathbf{k}} & -v_{B,3,\mathbf{k}} \\ u^*_{C,1,\mathbf{k}} & u^*_{C,2,\mathbf{k}} & u^*_{C,3,\mathbf{k}} & -v_{C,1,\mathbf{k}} & -v_{C,2,\mathbf{k}} & -v_{C,3,\mathbf{k}} \\ v^*_{A,1,\mathbf{k}} & v^*_{A,2,\mathbf{k}} & v^*_{A,3,\mathbf{k}} & u_{A,1,\mathbf{k}} & u_{A,2,\mathbf{k}} & u_{A,3,\mathbf{k}} \\ v^*_{B,1,\mathbf{k}} & v^*_{B,2,\mathbf{k}} & v^*_{B,3,\mathbf{k}} & u_{B,1,\mathbf{k}} & u_{B,2,\mathbf{k}} & u_{B,3,\mathbf{k}} \\ v^*_{C,1,\mathbf{k}} & v^*_{C,2,\mathbf{k}} & v^*_{C,3,\mathbf{k}} & u_{C,1,\mathbf{k}} & u_{C,2,\mathbf{k}} & u_{C,3,\mathbf{k}} \end{pmatrix}, \tag{5.5}$$

such the Hamiltonian is diagonalized

$$\mathbf{U}^*_\mathbf{k}\hat{H}(\mathbf{k})\mathbf{U}_\mathbf{k} = \begin{pmatrix} \xi_1 & & & & & \\ & \xi_2 & & & & \\ & & \xi_3 & & & \\ & & & -\xi_1 & & \\ & & & & -\xi_2 & \\ & & & & & -\xi_3 \end{pmatrix}, \tag{5.6}$$

with new basis

$$\tilde{\Psi}_{\mathbf{k}} = \begin{pmatrix} \gamma_{1,\mathbf{k},\uparrow} \\ \gamma_{2,\mathbf{k},\uparrow} \\ \gamma_{3,\mathbf{k},\uparrow} \\ \gamma^*_{1,-\mathbf{k},\downarrow} \\ \gamma^*_{2,-\mathbf{k},\downarrow} \\ \gamma^*_{3,-\mathbf{k},\downarrow} \end{pmatrix} = \mathbf{U}^\dagger_{\mathbf{k}} \Psi_{\mathbf{k}} = \mathbf{U}^\dagger_{\mathbf{k}} \begin{pmatrix} c_{A,\mathbf{k},\uparrow} \\ c_{B,\mathbf{k},\uparrow} \\ c_{C,\mathbf{k},\uparrow} \\ c^\dagger_{A,-\mathbf{k},\downarrow} \\ c^\dagger_{B,-\mathbf{k},\downarrow} \\ c^\dagger_{C,-\mathbf{k},\downarrow} \end{pmatrix}. \tag{5.7}$$

With the definition, We can find the relation of the Bogoliubov transformation

$$\begin{aligned} c_{\alpha,\mathbf{k},\uparrow} &= \sum_m \left(u^*_{\alpha,m,\mathbf{k}} \gamma_{m,\mathbf{k},\uparrow} - v_{\alpha,m,\mathbf{k}} \gamma^\dagger_{m,-\mathbf{k},\downarrow} \right) \\ c^\dagger_{\alpha,-\mathbf{k},\downarrow} &= \sum_m \left(v^*_{\alpha,m,\mathbf{k}} \gamma_{m,\mathbf{k},\uparrow} + u_{\alpha,m,\mathbf{k}} \gamma^\dagger_{m,-\mathbf{k},\downarrow} \right) \\ c^\dagger_{\alpha,\mathbf{k},\uparrow} &= \sum_m \left(u_{\alpha,m,\mathbf{k}} \gamma_{m,\mathbf{k},\uparrow} - v^*_{\alpha,m,\mathbf{k}} \gamma^\dagger_{m,-\mathbf{k},\downarrow} \right) \\ c_{\alpha,-\mathbf{k},\downarrow} &= \sum_m \left(v_{\alpha,m,\mathbf{k}} \gamma_{m,\mathbf{k},\uparrow} + u^*_{\alpha,m,\mathbf{k}} \gamma^\dagger_{m,-\mathbf{k},\downarrow} \right) \end{aligned} \tag{5.8}$$

Now we consider the spin susceptibility. The expression for the spin susceptibility with sublattice indices in the momentum space is

$$\chi^{+-}_{0,\alpha\beta}(\mathbf{q},\tau) = \frac{1}{\mathcal{N}^2} \sum_{\mathbf{k}\mathbf{k}'} \langle T_\tau c^\dagger_{\alpha,\mathbf{k}+\mathbf{q}\uparrow} c_{\alpha,\mathbf{k}\downarrow} c^\dagger_{\beta,\mathbf{k}'-\mathbf{q}\downarrow}(\tau) c_{\beta,\mathbf{k}'\uparrow}(\tau) \rangle. \tag{5.9}$$

We insert the relation of the Bogoliubov transformation Eq. (5.8) into the expression above, and after some calculation as shown in Appendix C, we can finally derive the spin susceptiblity for the multi-band system with sublattice indices

$$\begin{aligned} &\chi^{+-}_{0,\alpha\beta}(\mathbf{q},\tau) = \frac{1}{\mathcal{N}} \sum_{\mathbf{k},m,m'} \\ &\Bigg[\left(v^*_{\alpha,m,\mathbf{k}+\mathbf{q}} v_{\beta,m,\mathbf{k}+\mathbf{q}} u^*_{\alpha,m',\mathbf{k}} u_{\beta,m',\mathbf{k}} - v^*_{\alpha,m,\mathbf{k}+\mathbf{q}} u_{\beta,m,\mathbf{k}+\mathbf{q}} u^*_{\alpha,m',\mathbf{k}} v_{\beta,m',\mathbf{k}} \right) \frac{1 - f(E_{\mathbf{k}+\mathbf{q},m}) - f(E_{\mathbf{k},m'})}{i\omega_n + E_{\mathbf{k}+\mathbf{q},m} + E_{\mathbf{k},m'}} \\ &+ \left(u_{\alpha,m,\mathbf{k}+\mathbf{q}} u^*_{\beta,m,\mathbf{k}+\mathbf{q}} u^*_{\alpha,m',\mathbf{k}} u_{\beta,m',\mathbf{k}} + u_{\alpha,m,\mathbf{k}+\mathbf{q}} v^*_{\beta,m,\mathbf{k}+\mathbf{q}} u^*_{\alpha,m',\mathbf{k}} v_{\beta,m',\mathbf{k}} \right) \frac{f(E_{\mathbf{k}+\mathbf{q},m}) - f(E_{\mathbf{k},m'})}{i\omega_n + E_{\mathbf{k},m'} - E_{\mathbf{k}+\mathbf{q},m}} \\ &+ \left(v^*_{\alpha,m,\mathbf{k}+\mathbf{q}} v_{\beta,m,\mathbf{k}+\mathbf{q}} v_{\alpha,m',\mathbf{k}} v^*_{\beta,m',\mathbf{k}} + v^*_{\alpha,m,\mathbf{k}+\mathbf{q}} u_{\beta,m,\mathbf{k}+\mathbf{q}} v_{\alpha,m',\mathbf{k}} u^*_{\beta,m',\mathbf{k}} \right) \frac{f(E_{\mathbf{k},m'}) - f(E_{\mathbf{k}+\mathbf{q},m})}{i\omega_n + E_{\mathbf{k}+\mathbf{q},m} - E_{\mathbf{k},m'}} \\ &+ \left(u_{\alpha,m,\mathbf{k}+\mathbf{q}} u^*_{\beta,m,\mathbf{k}+\mathbf{q}} v_{\alpha,m',\mathbf{k}} v^*_{\beta,m',\mathbf{k}} - u_{\alpha,m,\mathbf{k}+\mathbf{q}} v^*_{\beta,m,\mathbf{k}+\mathbf{q}} v_{\alpha,m',\mathbf{k}} u^*_{\beta,m',\mathbf{k}} \right) \frac{f(E_{\mathbf{k}+\mathbf{q},m}) + f(E_{\mathbf{k},m'}) - 1}{i\omega_n - E_{\mathbf{k}+\mathbf{q},m} - E_{\mathbf{k},m'}} \Bigg]. \end{aligned} \tag{5.10}$$

Another question is that when calculating the spin susceptibility in a system with sublattice indices, how the summation over the sublattice indices works. The different ways of defining the basis will influence the result of the summation. We discuss this

question in Appendix D, where we have shown that by choosing the proper basis, the spin susceptibility is obtained with the summation over sublattice indices. However, some basis choice will introduce an extra phase factor, which will lead to a wrong result. In the correct basis, we define the spin susceptibility

$$\chi_0^{+-}(\mathbf{q},\tau) = \sum_{\alpha\beta} \chi_{0,\alpha\beta}^{+-}(\mathbf{q},\tau). \tag{5.11}$$

In the kagome lattice, in order to check which basis used in Eq. (4.23) and (5.4) is proper, we define the spin susceptibility calculated with Eq. (4.23) as $\chi_{0,AB}^{+-}(\mathbf{q},\omega)$, and with Eq. (5.4) $\tilde{\chi}_{0,AB}^{+-}(\mathbf{q},\omega)$. As shown in Fig. 5.1, the use of the basis Eq. (5.4) breaks the C_2 symmetry by a rotation of π around the principal axis [10]. By contrast, as shown in Fig. 5.1 (a), the spin susceptibility $\mathrm{Im}\,\chi_{0,AB}^{+-}(\mathbf{q},\omega)$ is invariant under a C_2 rotation.

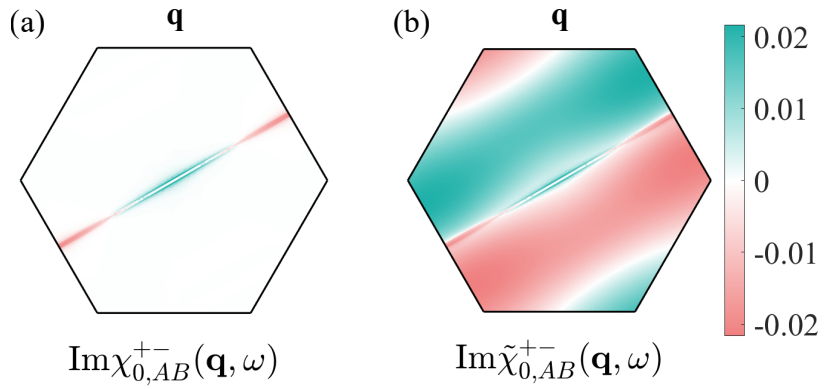

Figure 5.1: Panel (a) displays $\mathrm{Im}\,\chi_{0,AB}^{+-}(\mathbf{q},\omega)$ with the basis Eq. (4.23). Panel (b) displays $\mathrm{Im}\,\tilde{\chi}_{0,AB}^{+-}(\mathbf{q},\omega)$ with the basis choice of Eq. (5.4). (a) conserves the C_2 symmetry by a rotation of π around the principal axis; (b) breaks this symmetry.

However, by including a phase factor

$$\chi_{0,\alpha\beta}^{+-}(\mathbf{q},\omega) = \begin{pmatrix} \tilde{\chi}_{0,AA}^{+-} & e^{i(q_2-q_1)}\tilde{\chi}_{0,AB}^{+-} & e^{-iq_1}\tilde{\chi}_{0,AC}^{+-} \\ e^{i(q_1-q_2)}\tilde{\chi}_{0,BA}^{+-} & \tilde{\chi}_{0,BB}^{+-} & e^{-iq_2}\tilde{\chi}_{0,BC}^{+-} \\ e^{iq_1}\tilde{\chi}_{0,CA}^{+-} & e^{iq_2}\tilde{\chi}_{0,CB}^{+-} & \tilde{\chi}_{0,CC}^{+-} \end{pmatrix}, \tag{5.12}$$

one can recover the correct spin susceptibility. This symmetry breaking by an inappropriate choice of basis is also discussed in Ref. [41]. Thus we can use the basis in Eq. (4.23) with the size of the **k**-grid twice that of the first BZ. Alternatively, we can use the basis in Eq. (5.4) to calculate the spin susceptibility, and consider the phase factor to get the correct one.

5.2 Relaxation rate

The spin-lattice relaxation rate of the kagome lattice is also proportional to the spin susceptibility, where the only difference is the summation over the sublattice indices. It can be written as

$$\alpha \equiv \frac{1}{T_1 T} = \frac{C}{\omega}\frac{1}{\mathcal{N}}\sum_{\mathbf{q},\alpha\beta} \mathrm{Im}\chi^{+-}_{0,\alpha\beta}(\mathbf{q},\omega), \tag{5.13}$$

As shown in Fig. 5.2, both the s-wave and d-wave cases show the Hebel-Slichter peak. This is quite surprising, since the peak is expected to be wiped out due to the sign-changing effect. To explain this, we want to look at the coherence factors, since they are the key to the Hebel-Slichter peak as we have discussed before. However, it is hard to define such a coherence factor in a multi-band model Eq. (5.10), since we can not find a analytical expression for the u and v in the Bogoliubov transformation. This drives us to derive a effective model, by which we can define the effective coherence factor and understand why the unconventional d-wave kagome superconductor shows the Hebel-Slichter peak.

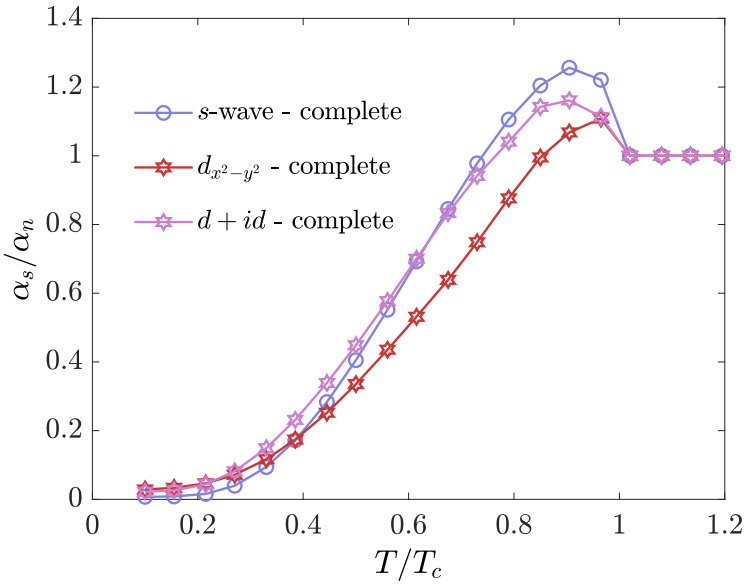

Figure 5.2: Temperature dependence of the spin-lattice relaxation rate ratio α_s/α_n for superconductivity on the kagome lattice. The label 'complete' means it is calculated with the three-band model using Eq. (5.10). The results are plotted for $\mathcal{N} = 1 \times 10^4$. $\omega = \eta = 0.015$ is applied in the calculation.

5.3 Effective model

We know that only the energies which are close to the Fermi level contribute to the spin susceptibility. For the kagome lattice, only the middle band is expected to contribute to the it when we are working on the upper Van Hove point. Having this argument, we can choose solely the middle and define an effective Hamiltonian,

$$H_{\text{eff}}(\mathbf{k}) = \begin{pmatrix} \xi_2(\mathbf{k}) & -\tilde{\Delta}_{22}(\mathbf{k}) \\ -\tilde{\Delta}^*_{22}(\mathbf{k}) & -\xi_2(\mathbf{k}) \end{pmatrix}, \tag{5.14}$$

where $\tilde{\Delta}_{22}$ is the order parameter defined in Eq. (4.25), and here we only consider the intra-band interaction of the middle band.

Now let's consider the spin susceptibility. Equation (5.9) is written in the sublattice space, while the effective Hamiltonian is defined in the band space. Thus a unitary transformation from the sublattice space to the band space is required for the expression of spin susceptibility. The unitary transformation that transforms the tight-binding Hamiltonian from the sublattice space to the band space is defined in Eq. (4.13). However, the transformation will not directly diagonalize the Hamiltonian like in the tight-binding model because of the off-diagonal components $\Delta(\mathbf{k})$; instead, it will transform the order parameter to the band space. To avoid confusion, we write the fermionic operators in the band space as $c_{n,\mathbf{k},\sigma}$ instead of $\gamma_{n,\mathbf{k},\sigma}$ as Eq. (4.14)

$$\begin{pmatrix} u_{A,1,\mathbf{k}} & u_{B,1,\mathbf{k}} & u_{C,1,\mathbf{k}} \\ u_{A,2,\mathbf{k}} & u_{B,2,\mathbf{k}} & u_{C,2,\mathbf{k}} \\ u_{A,3,\mathbf{k}} & u_{B,3,\mathbf{k}} & u_{C,3,\mathbf{k}} \end{pmatrix} \begin{pmatrix} c_{A,\mathbf{k},\sigma} \\ c_{B,\mathbf{k},\sigma} \\ c_{C,\mathbf{k},\sigma} \end{pmatrix} = \begin{pmatrix} c_{1,\mathbf{k},\sigma} \\ c_{2,\mathbf{k},\sigma} \\ c_{3,\mathbf{k},\sigma} \end{pmatrix}, \tag{5.15}$$

which gives the relation

$$c_{\alpha,\mathbf{k},\sigma} = \sum_m u^*_{\alpha,m,\mathbf{k}} c_{m,\mathbf{k},\sigma}. \tag{5.16}$$

The expression of the spin susceptibility Eq. 5.9, can be split into two terms according to Wick's theorem,

$$\begin{aligned} \chi_0^{+-}(\mathbf{q},\tau) = \frac{1}{\mathcal{N}} \sum_{\mathbf{k},\alpha\beta} [& -\langle T_\tau c^\dagger_{\alpha,\mathbf{k}+\mathbf{q}\uparrow} c^\dagger_{\beta,-\mathbf{k}-\mathbf{q}\downarrow}(\tau)\rangle\langle T_\tau c_{\alpha,\mathbf{k}\downarrow} c_{\beta,-\mathbf{k}\uparrow}(\tau)\rangle \\ & + \langle T_\tau c^\dagger_{\alpha,\mathbf{k}+\mathbf{q}\uparrow} c_{\beta,\mathbf{k}+\mathbf{q}\uparrow}(\tau)\rangle\langle T_\tau c_{\alpha,\mathbf{k}\downarrow} c^\dagger_{\beta,\mathbf{k}\downarrow}(\tau)\rangle]. \end{aligned} \tag{5.17}$$

We insert the relation Eq. (5.16) into the equation above with the approximation that only the middle band $n = 2$ is considered, and the first term which accounts for the

superconducting state gives an extra factor

$$g_{s,\alpha\beta}(\mathbf{k},\mathbf{q}) = u_{\alpha,2,\mathbf{k+q}} u_{\beta,2,\mathbf{k+q}} u^*_{\alpha,2,\mathbf{k}} u^*_{\beta,2,\mathbf{k}}. \tag{5.18}$$

The second term gives another factor

$$g_{n,\alpha\beta}(\mathbf{k},\mathbf{q}) = u_{\alpha,2,\mathbf{k+q}} u^*_{\beta,2,\mathbf{k+q}} u^*_{\alpha,2,\mathbf{k}} u_{\beta,2,\mathbf{k}}. \tag{5.19}$$

The expression thus becomes

$$\begin{aligned}\chi_0^{+-}(\mathbf{q},\tau) = \frac{1}{\mathcal{N}} \sum_{\mathbf{k},\alpha\beta} [& -g_{s,\alpha\beta}(\mathbf{k},\mathbf{q}) \langle T_\tau c^\dagger_{2,\mathbf{k+q}\uparrow} c^\dagger_{2,-\mathbf{k}-\mathbf{q}\downarrow}(\tau)\rangle \langle T_\tau c_{2,\mathbf{k}\downarrow} c_{2,-\mathbf{k}\uparrow}(\tau)\rangle \\ & + g_{n,\alpha\beta}(\mathbf{k},\mathbf{q}) \langle T_\tau c^\dagger_{2,\mathbf{k+q}\uparrow} c_{2,\mathbf{k+q}\uparrow}(\tau)\rangle \langle T_\tau c_{2,\mathbf{k}\downarrow} c^\dagger_{2,\mathbf{k}\downarrow}(\tau)\rangle].\end{aligned} \tag{5.20}$$

Under the basis choice Eq. (4.23), there is $g_{s,\alpha\beta}(\mathbf{k},\mathbf{q}) = g_{n,\alpha\beta}(\mathbf{k},\mathbf{q})$ because the eigenvectors are real. Thus we can write them as $g_{\alpha\beta}(\mathbf{k},\mathbf{q})$. After the same derivation as in Appendix B, the spin susceptibility is given by

$$\begin{aligned}\chi_0^{+-}(\mathbf{q},\omega) = \frac{1}{\mathcal{N}} \sum_{\mathbf{k},E>0} \left(\sum_{\alpha\beta} g_{\alpha\beta}(\mathbf{k},\mathbf{q}) \right) \Bigg[& \left(1 - \frac{\xi_\mathbf{k}\xi_\mathbf{k+q} + \Delta^*_\mathbf{k+q}\Delta_\mathbf{k}}{E_\mathbf{k}E_\mathbf{k+q}} \right) \frac{1 - f(E_\mathbf{k}) - f(E_\mathbf{k+q})}{\omega + E_\mathbf{k+q} + E_\mathbf{k} + i\eta} \\ & + \left(1 - \frac{\xi_\mathbf{k}\xi_\mathbf{k+q} + \Delta^*_\mathbf{k+q}\Delta_\mathbf{k}}{E_\mathbf{k}E_\mathbf{k+q}} \right) \frac{f(E_\mathbf{k}) + f(E_\mathbf{k+q}) - 1}{\omega - E_\mathbf{k+q} - E_\mathbf{k} + i\eta} \\ & + \left(1 + \frac{\xi_\mathbf{k}\xi_\mathbf{k+q} + \Delta^*_\mathbf{k+q}\Delta_\mathbf{k}}{E_\mathbf{k}E_\mathbf{k+q}} \right) \frac{f(E_\mathbf{k}) - f(E_\mathbf{k+q})}{\omega + E_\mathbf{k+q} - E_\mathbf{k} + i\eta} \\ & + \left(1 + \frac{\xi_\mathbf{k}\xi_\mathbf{k+q} + \Delta^*_\mathbf{k+q}\Delta_\mathbf{k}}{E_\mathbf{k}E_\mathbf{k+q}} \right) \frac{f(E_\mathbf{k+q}) - f(E_k)}{\omega + E_\mathbf{k} - E_\mathbf{k+q} + i\eta} \Bigg],\end{aligned} \tag{5.21}$$

where we have used the notation $\xi_\mathbf{k} \equiv \xi_2(\mathbf{k})$ and $\Delta_\mathbf{k} \equiv \Delta_{22}(\mathbf{k})$ for simplicity. This expression is the same expression as for the square lattice, except for an extra factor $\sum_{\alpha,\beta} g_{\alpha\beta}(\mathbf{k},\mathbf{q})$ arising from the transformation.

We can now evaluate the model. The result from the effective model is very similar to the complete one as seen in Fig. 5.3. The result from the complete model is slightly larger than the effective one, because the other bands also have a very small contribution. Despite the small difference, the result shows that it is enough to describe the behavior of the relaxation rate with the effective model.

5.4 Why is there a Hebel-Slichter peak?

In Chapter 3, we have defined the so-called B factor to explain the absence of the Hebel-Slichter peak with the unconventional d-wave superconducting order parameter

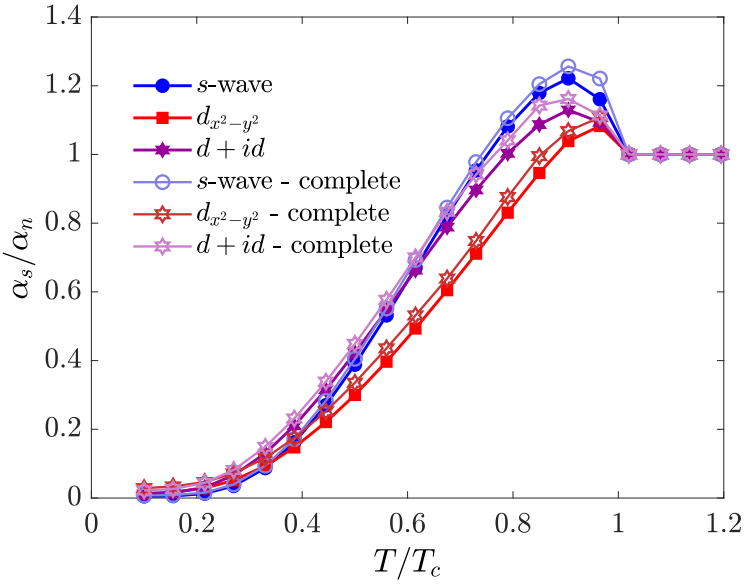

Figure 5.3: Temperature dependence of the spin-lattice relaxation rate ratio α_s/α_n for superconductivity on the kagome lattice. The effective models and the complete models are plotted for $\mathcal{N} = 4 \times 10^4$ and $\mathcal{N} = 1 \times 10^4$, respectively. And $\omega = \eta = 0.015$ is used in both cases. The blue and purple lines show the results calculated from the effective Hamiltonian $H_{\text{eff}}(\mathbf{k})$. The respective lines with open symbols show the results obtained from the complete three-band Hamiltonian $\hat{H}(\mathbf{k})$.

in the square lattice . Similarly, we can define a dressed coherence B factor given by

$$B_{\text{d}}(\mathbf{q}, \mathbf{k}_n) = \frac{\sum_{\alpha\beta} g_{\alpha\beta}(\mathbf{k}_n, \mathbf{q})}{Z} \frac{\Delta^*_{\mathbf{k}_n+\mathbf{q}} \Delta_{\mathbf{k}_n}}{E_{\mathbf{k}_n} E_{\mathbf{k}_n+\mathbf{q}}}, \tag{5.22}$$

where Z is a normalization factor defined by

$$Z = \frac{1}{\mathcal{N}^2} \sum_{\mathbf{k},\mathbf{q}} \sum_{\alpha\beta} g_{\alpha\beta}(\mathbf{k}, \mathbf{q}). \tag{5.23}$$

For comparison, we also define a bare coherence factor without the matrix element dressing from $g_{\alpha\beta}(\mathbf{k}, \mathbf{q})$

$$B_{\text{b}}(\mathbf{q}, \mathbf{k}_n) = \frac{\Delta^*_{\mathbf{k}_n+\mathbf{q}} \Delta_{\mathbf{k}_n}}{E_{\mathbf{k}_n} E_{\mathbf{k}_n+\mathbf{q}}}. \tag{5.24}$$

As seen in Fig. 5.4, we present both the bare and dressed B factors for the s- and d-wave order parameters of the kagome lattice. Let's first consider the conventional A_1 s-wave case in Fig. 5.4 (a,d,g). The dressing factor $\sum_{\alpha,\beta} g_{\alpha\beta}(\mathbf{k}, \mathbf{q})$ indeed changes the distribution of $B_{\text{b}}(\mathbf{q}, \mathbf{k}_n)$ in $\mathbf{q}$ space. However, the summed value $\sum_{\mathbf{q}} B_{\text{d}}(\mathbf{q}, \mathbf{k}_n)$ remains substantial and unchanged. Therefore, the corresponding spin-lattice relaxation rate $1/T_1T$ also remains unchanged, both showing a Hebel-Slichter peak in the bare and

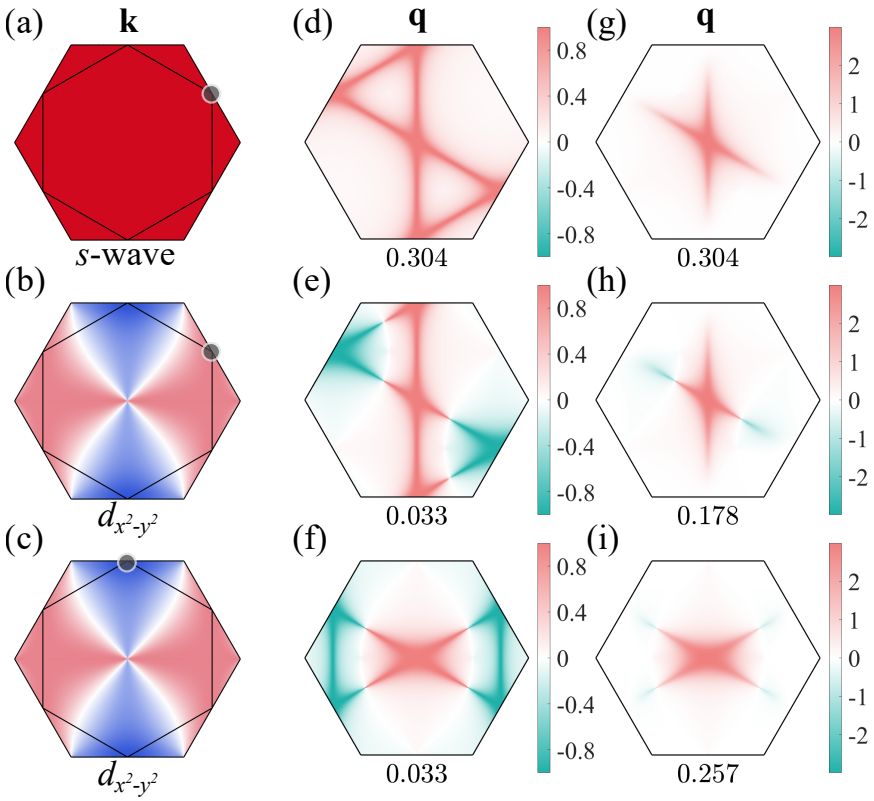

Figure 5.4: The s-wave order parameter (a) and the $d_{x^2-y^2}$ order parameter (b)-(c) in $\mathbf{k}$-space in the first BZ for the kagome lattice. The black lines indicate the Fermi surface at $\mu = 0$. Panel (d) displays the bare $B_{\mathrm{b}}(\mathbf{q}, \mathbf{k}_n)$ for the s-wave order parameter in $\mathbf{q}$-space and panels (e)-(f) are for the $d_{x^2-y^2}$ order parameter. Panel (g) displays the dressed $B_{\mathrm{d}}(\mathbf{q}, \mathbf{k}_n)$ in $\mathbf{q}$-space for the s-wave order parameters and panels (h)-(i) are for the $d_{x^2-y^2}$ order parameter. The chosen $\mathbf{k}_n$ for (d)-(i) is indicated by the black dots in (a)-(c) in the same row. The numbers below (d)-(f) and (g)-(i) display the summed values $\sum_{\mathbf{q}} B_{\mathrm{b}}(\mathbf{q}, \mathbf{k}_n)$ and $\sum_{\mathbf{q}} B_{\mathrm{d}}(\mathbf{q}, \mathbf{k}_n)$, respectively.

dressed cases as expected for s-wave superconductivity.

for the d-wave case the dressing factor $g_{\alpha\beta}(\mathbf{k}, \mathbf{q})$ originating from the sublattice to band space transformation becomes crucial as seen from comparing Fig. 5.4(e,f) to Fig. 5.4(h,i). There we compare the coherence factors $B_{\mathrm{b}}(\mathbf{q}, \mathbf{k}_n)$ and $B_{\mathrm{d}}(\mathbf{q}, \mathbf{k}_n)$ for the two $\mathbf{k}$-points highlighted in Fig. 5.4(b,c). Evidently, $g_{\alpha\beta}(\mathbf{k}, \mathbf{q})$ destroys the compensation (the near cancellation between positive and negative regions) seen in Fig. 5.4(e,f) and leads to substantial summed values of $\sum_{\mathbf{q}} B_{\mathrm{d}}(\mathbf{q}, \mathbf{k}_n)$, as seen from Fig. 5.4(h,i). This implies that while the bare d-wave case should not exhibit a Hebel-Slichter peak, the full (dressed) case should. Indeed, as seen from Fig. 5.5 this is the case. As a result, there exists a pronounced Hebel-Slichter peak in the case of d-wave superconductivity on the kagome lattice. This explains why there is a Hebel-Slichter peak in the kagome lattice.

The above conclusions are valid for the order parameters with $d_{x^2-y^2}$ and d_{xy} symmetries, which are the nodal d-wave cases However, for $d + id$ superconductivity, Δ_{d+id}

is a complex number. Thus, in principle, the imaginary part of $B(\mathbf{q},\mathbf{k})$ might contribute to $\chi_0^{+-}(\mathbf{q},\omega)$. If only the real part of $B(\mathbf{q},\mathbf{k})$ contributes to $\chi_0^{+-}(\mathbf{q},\omega)$, then only the imaginary part of the Fermi function term, which is only non-zero near the Fermi surface, contributes to the imaginary part of $\chi_0^{+-}(\mathbf{q},\omega)$, which is the basic condition of our analysis. Thus we want to check if it is true. To this end, we define

$$\Delta_{\mathbf{k}} = \Delta'_{\mathbf{k}} + i\Delta''_{\mathbf{k}}, \tag{5.25}$$

where $\Delta'_{\mathbf{k}}$ and $\Delta''_{\mathbf{k}}$ denote the real and imaginary parts of $\Delta_{\mathbf{k}}$. Both $\Delta'_{\mathbf{k}}$ and $\Delta''_{\mathbf{k}}$ have the time-reversal symmetry, while $\Delta_{\mathbf{k}}$ breaks the time-reversal symmetry. $B(\mathbf{q},\mathbf{k})$ can be written as

$$B(\mathbf{q},\mathbf{k}) = \frac{(\Delta'_{\mathbf{k+q}} - i\Delta''_{\mathbf{k+q}})(\Delta'_{\mathbf{k}} + i\Delta''_{\mathbf{k}})}{E_{\mathbf{k}}E_{\mathbf{k+q}}}, \tag{5.26}$$

and the imaginary part is

$$\mathrm{Im}\, B(\mathbf{q},\mathbf{k}) = \frac{\Delta'_{\mathbf{k+q}}\Delta''_{\mathbf{k}} - \Delta''_{\mathbf{k+q}}\Delta'_{\mathbf{k}}}{E_{\mathbf{k}}E_{\mathbf{k+q}}}. \tag{5.27}$$

Since we sum over $\mathbf{k}$ in $\chi_0^{+-}(\mathbf{q},\omega)$, we can do $\mathbf{k} \to -\mathbf{k} - \mathbf{q}$ for the first term of Eq. (5.27). Due to the even parity property $\Delta'_{\mathbf{k}} = \Delta'_{-\mathbf{k}}$, $\Delta''_{\mathbf{k}} = \Delta''_{-\mathbf{k}}$ and $E_{\mathbf{k}} = E_{-\mathbf{k}}$ together, the imaginary part gives zero. Thus for Δ_{d+id}, we can still only consider $\mathrm{Re}\, B(\mathbf{q},\mathbf{k})$.

Let's go back our discussion as the conclusion is also proved to be valid for the $d+id$ case. As seen from Fig. 5.4, the summed values $\sum_{\mathbf{q}} B_{\mathrm{d}}(\mathbf{q},\mathbf{k}_n)$ are smaller in the dressed d-wave cases as compared to the s-wave case, resulting in slightly smaller Hebel-Slichter peaks in d-wave cases. This, however, is only a quantitative difference, the important point being that unlike the bare case or d-wave order on the square lattice, the Hebel-Slichter peak is not wiped out despite the sign-changing gap.

In summary, because of the kagome sublattice structure, more specifically, the sublattice interference and localization of the sublattice weight, which appears as the dressing factor $g_{\alpha\beta}(\mathbf{k},\mathbf{q})$, the enhancement factor $\sum_{\mathbf{q}} B_{\mathrm{d}}(\mathbf{q},\mathbf{k}_n)$ in $\chi_0^{+-}(\mathbf{q},\omega)$ becomes substantial and d-wave superconductivity supports a Hebel-Slichter peak on the kagome lattice, as seen from Fig. 5.5.

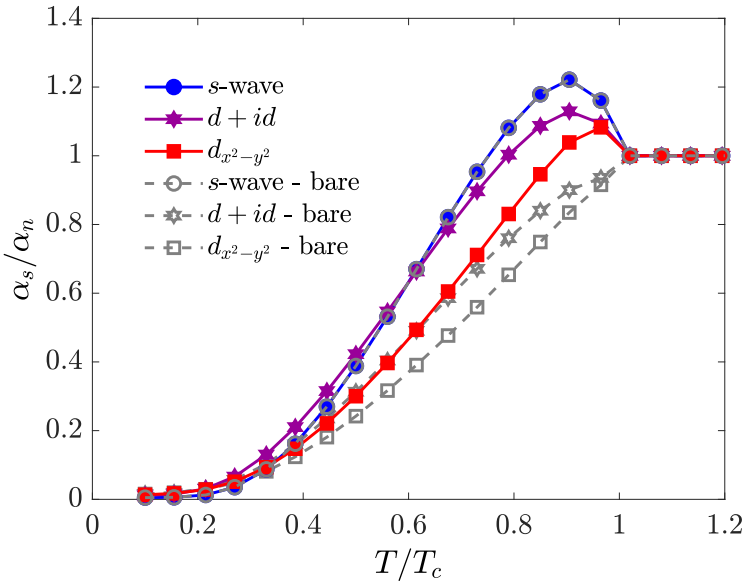

Figure 5.5: Temperature dependence of the spin-lattice relaxation rate ratio α_s/α_n for superconductivity on the kagome lattice. All cases are plotted for $\mathcal{N} = 4 \times 10^4$ and $\omega = \eta = 0.015$. The solid lines show the results calculated from the full $\chi_0^{+-}(\mathbf{q}, \omega)$, while the dashed lines display the results obtained from the spin susceptibility without the dressing factor $g_{\alpha\beta}(\mathbf{k}, \mathbf{q})$. As seen, $g_{\alpha\beta}(\mathbf{k}, \mathbf{q})$ restores the Hebel-Slichter peak even for the d-wave cases.

Chapter 6

Summary and Discussion

In this thesis, we investigated the spin-relaxation rate in the unconventional kagome superconductors. Surprisingly, the d-wave kagome superconductor will exhibit a Hebel-Slichter peak in the superconducting state despite a fully compensated sign-changing structure of the superconducting order parameter.

In previous studies, Hebel-Slichter peak was explained as a combined effect of the divergence of the DOS in superconducting state and the enhancement from coherence factor. In Chapter 2, we reviewed the spin-lattice relaxation rate and derived the coherence factor of relaxation rate from spin susceptibility. Then we investigated the role of each terms in the expression of spin-lattice relaxation rate, and found that the coherence factor is the key to the Hebel-Slichter peak in conventional BCS superconductors. Experimental results suggest that Hebel-Slichter peak should be absent in unconventional superconductors; thus in Chapter 3, we used the square lattice to explain the absence of the peak due to the coherence factor. Chapter 4 reviewed the model and the experiments of the kagome superconductors. Owing to the unique sublattice structure of the kagome lattice, the d-wave unconventional superconductivity can be unexpectedly robust to disorder on this lattice. Finally in Chapter 5, we calculated the spin-lattice relaxation rate of the kagome lattice, and proved the existence the Hebel-Slichter peak in the kagome lattice with d-wave symmetries of order parameters.

High sensitivity of critical temperature to disorder and absence of Hebel-Slichter peak are considered as strong evidences pointing to a sign-changing structure of order parameter. By contrast, superconductors which are not sensitive to disorder and exhibit Hebel-Slichter peak are always considered as conventional, non-sign-changing ones. However, this thesis together with Ref. [17] suggests that the special sublattice structure of kagome lattice may render these probes invalid in identifing the sign-changing gap structure on this lattice. Thus some of the current conclusions that the kagome superconductivity is the conventional BCS-type should be reconsidered. Just

like Søren Kierkegaard wrote in his book 'Fear and Trembling', the knight of infinity renounces the thing he loved most through the infinite resignation, but the knight of faith retrieves it by the power absurdity; the d-wave superconductor, through the sign-changing gap, abandons the Hebel-Slichter peak, but the kagome lattice, with the unique sublattice structure, recovers the Hebel-Slichter peak in the spin-lattice relaxation rate.

Currently, the nature of the superconductivity of the kagome lattice remains controversial. Experimental results can not clearly identify the nodal/nodeless structure of the kagome lattice. Besides, the experiments of the suppression of the critical temperature due to disorder on the lattice and the existence of the Hebel-Slichter peak, according to our work, can not serve as evidences for a non-sign-changing structure. Therefore, more probes are needed in the future in order to distinguish the superconducting states of the kagome lattice.

Appendix A

Derivation for the general spin-lattice relaxation rate

In this appendix, we derive the general expression of the spin-lattice relaxation rate. The relaxation process originates from the fluctuation of the nuclear energy level. The perturbation interaction can be described by the hyperfine Hamiltonian between a nuclear spin $\mathbf{I}$ and electron spins $\mathbf{S}$ [14, 25, 26, 28].

$$\mathcal{H}_{hf} = -\frac{8\pi}{3}\gamma_n\gamma_e\mathbf{I}\cdot\mathbf{S}\delta(\mathbf{r}), \tag{A.1}$$

where only the contact interaction is taken into account. In this expression, we have already set Planck constant $\hbar = 1$. γ_n and γ_e denotes the nuclear and the electronic gyromagnetic ratios. In general, the spin-lattice relaxation rate is defined by the fluctuation of the energy levels

$$\frac{1}{T_1} = 2\int_{-\infty}^{\infty} d\tau \cos(\omega_0\tau)\langle\{\mathcal{H}_{hf}^{+}(\tau), \mathcal{H}_{hf}^{-}(0)\}\rangle, \tag{A.2}$$

where ω_0 is the nuclear Larmor frequency. The operator is defined as $\{A, B\} = (AB + BA)/2$. In the second quantization representation, the Hamiltonian can be written as

$$\mathcal{H}_{hf}^{\pm} = -\frac{1}{\mathcal{N}}\sum_{\mathbf{q}}\gamma_n\gamma_e A_{\mathbf{q}} S_{\mathbf{q}}^{\pm}, \tag{A.3}$$

where $\mathcal{N}$ is the number of $\mathbf{q}$ space points. $A_{\mathbf{k},\mathbf{k+q}}$ is defined as

$$A_{\mathbf{k},\mathbf{k+q}} \equiv \frac{8\pi}{3}u_{\mathbf{k}}^{*}(0)u_{\mathbf{k+q}}(0), \tag{A.4}$$

where $u_{\mathbf{k}}$ is the wave function of the conduction electron at nuclear spin. We assume $A_{\mathbf{k},\mathbf{k+q}}$ is independent of $\mathbf{k}$ and is denoted by $A_{\mathbf{q}}$. The electronic spin operators are defined as

$$\begin{aligned} S^{+}_{\mathbf{q}} &= \frac{1}{\mathcal{N}} \sum_{\mathbf{k}} c^{\dagger}_{\mathbf{k+q}\uparrow} c_{\mathbf{k}\downarrow}, \\ S^{-}_{\mathbf{q}} &= \frac{1}{\mathcal{N}} \sum_{\mathbf{k}} c^{\dagger}_{\mathbf{k+q}\downarrow} c_{\mathbf{k}\uparrow}. \end{aligned} \tag{A.5}$$

Now insert the hyperfine Hamiltonian into Eq. (A.2) and it yields

$$\frac{1}{T_1} = 2\gamma_n^2\gamma_e^2 \int_{-\infty}^{\infty} d\tau \cos(\omega_0\tau) \sum_{\mathbf{q}} \langle\{S^{+}_{\mathbf{q}}(\tau), S^{-}_{-\mathbf{q}}(0)\}\rangle A_{\mathbf{q}} A_{-\mathbf{q}}. \tag{A.6}$$

According to the fluctuation-dissipation theorem, we can finally write the spin-lattice relaxation rate as

$$\frac{1}{T_1} = \frac{2\gamma_n^2\gamma_e^2(k_B T)}{\omega_0} \sum_{\mathbf{q}} A_{\mathbf{q}} A_{-\mathbf{q}} \mathrm{Im}\chi(\mathbf{q}, \omega_0). \tag{A.7}$$

Normally, when measuring the relaxation rate on the lattice site, the form factor $A_{\mathbf{q}}$ can be taken as a constant. Nevertheless, if the nearest neighbor effect to the wave function is taken into account, the form factor can show a $\mathbf{q}$ dependence and act as a filter for certain regions of the Brillouin zone [14, 33]. Previous studies have discussed the derivation of form factor [39] to explain the difference of the NMR spin-lattice relaxation rate measurement on different atom sites. The form factor can be derived from the position of the nearest atom sites. But we argue that the form factor will not influence the absence of the Hebel-Slichter peak in unconventional superconductors. This is because that the factor should act as a filter of certain $\mathbf{q}$ regions, which can potentially break the sign-changing compensation of unconventional order parameters and the superconductors are more likely to exhibit Hebel-Slichter peak. However, in experiments Hebel-Slichter peak is always absent in unconventional superconductors, which indicate that the form factor doesn't break the sign-changing structure. The form factor is more likely to select same areas of the positive region and the negative region of the $\mathbf{q}$ space as shown in Ref. [39]. Thus we can in principle ignore the form factor when discussing Hebel-Slichter peak.

Appendix B

Derivation for the one-band spin susceptibility

Fourier transform for homogeneous state

The definition for spin susceptibility is

$$\chi_0^{+-}(\mathbf{r}_i, \mathbf{r}_j, \tau) = \langle T_\tau \hat{S}_i^+(0)\hat{S}_j^-(\tau)\rangle, \tag{B.1}$$

where the operators $\hat{S}_i^+$ and $\hat{S}_i^+$ are defined as

$$\hat{S}_i^+ = c_{i\uparrow}^\dagger c_{i\downarrow}; \quad \hat{S}_i^- = c_{i\downarrow}^\dagger c_{i\uparrow}. \tag{B.2}$$

And there is relation

$$(\hat{S}_i^+)^\dagger = \hat{S}_i^-. \tag{B.3}$$

If we assume the state is homogeneous, we can define a Fourier transformation

$$\hat{S}^+(\mathbf{q}) = \int d\mathbf{r}_i \hat{S}_i^+ e^{i\mathbf{q}\mathbf{r}_i}; \quad \hat{S}^-(\mathbf{q}) = \int d\mathbf{r}_i \hat{S}_i^- e^{-i\mathbf{q}\mathbf{r}_i}, \tag{B.4}$$

and then

$$\begin{aligned} \chi_0^{+-}(\mathbf{q}, \tau) &= \int d\mathbf{r}_1 \int d\mathbf{r}_2 \langle T_\tau \hat{S}_i^+(0)\hat{S}_j^-(\tau)\rangle e^{i(\mathbf{r}_i - \mathbf{r}_j)\mathbf{q}} \\ &= \int d\mathbf{r}_1 \int d\mathbf{r}_2 \langle T_\tau c_{i\uparrow}^\dagger c_{i\downarrow} c_{j\downarrow}^\dagger(\tau) c_{j\uparrow}(\tau)\rangle e^{i(\mathbf{r}_i - \mathbf{r}_j)\mathbf{q}}. \end{aligned} \tag{B.5}$$

Next we perform the Fourier transform for the operators c and $c^\dagger$,

$$c_i^\dagger = \frac{1}{\sqrt{\mathcal{N}}} \sum_{\mathbf{k}} c_{\mathbf{k}}^\dagger e^{-i\mathbf{k}\mathbf{r}_i}; \quad c_i = \frac{1}{\sqrt{\mathcal{N}}} \sum_{\mathbf{k}} c_{\mathbf{k}} e^{i\mathbf{k}\mathbf{r}_i}, \tag{B.6}$$

where $\mathcal{N}$ is the number of $\mathbf{k}$ space points. Insert into the equation above we get

$$\begin{aligned}\chi_0^{+-}(\mathbf{q},\tau) =& \frac{1}{\mathcal{N}^2}\int d\mathbf{r}_1 \int d\mathbf{r}_2 \sum_{\mathbf{k}_1\mathbf{k}_2\mathbf{k}_3\mathbf{k}_4} \langle T_\tau c^\dagger_{\mathbf{k}_1\uparrow} c_{\mathbf{k}_2\downarrow} c^\dagger_{\mathbf{k}_3\downarrow}(\tau) c_{\mathbf{k}_4\uparrow}(\tau)\rangle e^{i(\mathbf{k}_2-\mathbf{k}_1)\mathbf{r}_i} e^{i(\mathbf{k}_4-\mathbf{k}_3)\mathbf{r}_j} e^{i(\mathbf{r}_i-\mathbf{r}_j)\mathbf{q}} \\ =& \frac{1}{\mathcal{N}^2}\sum_{\mathbf{k}_1\mathbf{k}_2\mathbf{k}_3\mathbf{k}_4} \delta(\mathbf{k}_2-\mathbf{k}_1+\mathbf{q})\delta(\mathbf{k}_4-\mathbf{k}_3-\mathbf{q})\langle T_\tau c^\dagger_{\mathbf{k}_1\uparrow} c_{\mathbf{k}_2\downarrow} c^\dagger_{\mathbf{k}_3\downarrow}(\tau) c_{\mathbf{k}_4\uparrow}(\tau)\rangle \\ =& \frac{1}{\mathcal{N}^2}\sum_{\mathbf{k}\mathbf{k}'}\langle T_\tau c^\dagger_{\mathbf{k}+\mathbf{q}\uparrow} c_{\mathbf{k}\downarrow} c^\dagger_{\mathbf{k}'-\mathbf{q}\downarrow}(\tau) c_{\mathbf{k}'\uparrow}(\tau)\rangle.\end{aligned} \tag{B.7}$$

Let's use Wick's theorem,

$$\begin{aligned}\chi_0^{+-}(\mathbf{q},\tau) = \frac{1}{\mathcal{N}^2}\sum_{\mathbf{k}\mathbf{k}'}[&\langle T_\tau c^\dagger_{\mathbf{k}+\mathbf{q}\uparrow} c_{\mathbf{k}\downarrow}\rangle\langle T_\tau c^\dagger_{\mathbf{k}'-\mathbf{q}\downarrow}(\tau) c_{\mathbf{k}'\uparrow}(\tau)\rangle \\ &-\langle T_\tau c^\dagger_{\mathbf{k}+\mathbf{q}\uparrow} c^\dagger_{\mathbf{k}'-\mathbf{q}\downarrow}(\tau)\rangle\langle T_\tau c_{\mathbf{k}\downarrow} c_{\mathbf{k}'\uparrow}(\tau)\rangle \\ &+\langle T_\tau c^\dagger_{\mathbf{k}+\mathbf{q}\uparrow} c_{\mathbf{k}'\uparrow}(\tau)\rangle\langle T_\tau c_{\mathbf{k}\downarrow} c^\dagger_{\mathbf{k}'-\mathbf{q}\downarrow}(\tau)\rangle].\end{aligned} \tag{B.8}$$

The first term simply gives zero. The second term is non zero when $\mathbf{k} = -\mathbf{k}'$, and it yields

$$\begin{aligned}&-\frac{1}{\mathcal{N}^2}\sum_{\mathbf{k}\mathbf{k}'}\langle T_\tau c^\dagger_{\mathbf{k}+\mathbf{q}\uparrow} c^\dagger_{\mathbf{k}'-\mathbf{q}\downarrow}(\tau)\rangle\langle T_\tau c_{\mathbf{k}\downarrow} c_{\mathbf{k}'\uparrow}(\tau)\rangle \\ =&-\frac{1}{\mathcal{N}}\sum_{\mathbf{k}}\langle T_\tau c^\dagger_{\mathbf{k}+\mathbf{q}\uparrow} c^\dagger_{-\mathbf{k}-\mathbf{q}\downarrow}(\tau)\rangle\langle T_\tau c_{\mathbf{k}\downarrow} c_{-\mathbf{k}\uparrow}(\tau)\rangle.\end{aligned} \tag{B.9}$$

The third term is non-zero when $\mathbf{k}' = \mathbf{k} + \mathbf{q}$, then it gives

$$\begin{aligned}&\frac{1}{\mathcal{N}^2}\sum_{\mathbf{k}\mathbf{k}'}\langle T_\tau c^\dagger_{\mathbf{k}+\mathbf{q}\uparrow} c_{\mathbf{k}'\uparrow}(\tau)\rangle\langle T_\tau c_{\mathbf{k}\downarrow} c^\dagger_{\mathbf{k}'-\mathbf{q}\downarrow}(\tau)\rangle \\ =&\frac{1}{\mathcal{N}}\sum_{\mathbf{k}}\langle T_\tau c^\dagger_{\mathbf{k}+\mathbf{q}\uparrow} c_{\mathbf{k}+\mathbf{q}\uparrow}(\tau)\rangle\langle T_\tau c_{\mathbf{k}\downarrow} c^\dagger_{\mathbf{k}\downarrow}(\tau)\rangle.\end{aligned} \tag{B.10}$$

Finally the susceptibility in momentum space reads

$$\chi_0^{+-}(\mathbf{q},\tau) = \frac{1}{\mathcal{N}}\sum_{\mathbf{k}}[-\langle T_\tau c^\dagger_{\mathbf{k}+\mathbf{q}\uparrow} c^\dagger_{-\mathbf{k}-\mathbf{q}\downarrow}(\tau)\rangle\langle T_\tau c_{\mathbf{k}\downarrow} c_{-\mathbf{k}\uparrow}(\tau)\rangle + \langle T_\tau c^\dagger_{\mathbf{k}+\mathbf{q}\uparrow} c_{\mathbf{k}+\mathbf{q}\uparrow}(\tau)\rangle\langle T_\tau c_{\mathbf{k}\downarrow} c^\dagger_{\mathbf{k}\downarrow}(\tau)\rangle]. \tag{B.11}$$

Bogoliubov transformation

Let's consider the Bogoliubov transformation. Assume the Hamiltonian is non-diagonal and can be written as

$$\mathbf{H}_{\mathbf{k}} = \begin{pmatrix} \xi_{\mathbf{k}} & \Delta_{\mathbf{k}} \\ \Delta_{\mathbf{k}}^{*} & -\xi_{\mathbf{k}} \end{pmatrix}, \tag{B.12}$$

and the basis

$$\mathbf{A}_{\mathbf{k}} = \begin{pmatrix} c_{\mathbf{k}\uparrow} \\ c_{-\mathbf{k}\downarrow}^{\dagger} \end{pmatrix}, \tag{B.13}$$

where we assumed the symmetry $\xi_{\mathbf{k}} = \xi_{-\mathbf{k}}$.

The unitary transformation defined in Bogoliubov transformation reads

$$\mathbf{U}_{\mathbf{k}} = \begin{pmatrix} u_{\mathbf{k}}^{*} & -v_{\mathbf{k}} \\ v_{\mathbf{k}}^{*} & u_{\mathbf{k}} \end{pmatrix}, \tag{B.14}$$

by which we can diagonalize the Hamiltonian

$$\mathbf{U}_{\mathbf{k}}^{\dagger}\mathbf{H}_{\mathbf{k}}\mathbf{U}_{\mathbf{k}} = \begin{pmatrix} E_{\mathbf{k}} & 0 \\ 0 & -E_{\mathbf{k}} \end{pmatrix}, \tag{B.15}$$

where

$$|u_{\mathbf{k}}|^2 = \frac{1}{2}\left(1 + \frac{\xi_{\mathbf{k}}}{E_{\mathbf{k}}}\right), \quad |v_{\mathbf{k}}|^2 = \frac{1}{2}\left(1 - \frac{\xi_{\mathbf{k}}}{E_{\mathbf{k}}}\right), \tag{B.16}$$

$$E_{\mathbf{k}} = \sqrt{\xi_{\mathbf{k}}^2 + |\Delta_{\mathbf{k}}|^2}. \tag{B.17}$$

The change of basis gives new eigenvector for the new diagonalized Hamiltonian

$$\mathbf{B}_{\mathbf{k}} = \begin{pmatrix} \gamma_{\mathbf{k}\uparrow} \\ \gamma_{-\mathbf{k}\downarrow}^{\dagger} \end{pmatrix} = \mathbf{U}_{\mathbf{k}}^{\dagger}\mathbf{A}_{\mathbf{k}} = \begin{pmatrix} u_{\mathbf{k}} & v_{\mathbf{k}} \\ -v_{\mathbf{k}}^{*} & u_{\mathbf{k}}^{*} \end{pmatrix} \begin{pmatrix} c_{\mathbf{k}\uparrow} \\ c_{-\mathbf{k}\downarrow}^{\dagger}. \end{pmatrix} \tag{B.18}$$

From that we can derive the relation for Bogoliubov transformation

$$\begin{aligned} c_{\mathbf{k}\uparrow} &= u_{\mathbf{k}}^{*}\gamma_{\mathbf{k}\uparrow} - v_{\mathbf{k}}\gamma_{-\mathbf{k}\downarrow}^{\dagger}, \\ c_{-\mathbf{k}\downarrow}^{\dagger} &= v_{\mathbf{k}}^{*}\gamma_{\mathbf{k}\uparrow} + u_{\mathbf{k}}\gamma_{-\mathbf{k}\downarrow}^{\dagger}, \\ c_{\mathbf{k}\uparrow}^{\dagger} &= u_{\mathbf{k}}\gamma_{\mathbf{k}\uparrow}^{\dagger} - v_{\mathbf{k}}^{*}\gamma_{-\mathbf{k}\downarrow}, \\ c_{-\mathbf{k}\downarrow} &= v_{\mathbf{k}}\gamma_{\mathbf{k}\uparrow}^{\dagger} + u_{\mathbf{k}}^{*}\gamma_{-\mathbf{k}\downarrow}, \end{aligned} \tag{B.19}$$

where $u_{\mathbf{k}}^2 = \frac{1}{2}\left(1 + \frac{\xi_{\mathbf{k}}}{E_{\mathbf{k}}}\right)$ and $v_{\mathbf{k}}^2 = \frac{1}{2}\left(1 - \frac{\xi_{\mathbf{k}}}{E_{\mathbf{k}}}\right)$.

Wake up in a lovely morning and do the calculation

Let's consider first the first term in eq. (B.11),

$$
\begin{aligned}
&-\frac{1}{\mathcal{N}}\sum_{\mathbf{k}}\langle T_\tau c^\dagger_{\mathbf{k+q}\uparrow} c^\dagger_{-\mathbf{k-q}\downarrow}(\tau)\rangle\langle T_\tau c_{\mathbf{k}\downarrow} c_{-\mathbf{k}\uparrow}(\tau)\rangle \\
=&-\frac{1}{\mathcal{N}}\sum_{\mathbf{k}}\langle T_\tau[u_{\mathbf{k+q}}\gamma^\dagger_{\mathbf{k+q}\uparrow} - v^*_{\mathbf{k+q}}\gamma_{-\mathbf{k-q}\downarrow}][v^*_{\mathbf{k+q}}\gamma_{\mathbf{k+q}\uparrow}(\tau) + u_{\mathbf{k+q}}\gamma^\dagger_{-\mathbf{k-q}\downarrow}(\tau)]\rangle\cdot \\
&\langle T_\tau[u^*_{\mathbf{k}}\gamma_{\mathbf{k}\downarrow} + v_{\mathbf{k}}\gamma^\dagger_{-\mathbf{k}\uparrow}][u^*_{\mathbf{k}}\gamma_{-\mathbf{k}\uparrow}(\tau) - v_{\mathbf{k}}\gamma^\dagger_{\mathbf{k}\downarrow}(\tau)]\rangle \\
=&-\frac{1}{\mathcal{N}}\sum_{\mathbf{k}}[-v^*_{\mathbf{k+q}}u_{\mathbf{k+q}}\langle T_\tau\gamma_{-\mathbf{k-q}\downarrow}\gamma^\dagger_{-\mathbf{k-q}\downarrow}(\tau)\rangle + u_{\mathbf{k+q}}v^*_{\mathbf{k+q}}\langle T_\tau\gamma^\dagger_{\mathbf{k+q}\uparrow}\gamma_{\mathbf{k+q}\uparrow}(\tau)\rangle]\cdot \\
&[-u^*_{\mathbf{k}}v_{\mathbf{k}}\langle T_\tau\gamma_{\mathbf{k}\downarrow}\gamma^\dagger_{\mathbf{k}\downarrow}(\tau)\rangle + v_{\mathbf{k}}u^*_{\mathbf{k}}\langle T_\tau\gamma^\dagger_{-\mathbf{k}\uparrow}\gamma_{-\mathbf{k}\uparrow}(\tau)\rangle] \\
=&\frac{1}{\mathcal{N}}\sum_{\mathbf{k}} v^*_{\mathbf{k+q}}u_{\mathbf{k+q}}u^*_{\mathbf{k}}v_{\mathbf{k}}[-\langle T_\tau\gamma_{-\mathbf{k-q}\downarrow}\gamma^\dagger_{-\mathbf{k-q}\downarrow}(\tau)\rangle\langle T_\tau\gamma_{\mathbf{k}\downarrow}\gamma^\dagger_{\mathbf{k}\downarrow}(\tau)\rangle + \langle T_\tau\gamma_{-\mathbf{k-q}\downarrow}\gamma^\dagger_{-\mathbf{k-q}\downarrow}(\tau)\rangle\cdot \\
&\langle T_\tau\gamma^\dagger_{-\mathbf{k}\uparrow}\gamma_{-\mathbf{k}\uparrow}(\tau)\rangle + \langle T_\tau\gamma^\dagger_{\mathbf{k+q}\uparrow}\gamma_{\mathbf{k+q}\uparrow}(\tau)\rangle\langle T_\tau\gamma_{\mathbf{k}\downarrow}\gamma^\dagger_{\mathbf{k}\downarrow}(\tau)\rangle - \langle T_\tau\gamma^\dagger_{\mathbf{k+q}\uparrow}\gamma_{\mathbf{k+q}\uparrow}(\tau)\rangle\langle T_\tau\gamma^\dagger_{-\mathbf{k}\uparrow}\gamma_{-\mathbf{k}\uparrow}(\tau)\rangle],
\end{aligned}
\tag{B.20}
$$

and use these relations

$$
\begin{aligned}
\langle T_\tau\gamma_n(\tau)\gamma^\dagger_n\rangle &= (1 - f(E_n))e^{-E_n\tau}, \\
\langle T_\tau\gamma^\dagger_n(\tau)\gamma_n\rangle &= f(E_n)e^{E_n\tau}, \\
\langle T_\tau\gamma_n\gamma^\dagger_n(\tau)\rangle &= -f(E_n)e^{E_n\tau}, \\
\langle T_\tau\gamma^\dagger_n\gamma_n(\tau)\rangle &= -(1 - f(E_n))e^{-E_n\tau},
\end{aligned}
\tag{B.21}
$$

which can be obtained under Heisenberg picture $\gamma_n(\tau) = e^{-E_n\tau}\gamma_n$, since the the Hamiltonian under the γ basis are diagonalized. Further, we assume there is spin degeneracy. Here $f(E_n) = 1/(e^{E_n/k_BT} + 1)$ is the Fermi-Dirac distribution. Then we get

$$
\begin{aligned}
= \frac{1}{\mathcal{N}}\sum_{\mathbf{k}} v^*_{\mathbf{k+q}}u_{\mathbf{k+q}}u^*_{\mathbf{k}}v_{\mathbf{k}}[&- f(E_{\mathbf{k+q}\downarrow})f(E_{\mathbf{k}\downarrow})e^{(E_{\mathbf{k+q}\downarrow}+E_{\mathbf{k}\downarrow})\tau} \\
&+ f(E_{\mathbf{k}\downarrow})(1 - f(E_{\mathbf{k+q}\uparrow}))e^{(E_{\mathbf{k}\downarrow}-E_{\mathbf{k+q}\uparrow})\tau} \\
&+ f(E_{\mathbf{k+q}\downarrow})(1 - f(E_{\mathbf{k}\uparrow}))e^{(E_{\mathbf{k+q}\downarrow}-E_{\mathbf{k}\uparrow})\tau} \\
&- (1 - f(E_{\mathbf{k+q}\uparrow}))(1 - f(E_{\mathbf{k}\uparrow}))e^{-(E_{\mathbf{k+q}\uparrow}+E_{\mathbf{k}\uparrow})\tau}].
\end{aligned}
\tag{B.22}
$$

We can further use these relations to simplify the result

$$\begin{aligned} f(x)f(y)b(x+y) &= 1-f(x)-f(y), \\ (1-f(x))(1-f(y))b(-x-y) &= f(x)+f(y)-1, \\ f(x)(1-f(y))b(x-y) &= f(y)-f(x), \end{aligned} \tag{B.23}$$

where $b(x) = e^{x\beta} - 1$. Then the first term becomes

$$\begin{aligned} \frac{1}{\mathcal{N}}\sum_{\mathbf{k}} v^*_{\mathbf{k}+\mathbf{q}} u_{\mathbf{k}+\mathbf{q}} u^*_{\mathbf{k}} v_{\mathbf{k}} \Bigg[& -\frac{1-f(E_{\mathbf{k}+\mathbf{q}\downarrow})-f(E_{\mathbf{k}\downarrow})}{e^{(E_{\mathbf{k}+\mathbf{q}\downarrow}+E_{\mathbf{k}\downarrow})\beta}-1} e^{(E_{\mathbf{k}+\mathbf{q}\downarrow}+E_{\mathbf{k}\downarrow})\tau} + \frac{f(E_{\mathbf{k}+\mathbf{q}\uparrow})-f(E_{\mathbf{k}\downarrow})}{e^{(E_{\mathbf{k}\downarrow}+E_{\mathbf{k}+\mathbf{q}\uparrow})\beta}-1} e^{(E_{\mathbf{k}\downarrow}-E_{\mathbf{k}+\mathbf{q}\uparrow})\tau} \\ & + \frac{f(E_{\mathbf{k}\uparrow})-f(E_{\mathbf{k}+\mathbf{q}\downarrow})}{e^{(E_{\mathbf{k}+\mathbf{q}\downarrow}-E_{\mathbf{k}\uparrow})\beta}-1} e^{(E_{\mathbf{k}+\mathbf{q}\downarrow}-E_{\mathbf{k}\uparrow})\tau} - \frac{f(E_{\mathbf{k}+\mathbf{q}\uparrow})+f(E_{\mathbf{k}\uparrow})-1}{e^{-((E_{\mathbf{k}\uparrow}+E_{\mathbf{k}+\mathbf{q}\downarrow}))\beta}-1} e^{-(E_{\mathbf{k}+\mathbf{q}\uparrow}+E_{\mathbf{k}\downarrow})\tau} \Bigg]. \end{aligned} \tag{B.24}$$

Transform to Matsubara frequency,

$$\begin{aligned} \frac{1}{\mathcal{N}}\int_0^\beta d\tau\ e^{i\omega_n\tau} \sum_{\mathbf{k}} v^*_{\mathbf{k}+\mathbf{q}} u_{\mathbf{k}+\mathbf{q}} u^*_{\mathbf{k}} v_{\mathbf{k}} \Bigg[& -\frac{1-f(E_{\mathbf{k}+\mathbf{q}\downarrow})-f(E_{\mathbf{k}\downarrow})}{e^{(E_{\mathbf{k}+\mathbf{q}\downarrow}+E_{\mathbf{k}\downarrow})\beta}-1} e^{(E_{\mathbf{k}+\mathbf{q}\downarrow}+E_{\mathbf{k}\downarrow})\tau} \\ & + \frac{f(E_{\mathbf{k}+\mathbf{q}\uparrow})-f(E_{\mathbf{k}\downarrow})}{e^{(E_{\mathbf{k}\downarrow}-E_{\mathbf{k}+\mathbf{q}\uparrow})\beta}-1} e^{(E_{\mathbf{k}\downarrow}-E_{\mathbf{k}+\mathbf{q}\uparrow})\tau} \\ & + \frac{f(E_{\mathbf{k}\uparrow})-f(E_{\mathbf{k}+\mathbf{q}\downarrow})}{e^{(E_{\mathbf{k}+\mathbf{q}\downarrow}-E_{\mathbf{k}\uparrow})\beta}-1} e^{(E_{\mathbf{k}+\mathbf{q}\downarrow}-E_{\mathbf{k}\uparrow})\tau} \\ & - \frac{f(E_{\mathbf{k}+\mathbf{q}\uparrow})+f(E_{\mathbf{k}\uparrow})-1}{e^{-((E_{\mathbf{k}\uparrow}+E_{\mathbf{k}+\mathbf{q}\uparrow}))\beta}-1} e^{-(E_{\mathbf{k}+\mathbf{q}\uparrow}+E_{\mathbf{k}\uparrow})\tau} \Bigg] \end{aligned} \tag{B.25}$$

$$\begin{aligned} = \frac{1}{\mathcal{N}}\sum_{\mathbf{k}} v^*_{\mathbf{k}+\mathbf{q}} u_{\mathbf{k}+\mathbf{q}} u^*_{\mathbf{k}} v_{\mathbf{k}} \Bigg[& -\frac{1-f(E_{\mathbf{k}+\mathbf{q}\downarrow})-f(E_{\mathbf{k}\downarrow})}{i\omega_n + E_{\mathbf{k}+\mathbf{q}\downarrow} + E_{\mathbf{k}\downarrow}} + \frac{f(E_{\mathbf{k}+\mathbf{q}\uparrow})-f(E_{\mathbf{k}\downarrow})}{i\omega_n + E_{\mathbf{k}\downarrow} - E_{\mathbf{k}+\mathbf{q}\uparrow}} \\ & + \frac{f(E_{\mathbf{k}\uparrow})-f(E_{\mathbf{k}+\mathbf{q}\downarrow})}{i\omega_n + E_{\mathbf{k}+\mathbf{q}\downarrow} - E_{\mathbf{k}\uparrow}} - \frac{f(E_{\mathbf{k}+\mathbf{q}\uparrow})+f(E_{\mathbf{k}\uparrow})-1}{i\omega_n - E_{\mathbf{k}+\mathbf{q}\uparrow} - E_{\mathbf{k}\uparrow}} \Bigg]. \end{aligned} \tag{B.26}$$

Next, we consider the second term

$$
\begin{aligned}
&\frac{1}{\mathcal{N}}\sum_{\mathbf{k}}\langle T_\tau c^\dagger_{\mathbf{k+q}\uparrow}c_{\mathbf{k+q}\uparrow}(\tau)\rangle\langle T_\tau c_{\mathbf{k}\downarrow}c^\dagger_{\mathbf{k}\downarrow}(\tau)\rangle\\
=&\frac{1}{\mathcal{N}}\sum_{\mathbf{k}}\langle T_\tau[u_{\mathbf{k+q}}\gamma^\dagger_{\mathbf{k+q}\uparrow}-v^*_{\mathbf{k+q}}\gamma_{-\mathbf{k}-\mathbf{q}\downarrow}][u^*_{\mathbf{k+q}}\gamma_{\mathbf{k+q}\uparrow}(\tau)-v_{\mathbf{k+q}}\gamma^\dagger_{-\mathbf{k}-\mathbf{q}\downarrow}(\tau)]\rangle\cdot\\
&\langle T_\tau[u^*_{\mathbf{k}}\gamma_{\mathbf{k}\downarrow}+v_{\mathbf{k}}\gamma^\dagger_{-\mathbf{k}\uparrow}][v^*_{\mathbf{k}}\gamma_{-\mathbf{k}\uparrow}(\tau)+u_{\mathbf{k}}\gamma^\dagger_{\mathbf{k}\downarrow}(\tau)]\rangle\\
=&\frac{1}{\mathcal{N}}\sum_{\mathbf{k}}[|v_{\mathbf{k+q}}|^2\langle\gamma_{-\mathbf{k}-\mathbf{q}\downarrow}\gamma^\dagger_{-\mathbf{k}-\mathbf{q}\downarrow}(\tau)\rangle+|u_{\mathbf{k+q}}|^2\langle\gamma^\dagger_{\mathbf{k+q}\uparrow}\gamma_{\mathbf{k+q}\uparrow}(\tau)\rangle]\cdot\\
&[|u_{\mathbf{k}}|^2\langle\gamma_{\mathbf{k}\downarrow}\gamma^\dagger_{\mathbf{k}\downarrow}(\tau)\rangle+|v_{\mathbf{k}}|^2\langle\gamma^\dagger_{-\mathbf{k}\uparrow}\gamma_{-\mathbf{k}\uparrow}(\tau)\rangle]\\
=&\frac{1}{\mathcal{N}}\sum_{\mathbf{k}}[|v_{\mathbf{k+q}}|^2f(E_{\mathbf{k+q}\downarrow})e^{E_{\mathbf{k+q}\downarrow}\tau}+|u_{\mathbf{k+q}}|^2(1-f(E_{\mathbf{k+q}\uparrow}))e^{-E_{\mathbf{k+q}\uparrow}\tau}]\cdot\\
&[|u_{\mathbf{k}}|^2f(E_{\mathbf{k}\downarrow})e^{E_{\mathbf{k}\downarrow}\tau}+|v_{\mathbf{k}}|^2(1-f(E_{\mathbf{k}\uparrow}))e^{-E_{\mathbf{k}\uparrow}\tau}]\\
=&\frac{1}{\mathcal{N}}\sum_{\mathbf{k}}[|v_{\mathbf{k+q}}|^2|u_{\mathbf{k}}|^2f(E_{\mathbf{k+q}\downarrow})f(E_{\mathbf{k}\downarrow})e^{(E_{\mathbf{k+q}\downarrow}+E_{\mathbf{k}\downarrow})\tau}\\
&+|v_{\mathbf{k+q}}|^2|v_{\mathbf{k}}|^2f(E_{\mathbf{k+q}\downarrow})(1-f(E_{\mathbf{k}\uparrow}))e^{(E_{\mathbf{k+q}\downarrow}-E_{\mathbf{k}\uparrow})\tau}\\
&+|u_{\mathbf{k+q}}|^2|u_{\mathbf{k}}|^2f(E_{\mathbf{k}\downarrow})(1-f(E_{\mathbf{k+q}\uparrow}))e^{(E_{\mathbf{k}\downarrow}-E_{\mathbf{k+q}\uparrow})\tau}\\
&+|u_{\mathbf{k+q}}|^2|v_{\mathbf{k}}|^2(1-f(E_{\mathbf{k}\uparrow}))(1-f(E_{\mathbf{k+q}\uparrow}))e^{-(E_{\mathbf{k}\uparrow}+E_{\mathbf{k+q}\uparrow})\tau}]\\
=&\frac{1}{\mathcal{N}}\sum_{\mathbf{k}}\Bigg[|v_{\mathbf{k+q}}|^2|u_{\mathbf{k}}|^2\frac{1-f(E_{\mathbf{k}\downarrow})-f(E_{\mathbf{k+q}\downarrow})}{e^{(E_{\mathbf{k+q}\downarrow}+E_{\mathbf{k}\downarrow})\beta}-1}e^{(E_{\mathbf{k+q}\downarrow}+E_{\mathbf{k}\downarrow})\tau}\\
&+|v_{\mathbf{k+q}}|^2|v_{\mathbf{k}}|^2\frac{f(E_{\mathbf{k}\uparrow})-f(E_{\mathbf{k+q}\downarrow})}{e^{(E_{\mathbf{k+q}\downarrow}-E_{\mathbf{k}\uparrow})\beta}-1}e^{(E_{\mathbf{k+q}\downarrow}-E_{\mathbf{k}\uparrow})\tau}\\
&+|u_{\mathbf{k+q}}|^2|u_{\mathbf{k}}|^2\frac{f(E_{\mathbf{k+q}\uparrow})-f(E_{\mathbf{k}\downarrow})}{e^{(E_{\mathbf{k}\downarrow}-E_{\mathbf{k+q}\uparrow})\beta}-1}e^{(E_{\mathbf{k}\downarrow}-E_{\mathbf{k+q}\uparrow})\tau}\\
&+|u_{\mathbf{k+q}}|^2|v_{\mathbf{k}}|^2\frac{f(E_{\mathbf{k}\uparrow})+f(E_{\mathbf{k+q}\uparrow})-1}{e^{-(E_{\mathbf{k+q}\uparrow}+E_{\mathbf{k}\uparrow})\beta}-1}e^{-(E_{\mathbf{k}\uparrow}+E_{\mathbf{k+q}\uparrow})\tau}\Bigg].
\end{aligned}
\tag{B.27}
$$

Transform to Matsubara frequency,

$$
\begin{aligned}
&\frac{1}{\mathcal{N}}\int_0^\beta d\tau\ e^{i\omega_n\tau}\sum_{\mathbf{k}}\Bigg[|v_{\mathbf{k+q}}|^2|u_{\mathbf{k}}|^2\frac{1-f(E_{\mathbf{k}\downarrow})-f(E_{\mathbf{k+q}\downarrow})}{e^{(E_{\mathbf{k+q}\downarrow}+E_{\mathbf{k}\downarrow})\beta}-1}e^{(E_{\mathbf{k+q}\downarrow}+E_{\mathbf{k}\downarrow})\tau}\\
&+|v_{\mathbf{k+q}}|^2|v_{\mathbf{k}}|^2\frac{f(E_{\mathbf{k}\uparrow})-f(E_{\mathbf{k+q}\downarrow})}{e^{(E_{\mathbf{k+q}\downarrow}-E_{\mathbf{k}\uparrow})\beta}-1}e^{(E_{\mathbf{k+q}\downarrow}-E_{\mathbf{k}\uparrow})\tau}\\
&+|u_{\mathbf{k+q}}|^2|u_{\mathbf{k}}|^2\frac{f(E_{\mathbf{k+q}\uparrow})-f(E_{\mathbf{k}\downarrow})}{e^{(E_{\mathbf{k}\downarrow}-E_{\mathbf{k+q}\uparrow})\beta}-1}e^{(E_{\mathbf{k}\downarrow}-E_{\mathbf{k+q}\uparrow})\tau}\\
&+|u_{\mathbf{k+q}}|^2|v_{\mathbf{k}}|^2\frac{f(E_{\mathbf{k}\uparrow})+f(E_{\mathbf{k+q}\uparrow})-1}{e^{-(E_{\mathbf{k+q}\uparrow}+E_{\mathbf{k}\downarrow})\beta}-1}e^{-(E_{\mathbf{k}\uparrow}+E_{\mathbf{k+q}\uparrow})\tau}\Bigg]\\
=&\frac{1}{\mathcal{N}}\sum_{\mathbf{k}}\Bigg[|v_{\mathbf{k+q}}|^2|u_{\mathbf{k}}|^2\frac{1-f(E_{\mathbf{k}\downarrow})-f(E_{\mathbf{k+q}\downarrow})}{i\omega_n+E_{\mathbf{k+q}\downarrow}+E_{\mathbf{k}\downarrow}}+|v_{\mathbf{k+q}}|^2|v_{\mathbf{k}}|^2\frac{f(E_{\mathbf{k}\uparrow})-f(E_{\mathbf{k+q}\downarrow})}{i\omega_n+E_{\mathbf{k+q}\downarrow}-E_{\mathbf{k}\uparrow}}\\
&+|u_{\mathbf{k+q}}|^2|u_{\mathbf{k}}|^2\frac{f(E_{\mathbf{k+q}\uparrow})-f(E_{\mathbf{k}\downarrow})}{i\omega_n+E_{\mathbf{k}\downarrow}-E_{\mathbf{k+q}\uparrow}}+|u_{\mathbf{k+q}}|^2|v_{\mathbf{k}}|^2\frac{f(E_{\mathbf{k}\uparrow})+f(E_{\mathbf{k+q}\uparrow})-1}{i\omega_n-E_{\mathbf{k+q}\uparrow}-E_{\mathbf{k}\uparrow}}\Bigg]
\end{aligned}
\tag{B.28}
$$

Combine the two terms from eq. (B.26) and eq. (B.28) together,

$$\begin{aligned}\chi_0^{+-}(\mathbf{q}, i\omega_n) = \frac{1}{\mathcal{N}}\sum_{\mathbf{k}}\Bigg[&(-v^*_{\mathbf{k+q}}u_{\mathbf{k+q}}u^*_{\mathbf{k}}v_{\mathbf{k}} + |v_{\mathbf{k+q}}|^2|u_{\mathbf{k}}|^2)\frac{1-f(E_{\mathbf{k}\downarrow})-f(E_{\mathbf{k+q}\downarrow})}{i\omega_n + E_{\mathbf{k+q}\downarrow} + E_{\mathbf{k}\downarrow}}\\ &+(v^*_{\mathbf{k+q}}u_{\mathbf{k+q}}u^*_{\mathbf{k}}v_{\mathbf{k}} + |v_{\mathbf{k+q}}|^2|v_{\mathbf{k}}|^2)\frac{f(E_{\mathbf{k}\uparrow})-f(E_{\mathbf{k+q}\downarrow})}{i\omega_n + E_{\mathbf{k+q}\downarrow} - E_{\mathbf{k}\uparrow}}\\ &+(v^*_{\mathbf{k+q}}u_{\mathbf{k+q}}u^*_{\mathbf{k}}v_{\mathbf{k}} + |u_{\mathbf{k+q}}|^2|u_{\mathbf{k}}|^2)\frac{f(E_{\mathbf{k+q}\uparrow})-f(E_{\mathbf{k}\downarrow})}{i\omega_n + E_{\mathbf{k}\downarrow} - E_{\mathbf{k+q}\uparrow}}\\ &+(-v^*_{\mathbf{k+q}}u_{\mathbf{k+q}}u^*_{\mathbf{k}}v_{\mathbf{k}} + |u_{\mathbf{k+q}}|^2|v_{\mathbf{k}}|^2)\frac{f(E_{\mathbf{k}\uparrow})+f(E_{\mathbf{k+q}\uparrow})-1}{i\omega_n - E_{\mathbf{k+q}\uparrow} - E_{\mathbf{k}\uparrow}}\Bigg].\end{aligned} \tag{B.29}$$

We can further simplify the result, and there is no approximation to be made. We can do some translation in $\mathbf{k}$ space to simplify the result. Define $\tilde{\mathbf{k}} = -\mathbf{k} - q$, then the second term in eq. (B.29) becomes

$$\frac{1}{\mathcal{N}}\sum_{\tilde{\mathbf{k}}}(v^*_{-\tilde{\mathbf{k}}}u_{-\tilde{\mathbf{k}}}u^*_{-\tilde{\mathbf{k}}-\mathbf{q}}v_{-\tilde{\mathbf{k}}-\mathbf{q}} + |v_{-\tilde{\mathbf{k}}}|^2|v_{-\tilde{\mathbf{k}}-\mathbf{q}}|^2)\frac{f(E_{-\tilde{\mathbf{k}}-\mathbf{q}\uparrow})-f(E_{-\tilde{\mathbf{k}}\downarrow})}{i\omega_n + E_{-\tilde{\mathbf{k}}\downarrow} - E_{-\tilde{\mathbf{k}}-\mathbf{q}\uparrow}}. \tag{B.30}$$

Because of time-reversal symmetry, the above is invariant under $\mathbf{k} \to -\mathbf{k}$. It can be written as

$$\frac{1}{\mathcal{N}}\sum_{\mathbf{k}}(v^*_{\mathbf{k+q}}u_{\mathbf{k+q}}u^*_{\mathbf{k}}v_{\mathbf{k}} + |v_{\mathbf{k+q}}|^2|v_{\mathbf{k}}|^2)\frac{f(E_{\mathbf{k+q}\uparrow})-f(E_{\mathbf{k}\downarrow})}{i\omega_n + E_{\mathbf{k}\downarrow} - E_{\mathbf{k+q}\uparrow}} \tag{B.31}$$

If we insert these relations from Bogoliubov transformation,

$$\begin{aligned}|u_{\mathbf{k}}|^2 &= \frac{E_{\mathbf{k}} + \xi_{\mathbf{k}}}{2E_{\mathbf{k}}},\\ |v_{\mathbf{k}}|^2 &= \frac{E_{\mathbf{k}} - \xi_{\mathbf{k}}}{2E_{\mathbf{k}}}\\ u^*_{\mathbf{k}}v_{\mathbf{k}} &= \frac{\Delta_{\mathbf{k}}}{2E_{\mathbf{k}}}\\ u_{\mathbf{k}}v^*_{\mathbf{k}} &= \frac{\Delta^*_{\mathbf{k}}}{2E_{\mathbf{k}}}\end{aligned} \tag{B.32}$$

Finally we get

$$\begin{aligned}\chi_0^{+-}(\mathbf{q}, i\omega_n) = \frac{1}{\mathcal{N}}\sum_{\mathbf{k}}\Bigg[&\frac{1}{4}\left(1 - \frac{\xi_{\mathbf{k}}\xi_{\mathbf{k+q}} + \Delta^*_{\mathbf{k+q}}\Delta_{\mathbf{k}}}{E_{\mathbf{k}}E_{\mathbf{k+q}}}\right)\frac{1-f(E_{\mathbf{k}})-f(E_{\mathbf{k+q}})}{i\omega_n + E_{\mathbf{k+q}} + E_{\mathbf{k}}}\\ &+\frac{1}{4}\left(1 - \frac{\xi_{\mathbf{k}}\xi_{\mathbf{k+q}} + \Delta^*_{\mathbf{k+q}}\Delta_{\mathbf{k}}}{E_{\mathbf{k}}E_{\mathbf{k+q}}}\right)\frac{f(E_{\mathbf{k}})+f(E_{\mathbf{k+q}})-1}{i\omega_n - E_{\mathbf{k+q}} - E_{\mathbf{k}}}\\ &+\frac{1}{2}\left(1 + \frac{\xi_{\mathbf{k}}\xi_{\mathbf{k+q}} + \Delta^*_{\mathbf{k+q}}\Delta_{\mathbf{k}}}{E_{\mathbf{k}}E_{\mathbf{k+q}}}\right)\frac{f(E_{\mathbf{k}})-f(E_{\mathbf{k+q}})}{i\omega_n + E_{\mathbf{k+q}} - E_{\mathbf{k}}}\Bigg].\end{aligned} \tag{B.33}$$

In a non-interacting electron system, the equation reduces to Lindhard function.

Nambu quasiparticle symmetry

In convention, we define the quasi-particle operators in this way,

$$\begin{pmatrix} u_{\mathbf{k}} & v_{\mathbf{k}} \\ -v_{\mathbf{k}}^* & u_{\mathbf{k}}^* \end{pmatrix} \begin{pmatrix} c_{\mathbf{k}\uparrow} \\ c_{-\mathbf{k}\downarrow}^\dagger \end{pmatrix} = \begin{pmatrix} \gamma_{1\mathbf{k}} \\ \gamma_{2\mathbf{k}}^\dagger \end{pmatrix}, \tag{B.34}$$

where in the normal state there is $\gamma_{1\mathbf{k}} = c_{\uparrow\mathbf{k}}$ and $\gamma_{2\mathbf{k}}^\dagger = c_{\downarrow-\mathbf{k}}^\dagger$

The diagonalized Hamiltonian is written as

$$\begin{aligned} H_\gamma &= \sum_{\mathbf{k}} \begin{pmatrix} \gamma_{1\mathbf{k}}^\dagger & \gamma_{2\mathbf{k}} \end{pmatrix} \begin{pmatrix} E_{1\mathbf{k}} & \\ & E_{2\mathbf{k}} \end{pmatrix} \begin{pmatrix} \gamma_{1\mathbf{k}} \\ \gamma_{2\mathbf{k}}^\dagger \end{pmatrix} \\ &= \sum_{\mathbf{k}} E_{1\mathbf{k}} \gamma_{1\mathbf{k}}^\dagger \gamma_{1\mathbf{k}} + E_{2\mathbf{k}} \gamma_{2\mathbf{k}} \gamma_{2\mathbf{k}}^\dagger \end{aligned} \tag{B.35}$$

The E_1 and E_2 are directly solved from the Hamiltonian matrix, so they will not change with the different definition of γ and $\gamma^\dagger$.

I have a look at this relation again,

$$\langle T_\tau \gamma_n \gamma_n^\dagger(\tau) \rangle = -f(E_n) e^{E_n \tau} \tag{B.36}$$

We need to pay attention to what do we insert here for E_n. In the textbook [6], they derived that for the free fermions, $E_n = \varepsilon_n c_n^\dagger c_n$. The quasi-particle we defined here are equivalent to non-interacting fermion. Thus for $\langle T_\tau \gamma_1 \gamma_1^\dagger(\tau) \rangle$ we insert E_1 while for $\langle T_\tau \gamma_2 \gamma_2^\dagger(\tau) \rangle$ we insert -E_2 (actually, we have already known that for this simple Hamiltonian there is $E_1 = -E_2$, so we can always insert E_1).

However, no one can stop us from using the 'strange' definition:

$$\begin{pmatrix} u_{\mathbf{k}} & v_{\mathbf{k}} \\ -v_{\mathbf{k}}^* & u_{\mathbf{k}}^* \end{pmatrix} \begin{pmatrix} c_{\mathbf{k}\uparrow} \\ c_{-\mathbf{k}\downarrow}^\dagger \end{pmatrix} = \begin{pmatrix} \gamma_{2\mathbf{k}}^\dagger \\ \gamma_{1\mathbf{k}} \end{pmatrix}, \tag{B.37}$$

where in the normal state there is $\gamma_{2\mathbf{k}}^\dagger = c_{\uparrow\mathbf{k}}$ and $\gamma_{1\mathbf{k}} = c_{\downarrow-\mathbf{k}}^\dagger$. This looks strange, but there is nothing wrong.

Then from the new definition, we write the Hamiltonian as

$$\begin{aligned} H_\gamma &= \sum_{\mathbf{k}} \begin{pmatrix} \gamma_{2\mathbf{k}} & \gamma_{1\mathbf{k}}^\dagger \end{pmatrix} \begin{pmatrix} E_{1\mathbf{k}} & \\ & E_{2\mathbf{k}} \end{pmatrix} \begin{pmatrix} \gamma_{2\mathbf{k}}^\dagger \\ \gamma_{1\mathbf{k}} \end{pmatrix} \\ &= \sum_{\mathbf{k}} E_{1\mathbf{k}} \gamma_{2\mathbf{k}} \gamma_{2\mathbf{k}}^\dagger + E_{2\mathbf{k}} \gamma_{1\mathbf{k}}^\dagger \gamma_{1\mathbf{k}} \end{aligned} \tag{B.38}$$

As I said above, $E_{1\mathbf{k}}$ and $E_{2\mathbf{k}}$ are not different from eq. (B.35) because they are diagonalized from the same matrix. However, here we should insert $E_{2\mathbf{k}}$ for $\langle T_\tau \gamma_1 \gamma_1^\dagger(\tau) \rangle$

and $-E_{1\mathbf{k}}$ for another. This also means that we can always insert $-E_{1\mathbf{k}}$ to this bra-ket.

Now let's see what happend to the Bogoliubov relation that we insert into the expression of spin susceptibility,

For the first definition,

$$\begin{aligned}\gamma_{1\mathbf{k}} &= u_{\mathbf{k}} c_{\mathbf{k}\uparrow} + v_{\mathbf{k}} c^{\dagger}_{-\mathbf{k}\downarrow} \\ \gamma^{\dagger}_{2\mathbf{k}} &= -v^{*}_{\mathbf{k}} c_{\mathbf{k}\uparrow} + u^{*}_{\mathbf{k}} c^{\dagger}_{-\mathbf{k}\downarrow}\end{aligned} \tag{B.39}$$

For another definition,

$$\begin{aligned}\gamma_{1\mathbf{k}} &= -v^{*}_{\mathbf{k}} c_{\mathbf{k}\uparrow} + u^{*}_{\mathbf{k}} c^{\dagger}_{-\mathbf{k}\downarrow} \\ \gamma^{\dagger}_{2\mathbf{k}} &= u_{\mathbf{k}} c_{\mathbf{k}\uparrow} + v_{\mathbf{k}} c^{\dagger}_{-\mathbf{k}\downarrow}\end{aligned} \tag{B.40}$$

We can observe that the two sets of Bogoliubov relations are replacing $u_{\mathbf{k}} \to -v^{*}_{\mathbf{k}}$ and $v_{\mathbf{k}} \to u^{*}_{\mathbf{k}}$. Since we have also changed the sign of the energy E_n we inserted, thus we can conclude this symmetry: $\{u_{\mathbf{k}}, v_{\mathbf{k}}, E_n \to -v^{*}_{\mathbf{k}}, u^{*}_{\mathbf{k}}, -E_n\}$. This symmetry is allowed when we insert them into the expression of spin susceptibility.

Sum over positive energy

For the first term in eq. (B.29), it can be written as

$$\begin{aligned}\frac{1}{\mathcal{N}}[&\sum_{E_{\mathbf{k}}>0}\sum_{E_{\mathbf{k+q}}>0}(-v^{*}_{\mathbf{k+q}}u_{\mathbf{k+q}}u^{*}_{\mathbf{k}}v_{\mathbf{k}} + |v_{\mathbf{k+q}}|^2|u_{\mathbf{k}}|^2)\frac{1-f(E_{\mathbf{k}\downarrow})-f(E_{\mathbf{k+q}\downarrow})}{i\omega_n + E_{\mathbf{k+q}\downarrow} + E_{\mathbf{k}\downarrow}} \\ &+ \sum_{E_{\mathbf{k}}>0}\sum_{E_{\mathbf{k+q}}<0}(-v^{*}_{\mathbf{k+q}}u_{\mathbf{k+q}}u^{*}_{\mathbf{k}}v_{\mathbf{k}} + |v_{\mathbf{k+q}}|^2|u_{\mathbf{k}}|^2)\frac{1-f(E_{\mathbf{k}\downarrow})-f(E_{\mathbf{k+q}\downarrow})}{i\omega_n + E_{\mathbf{k+q}\downarrow} + E_{\mathbf{k}\downarrow}} \\ &+ \sum_{E_{\mathbf{k}}<0}\sum_{E_{\mathbf{k+q}}>0}(-v^{*}_{\mathbf{k+q}}u_{\mathbf{k+q}}u^{*}_{\mathbf{k}}v_{\mathbf{k}} + |v_{\mathbf{k+q}}|^2|u_{\mathbf{k}}|^2)\frac{1-f(E_{\mathbf{k}\downarrow})-f(E_{\mathbf{k+q}\downarrow})}{i\omega_n + E_{\mathbf{k+q}\downarrow} + E_{\mathbf{k}\downarrow}} \\ &+ \sum_{E_{\mathbf{k}}<0}\sum_{E_{\mathbf{k+q}}<0}(-v^{*}_{\mathbf{k+q}}u_{\mathbf{k+q}}u^{*}_{\mathbf{k}}v_{\mathbf{k}} + |v_{\mathbf{k+q}}|^2|u_{\mathbf{k}}|^2)\frac{1-f(E_{\mathbf{k}\downarrow})-f(E_{\mathbf{k+q}\downarrow})}{i\omega_n + E_{\mathbf{k+q}\downarrow} + E_{\mathbf{k}\downarrow}}].\end{aligned} \tag{B.41}$$

We can use the symmetry $\{u_{\mathbf{k}}, v_{\mathbf{k}}, E_n \to -v^*_{\mathbf{k}}, u^*_{\mathbf{k}}, -E_n\}$, then the terms can be written as

$$\begin{aligned}\frac{1}{\mathcal{N}}\sum_{E_{\mathbf{k}}>0}\sum_{E_{\mathbf{k+q}}>0}[&(-v^*_{\mathbf{k+q}}u_{\mathbf{k+q}}u^*_{\mathbf{k}}v_{\mathbf{k}}+|v_{\mathbf{k+q}}|^2|u_{\mathbf{k}}|^2)\frac{1-f(E_{\mathbf{k}\downarrow})-f(E_{\mathbf{k+q}\downarrow})}{i\omega_n+E_{\mathbf{k+q}\downarrow}+E_{\mathbf{k}\downarrow}}\\&+(v^*_{\mathbf{k+q}}u_{\mathbf{k+q}}u^*_{\mathbf{k}}v_{\mathbf{k}}+|u_{\mathbf{k+q}}|^2|u_{\mathbf{k}}|^2)\frac{f(E_{\mathbf{k+q}\uparrow})-f(E_{\mathbf{k}\downarrow}))}{i\omega_n+E_{\mathbf{k}\downarrow}-E_{\mathbf{k+q}\uparrow}}\\&+(v^*_{\mathbf{k+q}}u_{\mathbf{k+q}}u^*_{\mathbf{k}}v_{\mathbf{k}}+|v_{\mathbf{k+q}}|^2|v_{\mathbf{k}}|^2)\frac{f(E_{\mathbf{k}\uparrow})-f(E_{\mathbf{k+q}\downarrow})}{i\omega_n+E_{\mathbf{k+q}\downarrow}-E_{\mathbf{k}\uparrow}}\\&+(-v^*_{\mathbf{k+q}}u_{\mathbf{k+q}}u^*_{\mathbf{k}}v_{\mathbf{k}}+|v_{\mathbf{k+q}}|^2|u_{\mathbf{k}}|^2)\frac{f(E_{\mathbf{k}\downarrow})+f(E_{\mathbf{k+q}\downarrow})-1}{i\omega_n-E_{\mathbf{k+q}\uparrow}-E_{\mathbf{k}\uparrow}}].\end{aligned} \tag{B.42}$$

The second term of eq. (B.29) can be written as

$$\begin{aligned}\frac{1}{\mathcal{N}}\sum_{E_{\mathbf{k}}>0}\sum_{E_{\mathbf{k+q}}>0}[&(v^*_{\mathbf{k+q}}u_{\mathbf{k+q}}u^*_{\mathbf{k}}v_{\mathbf{k}}+|v_{\mathbf{k+q}}|^2|v_{\mathbf{k}}|^2)\frac{f(E_{\mathbf{k}\uparrow})-f(E_{\mathbf{k+q}\downarrow})}{i\omega_n+E_{\mathbf{k+q}\downarrow}-E_{\mathbf{k}\uparrow}}\\&+(-v^*_{\mathbf{k+q}}u_{\mathbf{k+q}}u^*_{\mathbf{k}}v_{\mathbf{k}}+|u_{\mathbf{k+q}}|^2|v_{\mathbf{k}}|^2)\frac{f(E_{\mathbf{k}\uparrow})+f(E_{\mathbf{k}\uparrow})-1}{i\omega_n-E_{\mathbf{k+q}\uparrow}-E_{\mathbf{k}\uparrow}}\\&+(-v^*_{\mathbf{k+q}}u_{\mathbf{k+q}}u^*_{\mathbf{k}}v_{\mathbf{k}}+|v_{\mathbf{k+q}}|^2|v_{\mathbf{k}}|^2)\frac{1-f(E_{\mathbf{k}\downarrow})-f(E_{\mathbf{k+q}\downarrow})}{i\omega_n+E_{\mathbf{k+q}\downarrow}+E_{\mathbf{k}\downarrow}}\\&+(v^*_{\mathbf{k+q}}u_{\mathbf{k+q}}u^*_{\mathbf{k}}v_{\mathbf{k}}+|u_{\mathbf{k+q}}|^2|u_{\mathbf{k}}|^2)\frac{f(E_{\mathbf{k+q}\uparrow})-f(E_{\mathbf{k}\downarrow})}{i\omega_n+E_{\mathbf{k}\downarrow}-E_{\mathbf{k+q}\uparrow}}].\end{aligned} \tag{B.43}$$

The third term

$$\begin{aligned}\frac{1}{\mathcal{N}}\sum_{E_{\mathbf{k}}>0}\sum_{E_{\mathbf{k+q}}>0}[&(v^*_{\mathbf{k+q}}u_{\mathbf{k+q}}u^*_{\mathbf{k}}v_{\mathbf{k}}+|u_{\mathbf{k+q}}|^2|u_{\mathbf{k}}|^2)\frac{f(E_{\mathbf{k+q}\uparrow})-f(E_{\mathbf{k}\downarrow})}{i\omega_n+E_{\mathbf{k}\downarrow}-E_{\mathbf{k+q}\uparrow}}\\&+(-v^*_{\mathbf{k+q}}u_{\mathbf{k+q}}u^*_{\mathbf{k}}v_{\mathbf{k}}+|v_{\mathbf{k+q}}|^2|u_{\mathbf{k}}|^2)\frac{1-f(E_{\mathbf{k+q}\downarrow})-f(E_{\mathbf{k}\downarrow})}{i\omega_n+E_{\mathbf{k}\downarrow}+E_{\mathbf{k+q}\downarrow}}\\&+(-v^*_{\mathbf{k+q}}u_{\mathbf{k+q}}u^*_{\mathbf{k}}v_{\mathbf{k}}+|u_{\mathbf{k+q}}|^2|v_{\mathbf{k}}|^2)\frac{f(E_{\mathbf{k+q}\uparrow})+f(E_{\mathbf{k}\uparrow})-1}{i\omega_n-E_{\mathbf{k}\uparrow}-E_{\mathbf{k+q}\uparrow}}\\&+(v^*_{\mathbf{k+q}}u_{\mathbf{k+q}}u^*_{\mathbf{k}}v_{\mathbf{k}}+|v_{\mathbf{k+q}}|^2|v_{\mathbf{k}}|^2)\frac{f(E_{\mathbf{k}\uparrow})-f(E_{\mathbf{k+q}\downarrow})}{i\omega_n+E_{\mathbf{k+q}\downarrow}-E_{\mathbf{k}\uparrow}}].\end{aligned} \tag{B.44}$$

The last one,

$$\begin{aligned}\frac{1}{\mathcal{N}}\sum_{E_{\mathbf{k}}>0}\sum_{E_{\mathbf{k+q}}>0}[&(-v^*_{\mathbf{k+q}}u_{\mathbf{k+q}}u^*_{\mathbf{k}}v_{\mathbf{k}}+|u_{\mathbf{k+q}}|^2|v_{\mathbf{k}}|^2)\frac{f(E_{\mathbf{k}\uparrow})+f(E_{\mathbf{k+q}\uparrow})-1}{i\omega_n-E_{\mathbf{k+q}\uparrow}-E_{\mathbf{k}\uparrow}}\\&+(v^*_{\mathbf{k+q}}u_{\mathbf{k+q}}u^*_{\mathbf{k}}v_{\mathbf{k}}+|v_{\mathbf{k+q}}|^2|v_{\mathbf{k}}|^2)\frac{f(E_{\mathbf{k}\uparrow})-f(E_{\mathbf{k+q}\downarrow})}{i\omega_n+E_{\mathbf{k+q}\downarrow}-E_{\mathbf{k}\uparrow}}\\&+(v^*_{\mathbf{k+q}}u_{\mathbf{k+q}}u^*_{\mathbf{k}}v_{\mathbf{k}}+|u_{\mathbf{k+q}}|^2|u_{\mathbf{k}}|^2)\frac{f(E_{\mathbf{k+q}\uparrow})-f(E_{\mathbf{k}\downarrow})}{i\omega_n+E_{\mathbf{k}\downarrow}-E_{\mathbf{k+q}\uparrow}}\\&+(-v^*_{\mathbf{k+q}}u_{\mathbf{k+q}}u^*_{\mathbf{k}}v_{\mathbf{k}}+|v_{\mathbf{k+q}}|^2|u_{\mathbf{k}}|^2)\frac{1-f(E_{\mathbf{k}\downarrow})-f(E_{\mathbf{k+q}\downarrow})}{i\omega_n+E_{\mathbf{k+q}\downarrow}+E_{\mathbf{k}\downarrow}}].\end{aligned} \tag{B.45}$$

Combine them together,

$$\begin{aligned}\chi_0^{+-}(q,i\omega_n)=\frac{1}{\mathcal{N}}&\sum_{E_{\mathbf{k}}>0}\sum_{E_{\mathbf{k+q}}>0}\\&[(-4v^*_{\mathbf{k+q}}u_{\mathbf{k+q}}u^*_{\mathbf{k}}v_{\mathbf{k}}+4|v_{\mathbf{k+q}}|^2|u_{\mathbf{k}}|^2)\frac{1-f(E_{\mathbf{k}})-f(E_{\mathbf{k+q}})}{i\omega_n+E_{\mathbf{k+q}}+E_{\mathbf{k}}}\\&+(4v^*_{\mathbf{k+q}}u_{\mathbf{k+q}}u^*_{\mathbf{k}}v_{\mathbf{k}}4|v_{\mathbf{k+q}}|^2|v_{\mathbf{k}}|^2)\frac{f(E_{\mathbf{k}})-f(E_{\mathbf{k+q}})}{i\omega_n+E_{\mathbf{k+q}}-E_{\mathbf{k}}}\\&+(4v^*_{\mathbf{k+q}}u_{\mathbf{k+q}}u^*_{\mathbf{k}}v_{\mathbf{k}}+4|u_{\mathbf{k+q}}|^2|u_{\mathbf{k}}|^2)\frac{f(E_{\mathbf{k+q}})-f(E_{\mathbf{k}})}{i\omega_n+E_{\mathbf{k}}-E_{\mathbf{k+q}}}\\&+(-4v^*_{\mathbf{k+q}}u_{\mathbf{k+q}}u^*_{\mathbf{k}}v_{\mathbf{k}}+4|u_{\mathbf{k+q}}|^2|v_{\mathbf{k}}|^2)\frac{f(E_{\mathbf{k}})+f(E_{\mathbf{k+q}})-1}{i\omega_n-E_{\mathbf{k+q}}-E_{\mathbf{k}}}].\end{aligned} \tag{B.46}$$

Insert this relation to the expression above,

$$\begin{aligned}|u_{\mathbf{k}}|^2&=\frac{E_{\mathbf{k}}+\xi_{\mathbf{k}}}{2E_{\mathbf{k}}},\\|v_{\mathbf{k}}|^2&=\frac{E_{\mathbf{k}}-\xi_{\mathbf{k}}}{2E_{\mathbf{k}}}\\u^*_{\mathbf{k}}v_{\mathbf{k}}&=\frac{\Delta_{\mathbf{k}}}{2E_{\mathbf{k}}}\\u_{\mathbf{k}}v^*_{\mathbf{k}}&=\frac{\Delta^*_{\mathbf{k}}}{2E_{\mathbf{k}}},\end{aligned} \tag{B.47}$$

we get

$$
\begin{aligned}
4v^*_{\mathbf{k+q}}u_{\mathbf{k+q}}u^*_{\mathbf{k}}v_{\mathbf{k}} &= \frac{\Delta^*_{\mathbf{k+q}}\Delta_{\mathbf{k}}}{E_{\mathbf{k+q}}E_{\mathbf{k}}},\\
4|v_{\mathbf{k+q}}|^2|u_{\mathbf{k}}|^2 &= \left(1+\frac{-E_{\mathbf{k}}\xi_{\mathbf{k+q}}+E_{\mathbf{k+q}}\xi_{\mathbf{k}}-\xi_{\mathbf{k}}\xi_{\mathbf{k+q}}}{E_{\mathbf{k}}E_{\mathbf{k+q}}}\right),\\
4|u_{\mathbf{k+q}}|^2|v_{\mathbf{k}}|^2 &= \left(1+\frac{E_{\mathbf{k}}\xi_{\mathbf{k+q}}-E_{\mathbf{k+q}}\xi_{\mathbf{k}}-\xi_{\mathbf{k}}\xi_{\mathbf{k+q}}}{E_{\mathbf{k}}E_{\mathbf{k+q}}}\right),\\
4|v_{\mathbf{k+q}}|^2|v_{\mathbf{k}}|^2 &= \left(1+\frac{-E_{\mathbf{k}}\xi_{\mathbf{k+q}}-E_{\mathbf{k+q}}\xi_{\mathbf{k}}+\xi_{\mathbf{k}}\xi_{\mathbf{k+q}}}{E_{\mathbf{k}}E_{\mathbf{k+q}}}\right),\\
4|u_{\mathbf{k+q}}|^2|u_{\mathbf{k}}|^2 &= \left(1+\frac{E_{\mathbf{k}}\xi_{\mathbf{k+q}}+E_{\mathbf{k+q}}\xi_{\mathbf{k}}+\xi_{\mathbf{k}}\xi_{\mathbf{k+q}}}{E_{\mathbf{k}}E_{\mathbf{k+q}}}\right).
\end{aligned}
\tag{B.48}
$$

Insert these relations and finally we arrive at the form which only sums over the positive energy

$$
\begin{aligned}
\chi_0^{+-}(\mathbf{q},i\omega_n) = \frac{1}{\mathcal{N}}\sum_{\mathbf{k},E>0}\Bigg[&\left(1-\frac{\xi_{\mathbf{k}}\xi_{\mathbf{k+q}}+\Delta^*_{\mathbf{k+q}}\Delta_{\mathbf{k}}}{E_{\mathbf{k}}E_{\mathbf{k+q}}}\right)\frac{1-f(E_{\mathbf{k}})-f(E_{\mathbf{k+q}})}{i\omega_n+E_{\mathbf{k+q}}+E_{\mathbf{k}}}\\
&+\left(1-\frac{\xi_{\mathbf{k}}\xi_{\mathbf{k+q}}+\Delta^*_{\mathbf{k+q}}\Delta_{\mathbf{k}}}{E_{\mathbf{k}}E_{\mathbf{k+q}}}\right)\frac{f(E_{\mathbf{k}})+f(E_{\mathbf{k+q}})-1}{i\omega_n-E_{\mathbf{k+q}}-E_{\mathbf{k}}}\\
&+\left(1+\frac{\xi_{\mathbf{k}}\xi_{\mathbf{k+q}}+\Delta^*_{\mathbf{k+q}}\Delta_{\mathbf{k}}}{E_{\mathbf{k}}E_{\mathbf{k+q}}}\right)\frac{f(E_{\mathbf{k}})-f(E_{\mathbf{k+q}})}{i\omega_n+E_{\mathbf{k+q}}-E_{\mathbf{k}}}\\
&+\left(1+\frac{\xi_{\mathbf{k}}\xi_{\mathbf{k+q}}+\Delta^*_{\mathbf{k+q}}\Delta_{\mathbf{k}}}{E_{\mathbf{k}}E_{\mathbf{k+q}}}\right)\frac{f(E_{\mathbf{k+q}})-f(E_{\mathbf{k}})}{i\omega_n+E_{\mathbf{k}}-E_{\mathbf{k+q}}}\Bigg].
\end{aligned}
\tag{B.49}
$$

Appendix C

Derivation for the multi-band spin susceptibility

Now we start to calculate spin susceptibility,

$$\chi^{+-}_{\alpha\beta}(\mathbf{q},\tau) = \frac{1}{\mathcal{N}^2}\sum_{\mathbf{k}\mathbf{k}'}\langle T_\tau c^\dagger_{\alpha,\mathbf{k}+\mathbf{q}\uparrow} c_{\alpha,\mathbf{k}\downarrow} c^\dagger_{\beta,\mathbf{k}'-\mathbf{q}\downarrow}(\tau) c_{\beta,\mathbf{k}'\uparrow}(\tau)\rangle. \tag{C.1}$$

Wick's theorem gives two terms,

$$\begin{aligned}\chi^{+-}_{\alpha\beta}(\mathbf{q},\tau) = \frac{1}{\mathcal{N}}\sum_{\mathbf{k}}[&-\langle T_\tau c^\dagger_{\alpha,\mathbf{k}+\mathbf{q}\uparrow} c^\dagger_{\beta,-\mathbf{k}-\mathbf{q}\downarrow}(\tau)\rangle\langle T_\tau c_{\alpha,\mathbf{k}\downarrow} c_{\beta,-\mathbf{k}\uparrow}(\tau)\rangle \\ &+\langle T_\tau c^\dagger_{\alpha,\mathbf{k}+\mathbf{q}\uparrow} c_{\beta,\mathbf{k}+\mathbf{q}\uparrow}(\tau)\rangle\langle T_\tau c_{\alpha,\mathbf{k}\downarrow} c^\dagger_{\beta,\mathbf{k}\downarrow}(\tau)\rangle].\end{aligned} \tag{C.2}$$

The first term

$$
\begin{aligned}
&-\frac{1}{\mathcal{N}}\sum_{\mathbf{k}}\langle T_\tau c^\dagger_{\alpha,\mathbf{k}+\mathbf{q}\uparrow}c^\dagger_{\beta,-\mathbf{k}-\mathbf{q}\downarrow}(\tau)\rangle\langle T_\tau c_{\alpha,\mathbf{k}\downarrow}c_{\beta,-\mathbf{k}\uparrow}(\tau)\rangle\\
=&-\frac{1}{\mathcal{N}}\sum_{\mathbf{k},m_1\sim m_4}\langle T_\tau[u_{\alpha,m_1,\mathbf{k}+\mathbf{q}}\gamma^\dagger_{m_1,\mathbf{k}+\mathbf{q}\uparrow}-v^*_{\alpha,m_1,\mathbf{k}+\mathbf{q}}\gamma_{m_1,-\mathbf{k}-\mathbf{q}\downarrow}][v^*_{\beta,m_2,\mathbf{k}+\mathbf{q}}\gamma_{m_2,\mathbf{k}+\mathbf{q}\uparrow}(\tau)\\
&+u_{\beta,m_2,\mathbf{k}+\mathbf{q}}\gamma^\dagger_{m_2,-\mathbf{k}-\mathbf{q}\downarrow}(\tau)]\rangle\cdot\langle T_\tau[u^*_{\alpha,m_3,\mathbf{k}}\gamma_{m_3,\mathbf{k}\downarrow}+v_{\alpha,m_3,\mathbf{k}}\gamma^\dagger_{m_3,-\mathbf{k}\uparrow}][u^*_{\beta,m_4,\mathbf{k}}\gamma_{m_4,-\mathbf{k}\uparrow}(\tau)\\
&-v_{\beta,m_4,\mathbf{k}}\gamma^\dagger_{m_4,\mathbf{k}\downarrow}(\tau)]\rangle\\
=&-\frac{1}{\mathcal{N}}\sum_{\mathbf{k},m,m'}[u_{\alpha,m,\mathbf{k}+\mathbf{q}}v^*_{\beta,m,\mathbf{k}+\mathbf{q}}\langle T_\tau\gamma^\dagger_{m,\mathbf{k}+\mathbf{q}\uparrow}\gamma_{m,\mathbf{k}+\mathbf{q}\uparrow}(\tau)\rangle-v^*_{\alpha,m,\mathbf{k}+\mathbf{q}}u_{\beta,m,\mathbf{k}+\mathbf{q}}\langle T_\tau\gamma_{m,-\mathbf{k}-\mathbf{q}\downarrow}\gamma^\dagger_{m,-\mathbf{k}-\mathbf{q}\downarrow}(\tau)\rangle]\\
&\times[-u^*_{\alpha,m',\mathbf{k}}v_{\beta,m',\mathbf{k}}\langle T_\tau\gamma_{m',\mathbf{k}\downarrow}\gamma^\dagger_{m',\mathbf{k}\downarrow}(\tau)\rangle+v_{\alpha,m',\mathbf{k}}u^*_{\beta,m',\mathbf{k}}\langle T_\tau\gamma^\dagger_{m',-\mathbf{k}\uparrow}\gamma_{m',-\mathbf{k}\uparrow}(\tau)\rangle]\\
=&\frac{1}{\mathcal{N}}\sum_{\mathbf{k},m,m'}[u_{\alpha,m,\mathbf{k}+\mathbf{q}}v^*_{\beta,m,\mathbf{k}+\mathbf{q}}u^*_{\alpha,m',\mathbf{k}}v_{\beta,m',\mathbf{k}}\langle T_\tau\gamma^\dagger_{m,\mathbf{k}+\mathbf{q}\uparrow}\gamma_{m,\mathbf{k}+\mathbf{q}\uparrow}(\tau)\rangle\langle T_\tau\gamma_{m',\mathbf{k}\downarrow}\gamma^\dagger_{m',\mathbf{k}\downarrow}(\tau)\rangle\\
&-u_{\alpha,m,\mathbf{k}+\mathbf{q}}v^*_{\beta,m,\mathbf{k}+\mathbf{q}}v_{\alpha,m',\mathbf{k}}u^*_{\beta,m',\mathbf{k}}\langle T_\tau\gamma^\dagger_{m,\mathbf{k}+\mathbf{q}\uparrow}\gamma_{m,\mathbf{k}+\mathbf{q}\uparrow}(\tau)\rangle\langle T_\tau\gamma^\dagger_{m',-\mathbf{k}\uparrow}\gamma_{m',-\mathbf{k}\uparrow}(\tau)\rangle\\
&-v^*_{\alpha,m,\mathbf{k}+\mathbf{q}}u_{\beta,m,\mathbf{k}+\mathbf{q}}u^*_{\alpha,m',\mathbf{k}}v_{\beta,m',\mathbf{k}}\langle T_\tau\gamma_{m,-\mathbf{k}-\mathbf{q}\downarrow}\gamma^\dagger_{m,-\mathbf{k}-\mathbf{q}\downarrow}(\tau)\rangle\langle T_\tau\gamma_{m',\mathbf{k}\downarrow}\gamma^\dagger_{m',\mathbf{k}\downarrow}(\tau)\rangle\\
&+v^*_{\alpha,m,\mathbf{k}+\mathbf{q}}u_{\beta,m,\mathbf{k}+\mathbf{q}}v_{\alpha,m',\mathbf{k}}u^*_{\beta,m',\mathbf{k}}\langle T_\tau\gamma_{m,-\mathbf{k}-\mathbf{q}\downarrow}\gamma^\dagger_{m,-\mathbf{k}-\mathbf{q}\downarrow}(\tau)\rangle\langle T_\tau\gamma^\dagger_{m',-\mathbf{k}\uparrow}\gamma_{m',-\mathbf{k}\uparrow}(\tau)\rangle]
\end{aligned}
\tag{C.3}
$$

with the relations Eq (B.21) again, we can get

$$
\begin{aligned}
=&\frac{1}{\mathcal{N}}\sum_{\mathbf{k},m,m'}[-v^*_{\alpha,m,\mathbf{k}+\mathbf{q}}u_{\beta,m,\mathbf{k}+\mathbf{q}}u^*_{\alpha,m',\mathbf{k}}v_{\beta,m',\mathbf{k}}f(E_{\mathbf{k}+\mathbf{q},m})f(E_{\mathbf{k},m'})e^{E_{\mathbf{k},m'}+E_{\mathbf{k}+\mathbf{q},m}\tau}\\
&+u_{\alpha,m,\mathbf{k}+\mathbf{q}}v^*_{\beta,m,\mathbf{k}+\mathbf{q}}u^*_{\alpha,m',\mathbf{k}}v_{\beta,m',\mathbf{k}}f(E_{\mathbf{k},m'})(1-f(E_{\mathbf{k}+\mathbf{q},m}))e^{E_{\mathbf{k},m'}-E_{\mathbf{k}+\mathbf{q},m}\tau}\\
&+v^*_{\alpha,m,\mathbf{k}+\mathbf{q}}u_{\beta,m,\mathbf{k}+\mathbf{q}}v_{\alpha,m',\mathbf{k}}u^*_{\beta,m',\mathbf{k}}f(E_{\mathbf{k}+\mathbf{q},m})(1-f(E_{\mathbf{k},m'}))e^{(E_{\mathbf{k}+\mathbf{q},m}-E_{\mathbf{k},m'})\tau}\\
&-u_{\alpha,m,\mathbf{k}+\mathbf{q}}v^*_{\beta,m,\mathbf{k}+\mathbf{q}}v_{\alpha,m',\mathbf{k}}u^*_{\beta,m',\mathbf{k}}(1-f(E_{\mathbf{k}+\mathbf{q},m})(1-f(E_{\mathbf{k},m'})))e^{-(E_{\mathbf{k}+\mathbf{q},m}+E_{\mathbf{k},m'})\tau}].
\end{aligned}
\tag{C.4}
$$

And follow the same steps as Appendix B, we can write the first term of spin susceptibility as

$$
\begin{aligned}
=&\frac{1}{\mathcal{N}}\sum_{\mathbf{k},m,m'}[-v^*_{\alpha,m,\mathbf{k}+\mathbf{q}}u_{\beta,m,\mathbf{k}+\mathbf{q}}u^*_{\alpha,m',\mathbf{k}}v_{\beta,m',\mathbf{k}}\frac{1-f(E_{\mathbf{k}+\mathbf{q},m})-f(E_{\mathbf{k},m'})}{i\omega_n+E_{\mathbf{k}+\mathbf{q},m}+E_{\mathbf{k},m'}}\\
&+u_{\alpha,m,\mathbf{k}+\mathbf{q}}v^*_{\beta,m,\mathbf{k}+\mathbf{q}}u^*_{\alpha,m',\mathbf{k}}v_{\beta,m',\mathbf{k}}\frac{f(E_{\mathbf{k}+\mathbf{q},m})-f(E_{\mathbf{k},m'})}{i\omega_n+E_{\mathbf{k},m'}-E_{\mathbf{k}+\mathbf{q},m}}\\
&+v^*_{\alpha,m,\mathbf{k}+\mathbf{q}}u_{\beta,m,\mathbf{k}+\mathbf{q}}v_{\alpha,m',\mathbf{k}}u^*_{\beta,m',\mathbf{k}}\frac{f(E_{\mathbf{k},m'})-f(E_{\mathbf{k}+\mathbf{q},m})}{i\omega_n+E_{\mathbf{k}+\mathbf{q},m}-E_{\mathbf{k},m'}}\\
&-u_{\alpha,m,\mathbf{k}+\mathbf{q}}v^*_{\beta,m,\mathbf{k}+\mathbf{q}}v_{\alpha,m',\mathbf{k}}u^*_{\beta,m',\mathbf{k}}\frac{f(E_{\mathbf{k}+\mathbf{q},m})+f(E_{\mathbf{k},m'})-1}{i\omega_n-E_{\mathbf{k}+\mathbf{q},m}-E_{\mathbf{k},m'}}].
\end{aligned}
\tag{C.5}
$$

Let's calculate the second term,

$$
\begin{aligned}
&\frac{1}{\mathcal{N}}\sum_{\mathbf{k}}\langle T_\tau c^\dagger_{\alpha,\mathbf{k}+\mathbf{q}\uparrow}c_{\beta,\mathbf{k}+\mathbf{q}\uparrow}(\tau)\rangle\langle T_\tau c_{\alpha,\mathbf{k}\downarrow}c^\dagger_{\beta,\mathbf{k}\downarrow}(\tau)\rangle\\
=&\frac{1}{\mathcal{N}}\sum_{\mathbf{k},m_1\sim m_4}\langle T_\tau[u_{\alpha,m_1,\mathbf{k}+\mathbf{q}}\gamma^\dagger_{m_1,\mathbf{k}+\mathbf{q}\uparrow}-v^*_{\alpha,m_1,\mathbf{k}+\mathbf{q}}\gamma_{m_1,-\mathbf{k}-\mathbf{q}\downarrow}][u^*_{\beta,m_2,\mathbf{k}+\mathbf{q}}\gamma_{m_2,\mathbf{k}+\mathbf{q}\uparrow}(\tau)\\
&-v_{\beta,m_2,\mathbf{k}+\mathbf{q}}\gamma^\dagger_{m_2,-\mathbf{k}-\mathbf{q}\downarrow}(\tau)]\rangle\cdot\langle T_\tau[v_{\alpha,m_3,\mathbf{k}}\gamma^\dagger_{m_3,-\mathbf{k}\uparrow}+u^*_{\alpha,m_3,\mathbf{k}}\gamma_{m_3,\mathbf{k}\downarrow}][v^*_{\beta,m_4,\mathbf{k}}\gamma_{m_4,-\mathbf{k}\uparrow}(\tau)\\
&+u_{\beta,m_4,\mathbf{k}}\gamma^\dagger_{m_4,\mathbf{k}\downarrow}(\tau)]\rangle\\
=&\frac{1}{\mathcal{N}}\sum_{\mathbf{k},m,m'}[u_{\alpha,m,\mathbf{k}+\mathbf{q}}u^*_{\beta,m,\mathbf{k}+\mathbf{q}}\langle T_\tau\gamma^\dagger_{m,\mathbf{k}+\mathbf{q}\uparrow}\gamma_{m,\mathbf{k}+\mathbf{q}\uparrow}(\tau)\rangle+v^*_{\alpha,m,\mathbf{k}+\mathbf{q}}v_{\beta,m,\mathbf{k}+\mathbf{q}}\langle T_\tau\gamma_{m,-\mathbf{k}-\mathbf{q}\downarrow}\gamma^\dagger_{m,-\mathbf{k}-\mathbf{q}\downarrow}(\tau)\rangle]\\
&\times[v_{\alpha,m',\mathbf{k}}v^*_{\beta,m',\mathbf{k}}\langle T_\tau\gamma^\dagger_{m',-\mathbf{k}\uparrow}\gamma_{m',-\mathbf{k}\uparrow}(\tau)\rangle+u^*_{\alpha,m',\mathbf{k}}u_{\beta,m',\mathbf{k}}\langle T_\tau\gamma_{m',\mathbf{k}\downarrow}\gamma^\dagger_{m',\mathbf{k}\downarrow}(\tau)\rangle]\\
=&\frac{1}{\mathcal{N}}\sum_{\mathbf{k},m,m'}[u_{\alpha,m,\mathbf{k}+\mathbf{q}}u^*_{\beta,m,\mathbf{k}+\mathbf{q}}v_{\alpha,m',\mathbf{k}}v^*_{\beta,m',\mathbf{k}}\langle T_\tau\gamma^\dagger_{m,\mathbf{k}+\mathbf{q}\uparrow}\gamma_{m,\mathbf{k}+\mathbf{q}\uparrow}(\tau)\rangle\langle T_\tau\gamma^\dagger_{m',-\mathbf{k}\uparrow}\gamma_{m',-\mathbf{k}\uparrow}(\tau)\rangle\\
&+u_{\alpha,m,\mathbf{k}+\mathbf{q}}u^*_{\beta,m,\mathbf{k}+\mathbf{q}}u^*_{\alpha,m',\mathbf{k}}u_{\beta,m',\mathbf{k}}\langle T_\tau\gamma^\dagger_{m,\mathbf{k}+\mathbf{q}\uparrow}\gamma_{m,\mathbf{k}+\mathbf{q}\uparrow}(\tau)\rangle\langle T_\tau\gamma_{m',\mathbf{k}\downarrow}\gamma^\dagger_{m',\mathbf{k}\downarrow}(\tau)\rangle\\
&+v^*_{\alpha,m,\mathbf{k}+\mathbf{q}}v_{\beta,m,\mathbf{k}+\mathbf{q}}v_{\alpha,m',\mathbf{k}}v^*_{\beta,m',\mathbf{k}}\langle T_\tau\gamma_{m,-\mathbf{k}-\mathbf{q}\downarrow}\gamma^\dagger_{m,-\mathbf{k}-\mathbf{q}\downarrow}(\tau)\rangle\langle T_\tau\gamma^\dagger_{m',-\mathbf{k}\uparrow}\gamma_{m',-\mathbf{k}\uparrow}(\tau)\rangle\\
&+v^*_{\alpha,m,\mathbf{k}+\mathbf{q}}v_{\beta,m,\mathbf{k}+\mathbf{q}}u^*_{\alpha,m',\mathbf{k}}u_{\beta,m',\mathbf{k}}\langle T_\tau\gamma_{m,-\mathbf{k}-\mathbf{q}\downarrow}\gamma^\dagger_{m,-\mathbf{k}-\mathbf{q}\downarrow}(\tau)\rangle\langle T_\tau\gamma_{m',\mathbf{k}\downarrow}\gamma^\dagger_{m',\mathbf{k}\downarrow}(\tau)\rangle],
\end{aligned}
\tag{C.6}
$$

then

$$
\begin{aligned}
=&\frac{1}{\mathcal{N}}\sum_{\mathbf{k},m,m'}[u_{\alpha,m,\mathbf{k}+\mathbf{q}}u^*_{\beta,m,\mathbf{k}+\mathbf{q}}v_{\alpha,m',\mathbf{k}}v^*_{\beta,m',\mathbf{k}}(1-f(E_{\mathbf{k}+\mathbf{q},m}))(1-f(E_{\mathbf{k},m'}))e^{-(E_{\mathbf{k}+\mathbf{q},m}+E_{\mathbf{k},m'})\tau}\\
&+u_{\alpha,m,\mathbf{k}+\mathbf{q}}u^*_{\beta,m,\mathbf{k}+\mathbf{q}}u^*_{\alpha,m',\mathbf{k}}u_{\beta,m',\mathbf{k}}f(E_{\mathbf{k},m'})(1-f(E_{\mathbf{k}+\mathbf{q},m}))e^{(E_{\mathbf{k},m'}-E_{\mathbf{k}+\mathbf{q},m})\tau}\\
&+v^*_{\alpha,m,\mathbf{k}+\mathbf{q}}v_{\beta,m,\mathbf{k}+\mathbf{q}}v_{\alpha,m',\mathbf{k}}v^*_{\beta,m',\mathbf{k}}f(E_{\mathbf{k}+\mathbf{q},m})(1-f(E_{\mathbf{k},m'}))e^{(E_{\mathbf{k}+\mathbf{q},m}-E_{\mathbf{k},m'})\tau}\\
&+v^*_{\alpha,m,\mathbf{k}+\mathbf{q}}v_{\beta,m,\mathbf{k}+\mathbf{q}}u^*_{\alpha,m',\mathbf{k}}u_{\beta,m',\mathbf{k}}f(E_{\mathbf{k}+\mathbf{q},m})f(E_{\mathbf{k},m'})e^{(E_{\mathbf{k},m'}+E_{\mathbf{k}+\mathbf{q},m})\tau}].
\end{aligned}
\tag{C.7}
$$

And finally this term yields

$$
\begin{aligned}
=&\frac{1}{\mathcal{N}}\sum_{\mathbf{k},m,m'}[v^*_{\alpha,m,\mathbf{k}+\mathbf{q}}v_{\beta,m,\mathbf{k}+\mathbf{q}}u^*_{\alpha,m',\mathbf{k}}u_{\beta,m',\mathbf{k}}\frac{1-f(E_{\mathbf{k}+\mathbf{q},m})-f(E_{\mathbf{k},m'})}{i\omega_n+E_{\mathbf{k}+\mathbf{q},m}+E_{\mathbf{k},m'}}\\
&+u_{\alpha,m,\mathbf{k}+\mathbf{q}}u^*_{\beta,m,\mathbf{k}+\mathbf{q}}u^*_{\alpha,m',\mathbf{k}}u_{\beta,m',\mathbf{k}}\frac{f(E_{\mathbf{k}+\mathbf{q},m})-f(E_{\mathbf{k},m'})}{i\omega_n+E_{\mathbf{k},m'}-E_{\mathbf{k}+\mathbf{q},m}}\\
&+v^*_{\alpha,m,\mathbf{k}+\mathbf{q}}v_{\beta,m,\mathbf{k}+\mathbf{q}}v_{\alpha,m',\mathbf{k}}v^*_{\beta,m',\mathbf{k}}\frac{f(E_{\mathbf{k},m'})-f(E_{\mathbf{k}+\mathbf{q},m})}{i\omega_n+E_{\mathbf{k}+\mathbf{q},m}-E_{\mathbf{k},m'}}\\
&+u_{\alpha,m,\mathbf{k}+\mathbf{q}}u^*_{\beta,m,\mathbf{k}+\mathbf{q}}v_{\alpha,m',\mathbf{k}}v^*_{\beta,m',\mathbf{k}}\frac{f(E_{\mathbf{k}+\mathbf{q},m})+f(E_{\mathbf{k},m'})-1}{i\omega_n-E_{\mathbf{k}+\mathbf{q},m}-E_{\mathbf{k},m'}}].
\end{aligned}
\tag{C.8}
$$

By combining the two terms together, finally we get the expression for the spin

susceptibility of the kagome lattice

$$
\begin{aligned}
&\chi^{+-}_{\alpha\beta}(\mathbf{q},\tau)\\
=&\frac{1}{\mathcal{N}}\sum_{\mathbf{k},m,m'}\Big[\big(v^{*}_{\alpha,m,\mathbf{k+q}}v_{\beta,m,\mathbf{k+q}}u^{*}_{\alpha,m',\mathbf{k}}u_{\beta,m',\mathbf{k}}-v^{*}_{\alpha,m,\mathbf{k+q}}u_{\beta,m,\mathbf{k+q}}u^{*}_{\alpha,m',\mathbf{k}}v_{\beta,m',\mathbf{k}}\big)\frac{1-f(E_{\mathbf{k+q},m})-f(E_{\mathbf{k},m'})}{i\omega_n+E_{\mathbf{k+q},m}+E_{\mathbf{k},m'}}\\
&+\big(u_{\alpha,m,\mathbf{k+q}}u^{*}_{\beta,m,\mathbf{k+q}}u^{*}_{\alpha,m',\mathbf{k}}u_{\beta,m',\mathbf{k}}+u_{\alpha,m,\mathbf{k+q}}v^{*}_{\beta,m,\mathbf{k+q}}u^{*}_{\alpha,m',\mathbf{k}}v_{\beta,m',\mathbf{k}}\big)\frac{f(E_{\mathbf{k+q},m})-f(E_{\mathbf{k},m'})}{i\omega_n+E_{\mathbf{k},m'}-E_{\mathbf{k+q},m}}\\
&+\big(v^{*}_{\alpha,m,\mathbf{k+q}}v_{\beta,m,\mathbf{k+q}}v_{\alpha,m',\mathbf{k}}v^{*}_{\beta,m',\mathbf{k}}+v^{*}_{\alpha,m,\mathbf{k+q}}u_{\beta,m,\mathbf{k+q}}v_{\alpha,m',\mathbf{k}}u^{*}_{\beta,m',\mathbf{k}}\big)\frac{f(E_{\mathbf{k},m'})-f(E_{\mathbf{k+q},m})}{i\omega_n+E_{\mathbf{k+q},m}-E_{\mathbf{k},m'}}\\
&+\big(u_{\alpha,m,\mathbf{k+q}}u^{*}_{\beta,m,\mathbf{k+q}}v_{\alpha,m',\mathbf{k}}v^{*}_{\beta,m',\mathbf{k}}-u_{\alpha,m,\mathbf{k+q}}v^{*}_{\beta,m,\mathbf{k+q}}v_{\alpha,m',\mathbf{k}}u^{*}_{\beta,m',\mathbf{k}}\big)\frac{f(E_{\mathbf{k+q},m})+f(E_{\mathbf{k},m'})-1}{i\omega_n-E_{\mathbf{k+q},m}-E_{\mathbf{k},m'}}\Big].
\end{aligned}
\tag{C.9}
$$

Appendix D

Summing over sublattice indices

One dimensional chain model

In the previous appendices, we derived the general expression for spin susceptibility. In the monoatomic lattice systems such as the square lattice, we can easily calculate the spin susceptibility without thinking about the sublattice indices. However, when there are sublattice indices in the system, we have to consider how the summation over sublattice indices works, since in the end we only want to get one value of the relaxation rate rather than a matrix. It is hard to directly illustrate the summation in the kagome lattice, but we can start with an easy one-dimensional chain model.

We assume nearest neighbor interaction. The Hamiltonian of the 1D chain model is

$$\mathcal{H} = -t \sum_{r=0,a,2a,\ldots} c_r^\dagger c_{r+a} + H.C. + \mu \sum_{r=0,a,2a,\ldots} c_r^\dagger c_r. \tag{D.1}$$

Define Fourier transformation

$$c_r^\dagger = \frac{1}{\sqrt{\mathcal{V}}} \sum_k c_k^\dagger e^{-ikr}; \quad c_r = \frac{1}{\sqrt{\mathcal{V}}} \sum_k c_k e^{ikr}. \tag{D.2}$$

The Hamiltonian after Fourier transformation is

$$\begin{aligned} \mathcal{H} &= -t \sum_k c_k^\dagger c_k e^{ika} + c_k^\dagger c_k e^{-ika} + \mu \sum_k c_k^\dagger c_k \\ &= \left(2t\cos(ka) + \mu\right) c_k^\dagger c_k \end{aligned} \tag{D.3}$$

Now we consider another case. If we label the particles in this lattice as A and B like this

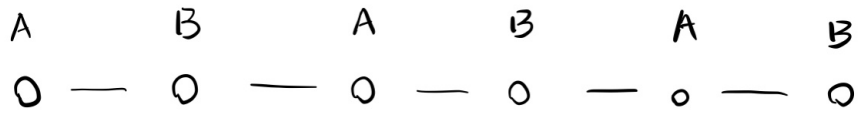

Even though there can be no difference between these two kinds of particles, we can still do so. We can think of two ways of defining the unit cell. The first one is to define each single particle as a unit cell.

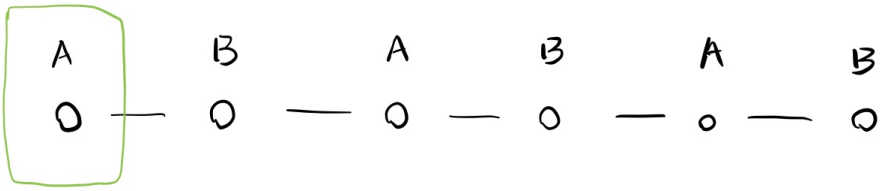

The Hamiltonian can be written as

$$\mathcal{H} = -t \sum_{r=0,2a,4a,\ldots} c^\dagger_{r,A} c_{r+a,B} + c^\dagger_{r+a,B} c_{r+2a,A} + H.C. + \mu \sum_{r=0,a,2a,\ldots} c^\dagger_r c_r. \tag{D.4}$$

The Fourier transformation with this unit cell is

$$c^\dagger_r = \frac{1}{\sqrt{\mathcal{V}}} \sum_k c^\dagger_k e^{-ikr}; \quad c_r = \frac{1}{\sqrt{\mathcal{V}}} \sum_k c_k e^{ikr}. \tag{D.5}$$

then the Hamiltonian under momentum basis is

$$\mathcal{H} = -\frac{t}{2} \sum_k c^\dagger_{k,A} c_{k,B} e^{ika} + c^\dagger_{k,B} c_{k,A} e^{ika} + c^\dagger_{k,B} c_{k,A} e^{-ika} + c^\dagger_{k,A} c_{k,B} e^{-ika} + \frac{\mu}{2} (c^\dagger_{k,A} c_{k,A} + c^\dagger_{k,B} c_{k,B}), \tag{D.6}$$

it can be written in matrix form

$$\mathcal{H} = \begin{pmatrix} c^\dagger_{k,A} & c^\dagger_{k,B} \end{pmatrix} \begin{pmatrix} \mu/2 & t\cos(ka) \\ t\cos(ka) & \mu/2 \end{pmatrix} \begin{pmatrix} c_{k,A} \\ c_{k,B} \end{pmatrix}. \tag{D.7}$$

The period is $\Delta k = \frac{2\pi}{a}$.
However, there are different ways of choosing unit cells, for example,

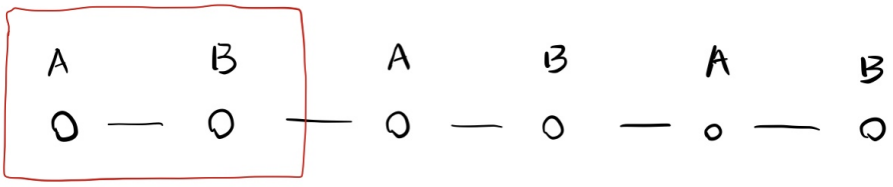

of which the unit cells consist of two particles. The Hamiltonian is

$$\mathcal{H} = -t \sum_{r=0,2a,4a,\ldots} c^{\dagger}_{r,A'} c_{r,B'} + c^{\dagger}_{r,B'} c_{r+2a,A'} + H.C. + \mu \sum_{r=0,a,2a,\ldots} c^{\dagger}_{r} c_{r}. \tag{D.8}$$

After Fourier transformation,

$$\mathcal{H} = -\frac{t}{2} \sum_{k} c^{\dagger}_{k,A'} c_{k,B'} + c^{\dagger}_{k,B'} c_{k,A'} e^{2ika} + c^{\dagger}_{k,B'} c_{k,A'} + c^{\dagger}_{k,A'} c_{k,B'} e^{-2ika} + \frac{\mu}{2} (c^{\dagger}_{k,A} c_{k,A} + c^{\dagger}_{k,B} c_{k,B}), \tag{D.9}$$

in the matrix form

$$\mathcal{H} = \begin{pmatrix} c^{\dagger}_{k,A'} & c^{\dagger}_{k,B'} \end{pmatrix} \begin{pmatrix} \mu/2 & (t/2)(1+e^{-2ika}) \\ (t/2)(1+e^{2ika}) & \mu/2 \end{pmatrix} \begin{pmatrix} c_{k,A'} \\ c_{k,B'} \end{pmatrix}. \tag{D.10}$$

The period in momentum space is smaller, $\Delta k = \frac{\pi}{a}$ The two matrix representations of Hamiltonian in eq. (D.7) and eq.D.10) can be transformed to each other by a unitary transformation

$$U = \begin{pmatrix} e^{-i\frac{1}{2}ka} & 0 \\ 0 & e^{i\frac{1}{2}ka} \end{pmatrix} \tag{D.11}$$

Now let's discuss the q sum over spin susceptibility. When doing the sum, we want to sum over each particles separately, i.e., the unit cells only contain one single particle. So the first form of Hamiltonian can provide correct result for eigenvectors, while the second one will lose the information of the relative phase inside the unit cell.

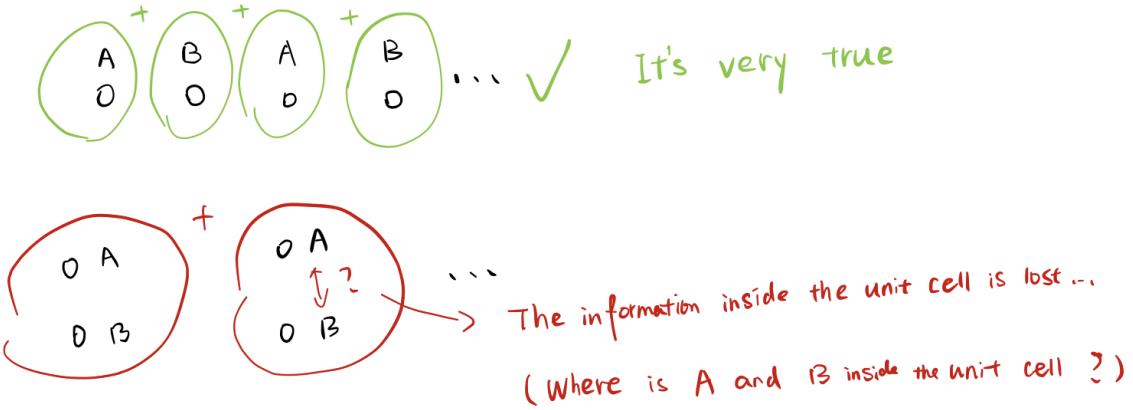

However, the period of the eigenvectors are smaller under the second basis, which means we can calculate fewer momentum space points in order to obtain the physical properties. We write the 'sublattice indices' in the second unit cell as A' and B', which means they are different from the original 'physical' sublattice indices A and B.

When we calculate the physical properties, we should do the unitary transformation to transform the basis back to the original sublattice indices A and B.

Spin susceptibility

What we are interested in is the nuclear relaxation rate. When we calculate the relaxation rate, we sum over q for spin susceptibility $\chi(q,\omega)$. Since in the real experiment, one can only measure one value for the relaxation rate rather than a matrix with sublattice indices, we want to check what operation will recover the value of spin susceptibility $\chi(q,\omega)$ without sublattice indices from the matrix $\chi_{\alpha\beta}(q,\omega)$.

Monoatomic lattice

For the lattice without sublattice indices, spin susceptibility is easily calculated from Lindhard function

$$\chi_0^{+-}(q,\omega) = \sum_k \frac{f(E_k) - f(E_{k+q})}{\omega + E_{k+q} - E_k + i\eta} \tag{D.12}$$

where $E(k) = 2t\cos(ka) + \mu$

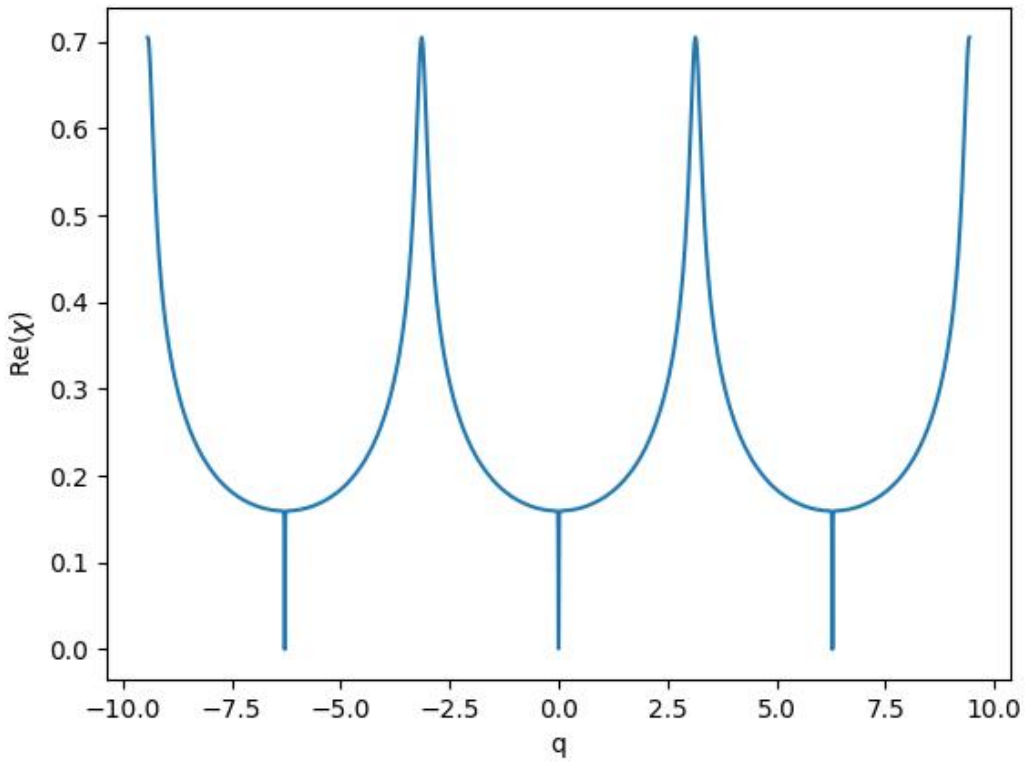

Unit cell with a single atom

Now let's look at the 'wrongly' labeled chain with sublattice indices A and B and see how does the spin susceptibility reduces to the single type particle case. The Hamiltonian in the matrix form is shown in eq. (D.7), and we can define the matrix

$$H = \begin{pmatrix} \mu/2 & t\cos(ka) \\ t\cos(ka) & \mu/2 \end{pmatrix} \tag{D.13}$$

The eigenvalues and eigenvectors of the matrix are

$$\begin{aligned} E_{k,1} &= \frac{\mu}{2} - t\cos(ka) \\ E_{k,2} &= \frac{\mu}{2} + t\cos(ka) \\ \mathbf{v} &= \begin{pmatrix} u_{A,1} & u_{A,2} \\ u_{B,1} & u_{B,2} \end{pmatrix} = \frac{1}{\sqrt{2}} \begin{pmatrix} -1 & 1 \\ 1 & 1 \end{pmatrix}. \end{aligned} \tag{D.14}$$

The spin susceptibility with sublattice indices are

$$\chi^{+-}_{\alpha\beta}(q, i\omega_n) = \frac{1}{\mathcal{V}} \sum_k \sum_{m,m'} u^*_{\alpha,m,k+q} u_{\beta,m,k+q} u_{\alpha,m',k} u^*_{\beta,m',k} \frac{f(E_{k+q,m}) - f(E_{k,m'})}{i\omega_n + E_{k,m'} - E_{k+q,m}}. \tag{D.15}$$

Then the four elements are

$$\begin{aligned} \chi^{+-}_{AA}(q, i\omega_n) =& \frac{1}{\mathcal{V}} \sum_k \Big(u^*_{A,1,k+q} u_{A,1,k+q} u_{A,1,k} u^*_{A,1,k} \frac{f(E_{k+q,1}) - f(E_{k,1})}{i\omega_n + E_{k,1} - E_{k+q,1}} \\ &+ u^*_{A,1,k+q} u_{A,1,k+q} u_{A,2,k} u^*_{A,2,k} \frac{f(E_{k+q,1}) - f(E_{k,2})}{i\omega_n + E_{k,2} - E_{k+q,1}} \\ &+ u^*_{A,2,k+q} u_{A,2,k+q} u_{A,1,k} u^*_{A,1,k} \frac{f(E_{k+q,2}) - f(E_{k,1})}{i\omega_n + E_{k,1} - E_{k+q,2}} \\ &+ u^*_{A,2,k+q} u_{A,2,k+q} u_{A,2,k} u^*_{A,2,k} \frac{f(E_{k+q,2}) - f(E_{k,2})}{i\omega_n + E_{k,2} - E_{k+q,2}} \Big) \\ =& \frac{1}{4\mathcal{V}} \sum_k \Big(\frac{f(E_{k+q,1}) - f(E_{k,1})}{i\omega_n + E_{k,1} - E_{k+q,1}} + \frac{f(E_{k+q,1}) - f(E_{k,2})}{i\omega_n + E_{k,2} - E_{k+q,1}} \\ &+ \frac{f(E_{k+q,2}) - f(E_{k,1})}{i\omega_n + E_{k,1} - E_{k+q,2}} + \frac{f(E_{k+q,2}) - f(E_{k,2})}{i\omega_n + E_{k,2} - E_{k+q,2}} \Big) \end{aligned} \tag{D.16}$$

$$\begin{aligned}\chi^{+-}_{AB}(q,i\omega_n) =&\frac{1}{\mathcal{V}}\sum_k(u^*_{A,1,k+q}u_{B,1,k+q}u_{A,1,k}u^*_{B,1,k}\frac{f(E_{k+q,1})-f(E_{k,1})}{i\omega_n+E_{k,1}-E_{k+q,1}}\\&+u^*_{A,1,k+q}u_{B,1,k+q}u_{A,2,k}u^*_{B,2,k}\frac{f(E_{k+q,1})-f(E_{k,2})}{i\omega_n+E_{k,2}-E_{k+q,1}}\\&+u^*_{A,2,k+q}u_{B,2,k+q}u_{A,1,k}u^*_{B,1,k}\frac{f(E_{k+q,2})-f(E_{k,1})}{i\omega_n+E_{k,1}-E_{k+q,2}}\\&+u^*_{A,2,k+q}u_{B,2,k+q}u_{A,2,k}u^*_{B,2,k}\frac{f(E_{k+q,2})-f(E_{k,2})}{i\omega_n+E_{k,2}-E_{k+q,2}})\\=&\frac{1}{4\mathcal{V}}\sum_k(\frac{f(E_{k+q,1})-f(E_{k,1})}{i\omega_n+E_{k,1}-E_{k+q,1}}-\frac{f(E_{k+q,1})-f(E_{k,2})}{i\omega_n+E_{k,2}-E_{k+q,1}}\\&-\frac{f(E_{k+q,2})-f(E_{k,1})}{i\omega_n+E_{k,1}-E_{k+q,2}}+\frac{f(E_{k+q,2})-f(E_{k,2})}{i\omega_n+E_{k,2}-E_{k+q,2}})\end{aligned} \tag{D.17}$$

$$\begin{aligned}\chi^{+-}_{BA}(q,i\omega_n) =&\frac{1}{\mathcal{V}}\sum_k(u^*_{B,1,k+q}u_{A,1,k+q}u_{B,1,k}u^*_{A,1,k}\frac{f(E_{k+q,1})-f(E_{k,1})}{i\omega_n+E_{k,1}-E_{k+q,1}}\\&+u^*_{B,1,k+q}u_{A,1,k+q}u_{B,2,k}u^*_{A,2,k}\frac{f(E_{k+q,1})-f(E_{k,2})}{i\omega_n+E_{k,2}-E_{k+q,1}}\\&+u^*_{B,2,k+q}u_{A,2,k+q}u_{B,1,k}u^*_{A,1,k}\frac{f(E_{k+q,2})-f(E_{k,1})}{i\omega_n+E_{k,1}-E_{k+q,2}}\\&+u^*_{B,2,k+q}u_{A,2,k+q}u_{B,2,k}u^*_{A,2,k}\frac{f(E_{k+q,2})-f(E_{k,2})}{i\omega_n+E_{k,2}-E_{k+q,2}})\\=&\frac{1}{4\mathcal{V}}\sum_k(\frac{f(E_{k+q,1})-f(E_{k,1})}{i\omega_n+E_{k,1}-E_{k+q,1}}-\frac{f(E_{k+q,1})-f(E_{k,2})}{i\omega_n+E_{k,2}-E_{k+q,1}}\\&-\frac{f(E_{k+q,2})-f(E_{k,1})}{i\omega_n+E_{k,1}-E_{k+q,2}}+\frac{f(E_{k+q,2})-f(E_{k,2})}{i\omega_n+E_{k,2}-E_{k+q,2}})\end{aligned} \tag{D.18}$$

$$\begin{aligned}\chi^{+-}_{BB}(q,i\omega_n) =&\frac{1}{\mathcal{V}}\sum_k(u^*_{B,1,k+q}u_{B,1,k+q}u_{B,1,k}u^*_{B,1,k}\frac{f(E_{k+q,1})-f(E_{k,1})}{i\omega_n+E_{k,1}-E_{k+q,1}}\\&+u^*_{B,1,k+q}u_{B,1,k+q}u_{B,2,k}u^*_{B,2,k}\frac{f(E_{k+q,1})-f(E_{k,2})}{i\omega_n+E_{k,2}-E_{k+q,1}}\\&+u^*_{B,2,k+q}u_{B,2,k+q}u_{B,1,k}u^*_{B,1,k}\frac{f(E_{k+q,2})-f(E_{k,1})}{i\omega_n+E_{k,1}-E_{k+q,2}}\\&+u^*_{B,2,k+q}u_{B,2,k+q}u_{B,2,k}u^*_{B,2,k}\frac{f(E_{k+q,2})-f(E_{k,2})}{i\omega_n+E_{k,2}-E_{k+q,2}})\\=&\frac{1}{4\mathcal{V}}\sum_k(\frac{f(E_{k+q,1})-f(E_{k,1})}{i\omega_n+E_{k,1}-E_{k+q,1}}+\frac{f(E_{k+q,1})-f(E_{k,2})}{i\omega_n+E_{k,2}-E_{k+q,1}}\\&+\frac{f(E_{k+q,2})-f(E_{k,1})}{i\omega_n+E_{k,1}-E_{k+q,2}}+\frac{f(E_{k+q,2})-f(E_{k,2})}{i\omega_n+E_{k,2}-E_{k+q,2}}).\end{aligned} \tag{D.19}$$

We can see that for this special case there are $\chi^{+-}_{AA} = \chi^{+-}_{BB}$ and $\chi^{+-}_{AB} = \chi^{+-}_{BA}$. We can plot their dependence of q for the elements,

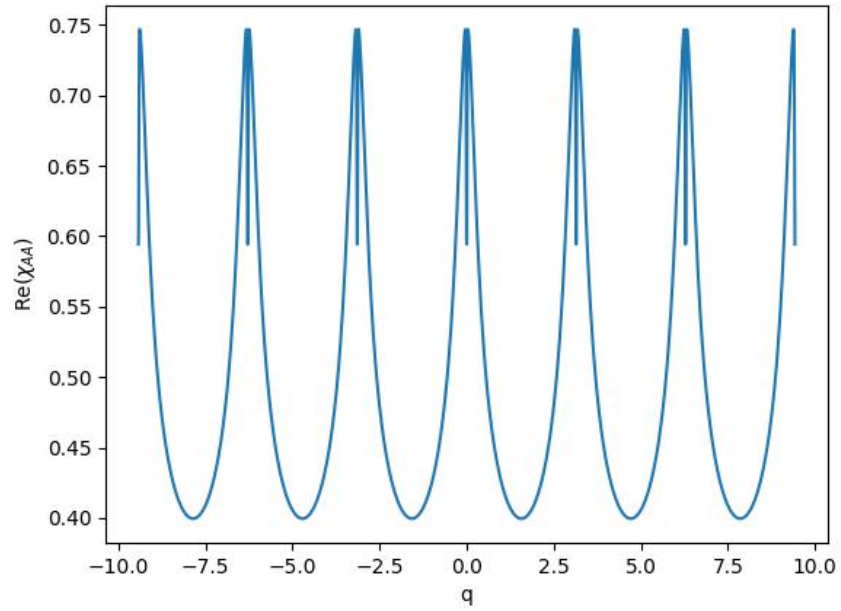

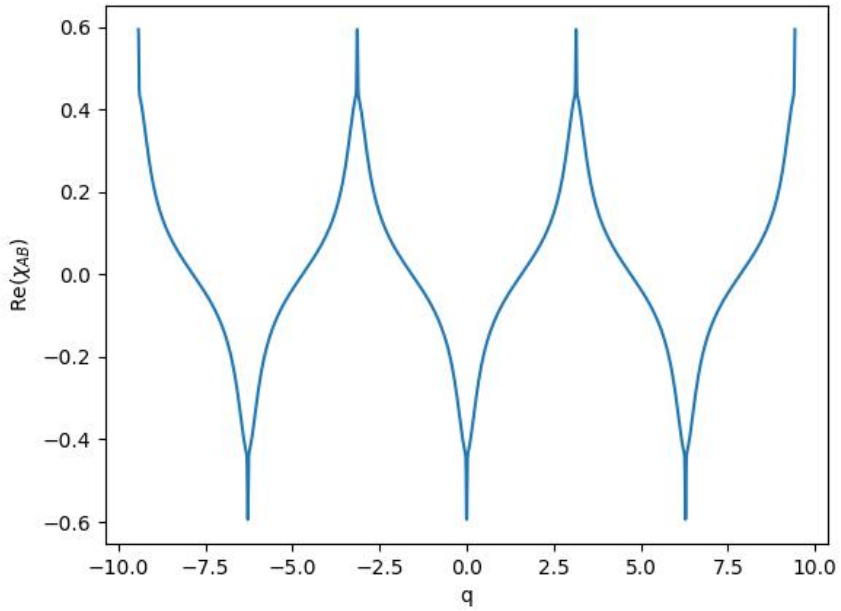

and sum the elements up, then divide them by four,

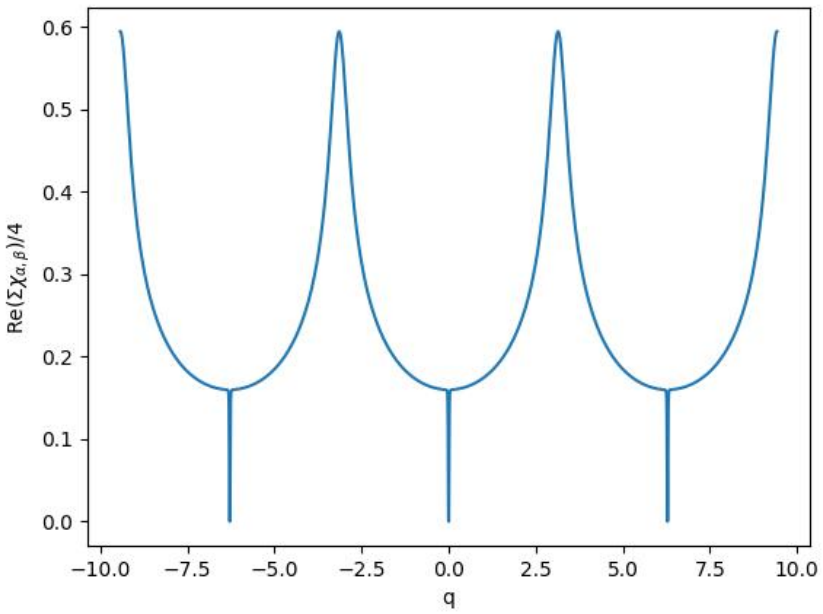

Compare it with the one without sublattice indices, we can find they are the same.

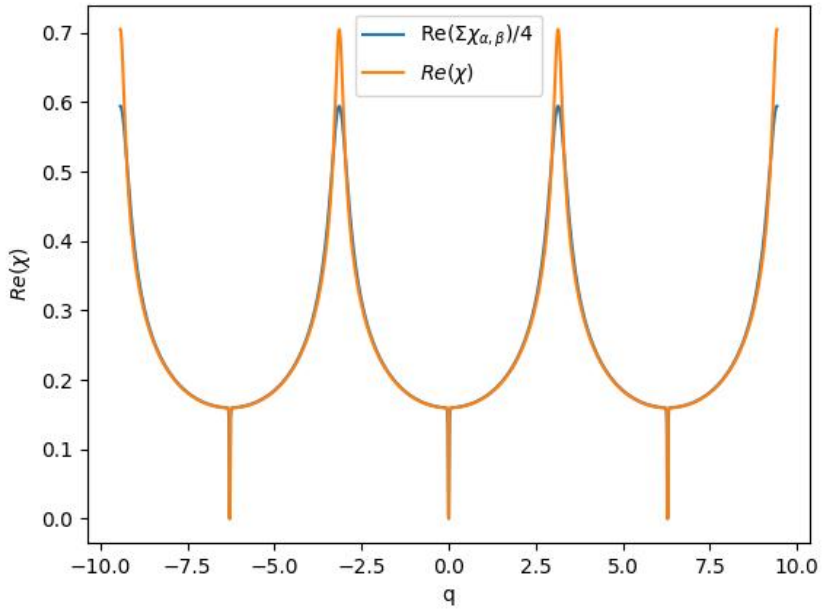

Unit cell with two atoms

In the second way of defining unit cells, we have two particles per unit cell. The matrix of the Hamiltonian is

$$H = \begin{pmatrix} \mu/2 & (t/2)(1+e^{-2ika}) \\ (t/2)(1+e^{2ika}) & \mu/2 \end{pmatrix}. \tag{D.20}$$

With the eigenvector

$$\mathbf{v} = \begin{pmatrix} u_{A,1} & u_{A,2} \\ u_{B,1} & u_{B,2} \end{pmatrix} = \frac{1}{\sqrt{2}} \begin{pmatrix} -e^{-\frac{1}{2}ika} & e^{-\frac{1}{2}ika} \\ e^{\frac{1}{2}ika} & e^{\frac{1}{2}ika} \end{pmatrix}, \tag{D.21}$$

we get the same eigenvalues as eq. (D.14). Now the elements of spin susceptibility are

$$\begin{aligned} \chi^{+-}_{AA}(q, i\omega_n) = &\frac{1}{4\mathcal{V}} \sum_k \Big(\frac{f(E_{k+q,1}) - f(E_{k,1})}{i\omega_n + E_{k,1} - E_{k+q,1}} + \frac{f(E_{k+q,1}) - f(E_{k,2})}{i\omega_n + E_{k,2} - E_{k+q,1}} \\ &+ \frac{f(E_{k+q,2}) - f(E_{k,1})}{i\omega_n + E_{k,1} - E_{k+q,2}} + \frac{f(E_{k+q,2}) - f(E_{k,2})}{i\omega_n + E_{k,2} - E_{k+q,2}} \Big) \end{aligned} \tag{D.22}$$

$$\begin{aligned} \chi^{+-}_{AB}(q, i\omega_n) = &\frac{1}{4\mathcal{V}} e^{iqa} \sum_k \Big(\frac{f(E_{k+q,1}) - f(E_{k,1})}{i\omega_n + E_{k,1} - E_{k+q,1}} - \frac{f(E_{k+q,1}) - f(E_{k,2})}{i\omega_n + E_{k,2} - E_{k+q,1}} \\ &- \frac{f(E_{k+q,2}) - f(E_{k,1})}{i\omega_n + E_{k,1} - E_{k+q,2}} + \frac{f(E_{k+q,2}) - f(E_{k,2})}{i\omega_n + E_{k,2} - E_{k+q,2}} \Big) \end{aligned} \tag{D.23}$$

$$\begin{aligned} \chi^{+-}_{BA}(q, i\omega_n) = &\frac{1}{4\mathcal{V}} e^{-iqa} \sum_k \Big(\frac{f(E_{k+q,1}) - f(E_{k,1})}{i\omega_n + E_{k,1} - E_{k+q,1}} - \frac{f(E_{k+q,1}) - f(E_{k,2})}{i\omega_n + E_{k,2} - E_{k+q,1}} \\ &- \frac{f(E_{k+q,2}) - f(E_{k,1})}{i\omega_n + E_{k,1} - E_{k+q,2}} + \frac{f(E_{k+q,2}) - f(E_{k,2})}{i\omega_n + E_{k,2} - E_{k+q,2}} \Big) \end{aligned} \tag{D.24}$$

$$\begin{aligned} \chi^{+-}_{BB}(q, i\omega_n) = &\frac{1}{4\mathcal{V}} \sum_k \Big(\frac{f(E_{k+q,1}) - f(E_{k,1})}{i\omega_n + E_{k,1} - E_{k+q,1}} + \frac{f(E_{k+q,1}) - f(E_{k,2})}{i\omega_n + E_{k,2} - E_{k+q,1}} \\ &+ \frac{f(E_{k+q,2}) - f(E_{k,1})}{i\omega_n + E_{k,1} - E_{k+q,2}} + \frac{f(E_{k+q,2}) - f(E_{k,2})}{i\omega_n + E_{k,2} - E_{k+q,2}} \Big). \end{aligned} \tag{D.25}$$

And the result of simply summing the elements are different from the lattice without sublattice indices.

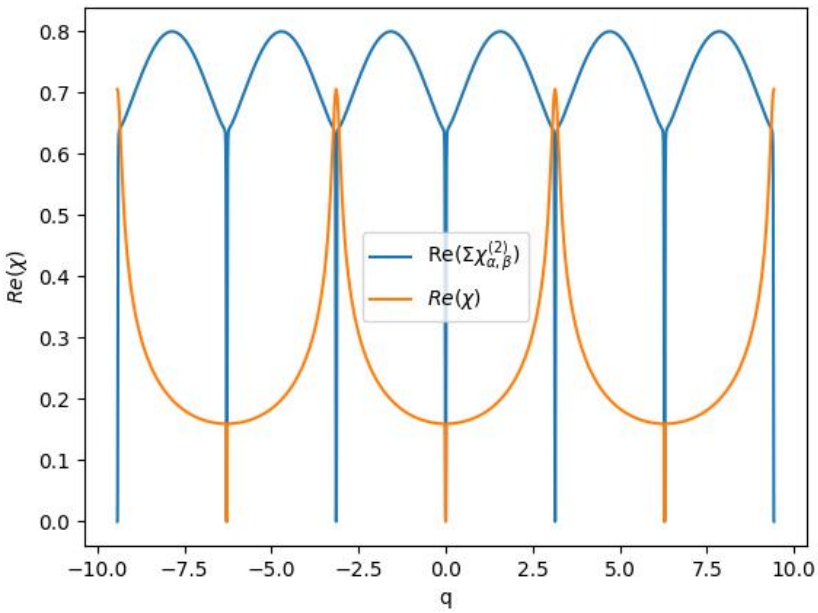

To conclude, if we want to get the 'physical' relaxation rate, we need to do the unitary transformation to transform the eigenvectors back to the single particle unit cell. Other wise the extra phase factors will lead to a wrong result.

Bibliography

[1] B. M. Andersen, A. Kreisel, and P. J. Hirschfeld. Spontaneous time-reversal symmetry breaking by disorder in superconductors. *Front. Phys.*, 12, 2024. doi: 10.3389/fphy.2024.1353425. URL https://www.frontiersin.org/articles/10.3389/fphy.2024.1353425/abstract.

[2] K. Asayama, Y. Kitaoka, G. Q. Zheng, and K. Ishida. NMR studies of high Tc superconductors. *Progress in Nuclear Magnetic Resonance Spectroscopy*, 28(3):221–253, 1996. ISSN 0079-6565. doi: https://doi.org/10.1016/0079-6565(95)01025-4. URL https://www.sciencedirect.com/science/article/pii/0079656595010254.

[3] J. Bardeen, L. N. Cooper, and J. R. Schrieffer. Theory of superconductivity. *Phys. Rev.*, 108:1175–1204, Dec 1957. doi: 10.1103/PhysRev.108.1175. URL https://link.aps.org/doi/10.1103/PhysRev.108.1175.

[4] J. G. Bednorz and K. A. Müller. *Possible High Tc Superconductivity in the Ba-La-Cu-O System*, pages 267–271. Springer Netherlands, Dordrecht, 1993. ISBN 978-94-011-1622-0. doi: 10.1007/978-94-011-1622-0_32. URL https://doi.org/10.1007/978-94-011-1622-0_32.

[5] S. Blundell. *Magnetism in Condensed Matter*. Oxford Master Series in Condensed Matter Physics 4. OUP Oxford, 2001. ISBN 9780198505921.

[6] H. Bruus and K. Flensberg. *Many-Body Quantum Theory in Condensed Matter Physics*. Oxford University Press, 2004. ISBN 0198566336.

[7] L. Buiarelli. Structural properties of kagome-layered crystals. *Master's thesis*, 2023.

[8] D. C. Cavanagh and B. J. Powell. Fate of the Hebel-Slichter peak in superconductors with strong antiferromagnetic fluctuations. *Phys. Rev. Res.*, 3:013241, Mar 2021. doi: 10.1103/PhysRevResearch.3.013241. URL https://link.aps.org/doi/10.1103/PhysRevResearch.3.013241.

[9] N. Curro, T. Caldwell, and E. e. a. Bauer. Unconventional superconductivity in $PuCoGa_5$. *Nature*, 434:622–625, 2005. doi: 10.1038/nature03428. URL https://doi.org/10.1038/nature03428.

[10] Y. Dai, A. Kreisel, and B. M. Andersen. Existence of hebel-slichter peak in unconventional kagome superconductors. *arXiv*, 2024.

[11] W. Duan, Z. Nie, S. Luo, F. Yu, B. R. Ortiz, L. Yin, H. Su, F. Du, A. Wang, Y. Chen, X. Lu, J. Ying, S. D. Wilson, X. Chen, Y. Song, and H. Yuan. Nodeless superconductivity in the kagome metal CsV_3Sb_5. *Sci. China: Phys. Mech. Astron.*, 64(10):107462, Jul 2021. ISSN 1869-1927. doi: 10.1007/s11433-021-1747-7. URL https://doi.org/10.1007/s11433-021-1747-7.

[12] Z. Guguchia, C. Mielke, D. Das, R. Gupta, J.-X. Yin, H. Liu, Q. Yin, M. H. Christensen, Z. Tu, C. Gong, N. Shumiya, M. S. Hossain, T. Gamsakhurdashvili, M. Elender, P. Dai, A. Amato, Y. Shi, H. C. Lei, R. M. Fernandes, M. Z. Hasan, H. Luetkens, and R. Khasanov. Tunable unconventional kagome superconductivity in charge ordered RbV_3Sb_5 and KV_3Sb_5. *Nature Communications*, 14 (1):153, Jan 2023. ISSN 2041-1723. doi: 10.1038/s41467-022-35718-z. URL https://doi.org/10.1038/s41467-022-35718-z.

[13] R. Gupta, D. Das, C. H. Mielke III, Z. Guguchia, T. Shiroka, C. Baines, M. Bartkowiak, H. Luetkens, R. Khasanov, Q. Yin, Z. Tu, C. Gong, and H. Lei. Microscopic evidence for anisotropic multigap superconductivity in the CsV_3Sb_5 kagome superconductor. *npj Quantum Mater.*, 7(1):49, Apr 2022. ISSN 2397-4648. doi: 10.1038/s41535-022-00453-7. URL https://doi.org/10.1038/s41535-022-00453-7.

[14] F. Hammerath. *Magnetism and Superconductivity in Iron-based Superconductors as Probed by Nuclear Magnetic Resonance*. Springer Spektrum, 2012. ISBN 978-3-8348-2422-6.

[15] L. C. Hebel and C. P. Slichter. Nuclear spin relaxation in normal and superconducting aluminum. *Phys. Rev.*, 113:1504–1519, Mar 1959. doi: 10.1103/PhysRev.113.1504. URL https://link.aps.org/doi/10.1103/PhysRev.113.1504.

[16] E. Hellebek. Charge order in kagome metals. *Master's thesis*, 2022.

[17] S. C. Holbæk, M. H. Christensen, A. Kreisel, and B. M. Andersen. Unconventional superconductivity protected from disorder on the kagome lattice. *Phys. Rev. B*, 108:144508, Oct 2023. doi: 10.1103/PhysRevB.108.144508. URL https://link.aps.org/doi/10.1103/PhysRevB.108.144508.

[18] S. C. Holbæk. Superconductivity in kagome materials. *Master's thesis*, 2023.

[19] K. Ishida, H. Mukuda, Y. Kitaoka, K. Asayama, Z. Q. Mao, Y. Mori, and Y. Maeno. Spin-triplet superconductivity in Sr_2RuO_4 identified by ^{17}O Knight shift. *Nature*, 396:658–660, Dec 1998. doi: 10.1038/25315. URL https://doi.org/10.1038/25315.

[20] R. Khasanov, D. Das, R. Gupta, C. Mielke, M. Elender, Q. Yin, Z. Tu, C. Gong, H. Lei, E. T. Ritz, R. M. Fernandes, T. Birol, Z. Guguchia, and H. Luetkens. Time-reversal symmetry broken by charge order in CsV_3Sb_5. *Phys. Rev. Res.*, 4:023244, Jun 2022. doi: 10.1103/PhysRevResearch.4.023244. URL https://link.aps.org/doi/10.1103/PhysRevResearch.4.023244.

[21] Y. Kitaoka, S. Hiramatsu, Y. Kohori, K. Ishida, T. Kondo, H. Shibai, K. Asayama, H. Takagi, S. Uchida, H. Iwabuchi, and S. Tanaka. Nuclear relaxation and Knight shift studies of^{63}Cu in ^{90}K-and ^{60}K-class $YBa_2Cu_3O_{7y}$. *Physica C: Superconductivity*, 153-155:83–86, 1988. ISSN 0921-4534. doi: https://doi.org/10.1016/0921-4534(88)90499-6. URL https://www.sciencedirect.com/science/article/pii/0921453488904996.

[22] Y. Kohori, Y. Yamato, Y. Iwamoto, T. Kohara, E. D. Bauer, M. B. Maple, and J. L. Sarrao. NMR and NQR studies of the heavy fermion superconductors CeTIn$_5$(T = Co and Ir). *Phys. Rev. B*, 64:134526, Sep 2001. doi: 10.1103/PhysRevB.64.134526. URL https://link.aps.org/doi/10.1103/PhysRevB.64.134526.

[23] C. Mielke, D. Das, J.-X. Yin, H. Liu, R. Gupta, Y.-X. Jiang, M. Medarde, X. Wu, H. C. Lei, J. Chang, P. Dai, Q. Si, H. Miao, R. Thomale, T. Neupert, Y. Shi, R. Khasanov, M. Z. Hasan, H. Luetkens, and Z. Guguchia. Time-reversal symmetry-breaking charge order in a kagome superconductor. *Nature*, 602(7896):245–250, Feb 2022. ISSN 1476-4687. doi: 10.1038/s41586-021-04327-z. URL https://doi.org/10.1038/s41586-021-04327-z.

[24] A. Mine, Y. Zhong, J. Liu, T. Suzuki, S. Najafzadeh, T. Uchiyama, J.-X. Yin, X. Wu, X. Shi, Z. Wang, Y. Yao, and K. Okazaki. Direct observation of anisotropic cooper pairing in kagome superconductor csv3sb5. *arXiv e-prints*, 2024.

[25] T. Moriya. Nuclear Magnetic Relaxation in Antiferromagnetics. *Progress of Theoretical Physics*, 16(1):23–44, 07 1956. ISSN 0033-068X. doi: 10.1143/PTP.16.23. URL https://doi.org/10.1143/PTP.16.23.

[26] T. Moriya. The effect of electron-electron interaction on the nuclear spin relaxation in metals. *Journal of the Physical Society of Japan*, 18(4):516–520, 1963. doi: 10.1143/JPSJ.18.516. URL https://doi.org/10.1143/JPSJ.18.516.

[27] C. Mu, Q. Yin, Z. Tu, C. Gong, H. Lei, Z. Li, and J. Luo. S-Wave Superconductivity in Kagome Metal CsV_3Sb_5 Revealed by $^{121/123}$Sb NQR and ^{51}V NMR Measurements. *Chin. Phys. Lett.*, 38(7):077402, jul 2021. doi: 10.1088/0256-307x/38/7/077402. URL https://doi.org/10.1088/0256-307x/38/7/077402.

[28] A. Narath and H. T. Weaver. Effects of electron-electron interactions on nuclear spin-lattice relaxation rates and knight shifts in alkali and noble metals. *Phys. Rev.*, 175:373–382, Nov 1968. doi: 10.1103/PhysRev.175.373. URL https://link.aps.org/doi/10.1103/PhysRev.175.373.

[29] B. R. Ortiz, L. C. Gomes, J. R. Morey, M. Winiarski, M. Bordelon, J. S. Mangum, I. W. H. Oswald, J. A. Rodriguez-Rivera, J. R. Neilson, S. D. Wilson, E. Ertekin, T. M. McQueen, and E. S. Toberer. New kagome prototype materials: discovery of KV_3Sb_5, RbV_3Sb_5, and CsV_3Sb_5. *Phys. Rev. Materials*, 3:094407, Sep 2019. doi: 10.1103/PhysRevMaterials.3.094407. URL https://link.aps.org/doi/10.1103/PhysRevMaterials.3.094407.

[30] B. R. Ortiz, S. M. L. Teicher, Y. Hu, J. L. Zuo, P. M. Sarte, E. C. Schueller, A. M. M. Abeykoon, M. J. Krogstad, S. Rosenkranz, R. Osborn, R. Seshadri, L. Balents, J. He, and S. D. Wilson. CsV_3Sb_5: A $\mathbb{Z}_2$ Topological Kagome Metal with a Superconducting Ground State. *Phys. Rev. Lett.*, 125:247002, Dec 2020. doi: 10.1103/PhysRevLett.125.247002. URL https://link.aps.org/doi/10.1103/PhysRevLett.125.247002.

[31] B. R. Ortiz, P. M. Sarte, E. M. Kenney, M. J. Graf, S. M. L. Teicher, R. Seshadri, and S. D. Wilson. Superconductivity in the $\mathbb{Z}_2$ kagome metal KV_3Sb_5. *Phys. Rev. Materials*, 5:034801, Mar 2021. doi: 10.1103/PhysRevMaterials.5.034801. URL https://link.aps.org/doi/10.1103/PhysRevMaterials.5.034801.

[32] D. Parker, O. V. Dolgov, M. M. Korshunov, A. A. Golubov, and I. I. Mazin. Extended $s_\pm$ scenario for the nuclear spin-lattice relaxation rate in superconducting pnictides. *Phys. Rev. B*, 78:134524, Oct 2008. doi: 10.1103/PhysRevB.78.134524. URL https://link.aps.org/doi/10.1103/PhysRevB.78.134524.

[33] A. Rigamonti. NMR-NQR studies of structural phase transitions. *Advances in Physics*, 33(2):115–191, 1984. doi: 10.1080/00018738400101651. URL https://doi.org/10.1080/00018738400101651.

[34] A. T. Rømer, S. Bhattacharyya, R. Valentí, M. H. Christensen, and B. M. Andersen. Superconductivity from repulsive interactions on the kagome lattice. *Phys. Rev. B*, 106:174514, Nov 2022. doi: 10.1103/PhysRevB.106.174514. URL https://link.aps.org/doi/10.1103/PhysRevB.106.174514.

[35] M. Roppongi, K. Ishihara, Y. Tanaka, K. Ogawa, K. Okada, S. Liu, K. Mukasa, Y. Mizukami, Y. Uwatoko, R. Grasset, M. Konczykowski, B. R. Ortiz, S. D. Wilson, K. Hashimoto, and T. Shibauchi. Bulk evidence of anisotropic s-wave pairing with no sign change in the kagome superconductor CsV_3Sb_5. *Nature Communications*, 14(1):667, Feb 2023. ISSN 2041-1723. doi: 10.1038/s41467-023-36273-x. URL https://doi.org/10.1038/s41467-023-36273-x.

[36] D. J. Scalapino. A common thread: The pairing interaction for unconventional superconductors. *Rev. Mod. Phys.*, 84:1383–1417, Oct 2012. doi: 10.1103/RevModPhys.84.1383. URL https://link.aps.org/doi/10.1103/RevModPhys.84.1383.

[37] J. R. Schriffer. *Theory of superconductivity.* The Benjamin/Cummings Publishing Company, 1983. ISBN 0-8053-8502-9.

[38] M. Sigrist and K. Ueda. Phenomenological theory of unconventional superconductivity. *Rev. Mod. Phys.*, 63:239–311, Apr 1991. doi: 10.1103/RevModPhys.63.239. URL https://link.aps.org/doi/10.1103/RevModPhys.63.239.

[39] A. Smerald and N. Shannon. Angle-resolved NMR: Quantitative theory of ^{75}As T_1 relaxation rate in $BaFe_2As_2$. *Phys. Rev. B*, 84:184437, Nov 2011. doi: 10.1103/PhysRevB.84.184437. URL https://link.aps.org/doi/10.1103/PhysRevB.84.184437.

[40] G. R. Stewart. Unconventional superconductivity. *Advances in Physics*, 66(2): 75–196, Apr. 2017. ISSN 1460-6976. doi: 10.1080/00018732.2017.1331615. URL http://dx.doi.org/10.1080/00018732.2017.1331615.

[41] S. Sumita, M. Naka, and H. Seo. Fulde-Ferrell-Larkin-Ovchinnikov state induced by antiferromagnetic order in κ-type organic conductors. *Phys. Rev. Res.*, 5(4): 043171, Nov. 2023. ISSN 2643-1564. doi: 10.1103/PhysRevResearch.5.043171.

[42] C. Timm. *Theory of Super Conductivity: Winter Semester 2011/2012 TU Dresden Institute of Theoretical Physics.* Independently Published, 2021. ISBN 9798524125262. URL https://books.google.dk/books?id=UnSKzgEACAAJ.

[43] M. Tinkham. *Introduction to superconductivity.* McGraw-Hill New York, 1975. ISBN 0070648778.

[44] L. Van Hove. The Occurrence of Singularities in the Elastic Frequency Distribution of a Crystal. *Phys. Rev.*, 89:1189–1193, Mar 1953. doi: 10.1103/PhysRev.89.1189. URL https://link.aps.org/doi/10.1103/PhysRev.89.1189.

[45] S. D. Wilson and B. R. Ortiz. AV_3Sb_5 Kagome Superconductors: Progress and Future Directions. *arXiv e-prints*, art. arXiv:2311.05946, Nov. 2023. doi: 10.48550/arXiv.2311.05946.

[46] Q. Yin, Z. Tu, C. Gong, Y. Fu, S. Yan, and H. Lei. Superconductivity and Normal-State Properties of Kagome Metal RbV_3Sb_5 Single Crystals. *Chin. Phys. Lett.*, 38(3):037403, mar 2021. doi: 10.1088/0256-307x/38/3/037403.

[47] S.-L. Yu and J.-X. Li. Chiral superconducting phase and chiral spin-density-wave phase in a hubbard model on the kagome lattice. *Phys. Rev. B*, 85:144402, Apr 2012. doi: 10.1103/PhysRevB.85.144402. URL https://link.aps.org/doi/10.1103/PhysRevB.85.144402.

[48] W. Zhang, X. Liu, L. Wang, C. W. Tsang, Z. Wang, S. T. Lam, W. Wang, J. Xie, X. Zhou, Y. Zhao, S. Wang, J. Tallon, K. T. Lai, and S. K. Goh. Nodeless Superconductivity in Kagome Metal CsV_3Sb_5 with and without Time Reversal Symmetry Breaking. *Nano Letters*, 23(3):872–879, Feb 2023. ISSN 1530-6984. doi: 10.1021/acs.nanolett.2c04103.

[49] Y. Zhong, J. Liu, X. Wu, Z. Guguchia, J.-X. Yin, A. Mine, Y. Li, S. Najafzadeh, D. Das, C. Mielke, R. Khasanov, H. Luetkens, T. Suzuki, K. Liu, X. Han, T. Kondo, J. Hu, S. Shin, Z. Wang, X. Shi, Y. Yao, and K. Okazaki. Nodeless electron pairing in CsV_3Sb_5-derived kagome superconductors. *Nature*, 617 (7961):488–492, May 2023. ISSN 1476-4687. doi: 10.1038/s41586-023-05907-x. URL https://doi.org/10.1038/s41586-023-05907-x.